Challenges of initial Thorium and Approaches to Robust Speleothem Age Models: A case study from the Yucatán peninsula, Mexico

Nils Schorndorf[1,2], Sophie F. Warken[1,2*], René Eichstädter[1†], Aaron S. Mielke[1,2], Jerónimo Avilés Olguín[3,4], Frank Keppler[2], Dominik Hennhöfer[5], Fátima Tec Pool[4,6], Carlos Evia[4], María José Gómez[4], Wolfgang Stinnesbeck[2] and Norbert Frank[1,2*]

[1] Institute of Environmental Physics, Heidelberg University, Heidelberg, 69120 Heidelberg, Germany
[2] Institute of Earth Sciences, Heidelberg University, Heidelberg, 69120 Heidelberg, Germany
[3] Museo del Desierto, Saltillo 25022, Coahuila, Mexico
[4] Grupo Espeleológico Ajau, Merida, Yucatán, Mexico
[5] Hessisches Landesmuseum Darmstadt, Friedensplatz 1, 64283 Darmstadt, Germany
[6] Department of Comparative Religion, Faculty of Arts, Comenius University, Bratislava, Slovakia

Correspondence to: Sophie Warken (sophie.warken@iup.uni-heidelberg.de)

Abstract. Speleothems, such as stalagmites and flowstones, are invaluable archives of past environmental and climatic conditions due to their layered growth and suitability for precise ^{230}Th/U dating. In tropical karst settings, however, elevated and variable detrital thorium contamination can severely compromise age accuracy, especially for young speleothems. Here, a suite of stalagmites from Áaktun Kóopo' Cave from the Yucatán Peninsula is used as a case study to develop and evaluate a multi-method framework for constraining initial thorium and constructing robust age–depth models. We combine extensive ^{230}Th/U dating with local isochron analysis, stratigraphic approaches, and annual Sr/Ca layer counting to constrain elevated and initial (^{230}Th/^{232}Th) activity ratios and resolve pronounced chronological inversions. High uranium concentrations in the speleothems (average c. 1 ppm) allow precise measurements, yet we infer a high and largely unsystematic variability of high initial (^{230}Th/^{232}Th) activity ratios in space and time, with values spanning between 4 and 68, thus far exceeding standard bulk-Earth values. This variability demonstrates that elevated and temporally variable initial Th may be common in tropical karst settings and that multiple, independent constraints on initial (^{230}Th/^{232}Th) activity ratios are essential for reliable chronologies in such environments. Applying this framework to Áaktun Kóopo' cave stalagmites yields internally consistent stalagmite age–depth models spanning the past 2.7 kyr, as well as evidence for earlier glacial and interglacial growth phases. These chronologies provide the basis for high-resolution, multi-proxy reconstructions of climatic and environmental changes in the northeastern Yucatán Peninsula during the entire era of Maya cultural evolution, and they illustrate how robust speleothem chronologies can be obtained even in cave systems affected by elevated and highly variable initial thorium.

Formatted: Superscript

Formatted: German

Deleted: (sophie.warken@uni-heidelberg.de)

Formatted: Font: 11 pt, Font color: Text 1

Deleted: These natural formations record hydroclimatic variability over time, offering insights into how environmental changes have influenced ecosystems and human societies. In the context of Mesoamerica, speleothem records provide an opportunity to explore potential links between climate variability and sociopolitical transformations during Maya cultural evolution. Paleoclimate archives from this region document severe dry conditions during the Terminal Classic Period (~800–1000 AD), a time marked by societal decline and urban abandonment among the Maya. Yet, existing records often suffer from limited chronological precision, and high-resolution multi-proxy datasets from the area remain scarce. This study presents extensive ^{230}Th/U dating of several speleothems from Áaktun Kóopo Cave, Yucatán, revealing continuous carbonate deposition over the past 2.7 kyr, encompassing the entire era of Maya cultural evolution, as well as evidence of speleothem growth during earlier glacial and interglacial periods. High uranium concentrations in the speleothems (averaging 1 ppm) enabled precise dating, despite challenges from elevated and variable detrital thorium contamination. These challenges were addressed by combining multiple techniques, including isochron analysis, stratigraphic approaches, and annual layer counting, to constrain elevated and initial (^{230}Th/^{232}Th) activity ratios. Notably,

Formatted: Font: 11 pt, Font color: Text 1, English (US)

Formatted: Font color: Text 1

Deleted: . Still, our approach yields stalagmite chronologies from Áaktun Kóopo Cave that provide a robust foundation for detailed multi-proxy reconstructions of hydroclimate and vegetation changes over the past 2.7 kyr. These chronologies address a critical gap in high-resolution data for this region and enable future studies to better resolve environmental conditions throughout Maya history

Formatted: Font: 11 pt, Font color: Text 1, English (US)

Formatted: Font: 11 pt, Font color: Text 1

1 Introduction

Reconstructing past environmental and climatic variability relies on archives that combine continuity, sensitivity to climate, and robust dating methods (Fairchild and Baker, 2012; Koltai et al., 2026; Medici et al., 2026). Speleothems fulfil these criteria, as their layered carbonate growth can be precisely dated using U-series disequilibrium dating (Wendt et al., 2021; Scholz and Hoffmann, 2008; Cheng et al., 2013). Constructing accurate age models based on a large number of individual ^{230}Th/U ages is fundamental for interpreting speleothem climate proxy records, as chronological uncertainties directly affect the absolute timing of events, its duration, and partially the magnitude (smoothing) of inferred climate variability (Comas-Bru et al., 2020; Moseley et al., 2016). However, ^{230}Th/U dating assumes a closed system for the exchange of Uranium and its decay products upon speleothem formation, and it further presumes absence of initial ^{230}Th. In such an ideal theoretical scenario the Th/U age precision and accuracy will solely depend on the analytical precision and accuracy of isotope ratio measurements and isotope half-lives (Cheng et al., 2013). Any deviation of the carbonate precipitating environment from this ideal scenario may influence the age accuracy, either through U-series system opening via dissolution and reprecipitation of carbonate, or via a variable degree of initial Th contamination. To date, U-series system opening cannot be corrected for cave deposits due to the lack of constant boundary conditions such as a time-invariant U-isotope composition of drip water. Such U-series open system models only exist for well-preserved marine carbonates and assume a near constancy of seawater U-isotope ratios as additional constraint (Frank et al., 2006). For the presence of initial ^{230}Th, however, several strategies exist to correct for its influence. In most cases ^{230}Th is related to the detrital origin of ^{232}Th assuming a constant detrital activity ratio for linear correction models applied to the measured ^{230}Th/^{238}U activity ratio. Appropriate correction techniques have to be applied, which are, however, associated with relatively large uncertainties. Consequently, high Th contamination and young ages of speleothems result in ^{230}Th/U-age errors exceeding analytical precision by orders of magnitude (Ludwig and Titterington, 1994). This issue is particularly problematic for speleothems with low uranium concentrations and visible non-carbonate traces, since even small amounts of initial Th can lead to erroneously old age estimates (e.g., Faraji et al., 2023; Kerber et al., 2025; Fensterer et al., 2010).

A primary challenge with initial Th correction arises from the difficulty in accurately estimating the initial (^{230}Th/^{232}Th) activity ratio of detrital material (further on referred to as R02i), which can vary depending on the characteristics of the host rock, soil, and chemical complexing agents during aqueous transport of Th (Ivanovich and Harmon, 1992). For geological material in ^{238}U–^{234}U–^{230}Th secular equilibrium, and assuming a crustal ^{232}Th/^{238}U activity ratio of 3.8 (Taylor and Mclennan, 1985), the resulting atomic ^{230}Th/^{232}Th ratio is 4.4 ± 2.2 ×

Deleted: .

Deleted: (Wendt et al., 2021; Scholz and Hoffmann, 2008; Cheng et al., 2013).

Deleted: (Comas-Bru et al., 2020; Moseley et al., 2016).

Deleted: (Cheng et al., 2013).

Deleted: (Frank et al., 2006).

Deleted: (Ludwig and Titterington, 1994).

Deleted: (e.g., Faraji et al., 2023; Kerber et al., 2025; Fensterer et al., 2010).

Deleted: (Ivanovich and Harmon, 1992).

Deleted: (Taylor and Mclennan, 1985),

10^{-6} (with an assumed error of 50%), equivalent to an activity ratio of ~0.8. This ratio, widely utilized for detrital ^{230}Th correction (Spötl et al., 2002), is commonly often applied to estimate initial ^{230}Th and correct ^{230}Th/U ages. This is particularly effective when absolute ^{232}Th concentrations are low (< a few ng) and speleothems are older than several thousand years. However, tropical karst systems frequently exhibit elevated and variable R02i in drip waters, modern carbonates, and speleothems, sometimes up to 80 times higher than the commonly assumed value of ~ 0.8 for the upper continental crust. For example, speleothem studies from Mexico report a wide range of R02i between 3.5 and 32 (Moseley et al., 2015; Kennett et al., 2022; Stinnesbeck et al., 2020). R02i ranging from 8 to 41 have been used to correct a Belizean stalagmite (Ridley et al., 2015), and values between 11 and 61 were applied to Puerto Rican stalagmites (Kerber et al., 2025; Vieten et al., 2024a; Vieten et al., 2024b; Warken et al., 2020; Rivera-Collazo et al., 2015). Also at other sites including the Bahamas (Beck et al., 2001; Arienzo et al., 2015; Hoffmann et al., 2010; Richards and Dorale, 2003), Cuba (Fensterer et al., 2010), or in the tropical Pacific (Faraji et al., 2021; Partin et al., 2007; Carolin et al., 2013) elevated R02i were found. These observations thus demonstrate a vast range of initial Th variability, also within single cave sites. However, large (and poorly constrained) variations in R02i directly translate into additional, often dominant, age uncertainties, particularly for young and/or strongly contaminated speleothems. Classical correction schemes based on a single bulk-Earth detrital ratio can therefore produce stratigraphic age inversions and biased chronologies when applied in such settings.

In general, there are two main approaches to assess R02i in speleothems: (1) direct measurement of the contaminating phase, e.g., from cave drip water, soil, or zero-age carbonate (ZAC) (Kerber et al., 2025; Hu et al., 2008; Li et al., 2022; Wortham et al., 2022); and (2) estimation of R02i using linear binary mixing models or a priori assumptions to obtain continuous chronologies. In cases where direct measurement is not possible, the isochron method can serve as a first order alternative (Kaufman, 1993; Richards and Dorale, 2003; Frank et al., 2002; Ludwig and Titterington, 1994). However, for this technique to be effective, multiple sub-samples from the same lamina (or group of laminae) must exhibit varying ^{232}Th/^{238}U ratios and follow first-order binary linear mixing behaviour (Wenz et al., 2016; Ludwig and Titterington, 1994). Another approach is the stratigraphic constraint method, where R02i is estimated by ensuring that the corrected ages increase steadily with distance from the top (dft) of the stalagmite (Roy-Barman and Pons-Branchu, 2016; Hellstrom, 2006). While monitoring detrital activity ratios in ZAC and drip waters provides useful information about initial activity ratios, it offers little insight into whether and how these ratios change over time. Overall, most studies still rely on only one of these methods, and the resulting uncertainty in initial Th variability is often poorly quantified. This highlights the need for more systematic assessments of initial Th when correcting ^{230}Th/U ages from such environments.

Deleted: (Spötl et al., 2002),

Deleted: –

Deleted: the Bahamas report a wide range of R02i between 2.2 to 18.7 (Beck et al., 2001; Arienzo et al., 2015; Hoffmann et al., 2010; Richards and Dorale, 2003). R02i ranging from 8 to 41 have been used to correct a Belizean stalagmite (Ridley et al., 2015), and values between 11 and 61 were applied to Puerto Rican stalagmites (Kerber et al., 2025; Vieten et al., 2024a; Vieten et al., 2024b; Warken et al., 2020; Rivera-Collazo et al., 2015). Also at other sites including Cuba (Fensterer et al., 2010), Mexico (Moseley et al., 2015; Kennett et al., 2022; Stinnesbeck et al., 2020) or in the tropical Pacific (Faraji et al., 2021; Partin et al., 2007; Carolin et al., 2013) elevated R02i were found. These observations underscore the necessity of addressing variability in initial Th activity ratios when correcting ^{230}Th/U ages from such environments.

Deleted: (Kerber et al., 2025; Hu et al., 2008; Li et al., 2022; Wortham et al., 2022);

Deleted: (binary mixing)

Deleted: .

Deleted: in order

Deleted: (Wenz et al., 2016; Ludwig and Titterington, 1994).

Deleted: (Roy-Barman and Pons-Branchu, 2016; Hellstrom, 2006).

High-resolution stalagmite records from the Yucatán Peninsula (YP) have been analysed to explore hydroclimate variability and its intersection with Maya sociopolitical evolution (e.g., Kennett et al., 2012; Medina-Elizalde et al., 2010; James et al., 2026). However, in the northeastern YP, high-resolution records are few, with only one stalagmite record available, spanning 1037 BCE to 397 AD (Medina-Elizalde et al., 2016b). Critically, YP records often face dating challenges due to low uranium concentrations or high detrital contamination (e.g., Frappier et al., 2014; Webster et al., 2007; Akers et al., 2016; Akers et al., 2019; James et al., 2025; Medina-Elizalde et al., 2010; Kennett et al., 2022; James et al., 2026). These complexities make it difficult to reconstruct past climate and environmental changes with precision, obscuring the evaluation of their effects on Maya cultural evolution, particularly during the Terminal Classic Period (TCP; ~800–1000 AD), a time of profound social and political upheaval marked by widespread population decline and the abandonment of many urban centres (e.g., Douglas et al., 2015).

This study focuses on constructing precise ^{230}Th/U chronologies for stalagmites from Áaktun Kóopo' Cave, located in the northeastern YP. Through a detailed study of (i) the speleothems' U and Th isotope compositions, (ii) their micro-facies and geochemistry, as well as (iii) their stable isotope compositions we establish multiple age-depth models that demonstrate active speleothem deposition over the past 2.7 kyr. These chronologies will allow to fill a notable gap in high-resolution paleoclimate records for the region and provide a foundation for future investigations into hydroclimatic and environmental changes, particularly during periods of profound Maya societal changes. Crucially, our study reveals highly variable initial ^{230}Th coprecipitation within the karst system that impacts, and in some layers inhibits, high-precision ^{230}Th/U age determination, thereby limiting the accuracy of speleothem chronologies. The chemical transport processes of Th isotopes in meteoric water, however, remain poorly understood.

2 Material and Methods

2.1 Study site

Áaktun Kóopo' Cave is situated in La Estrella, a small Maya community in the northeastern YP (Figure 1a), approximately 30 km northeast of Chemax and 7 km southwest of Xcan, at 20°48'26.7"N, 87°44'15.8"W. This region experiences a warm, humid tropical climate with highly seasonal rainfall (wet season June–November), high year-round humidity and frequent tropical storms and hurricanes (Romero and Alfaro, 2024; Medina-Elizalde et al., 2016a) and the soils are typically thin and variable, with pockets rarely reaching 0.5 m between areas of exposed bedrock (Lases-Hernandez et al., 2019).

Deleted: (e.g., Kennett et al., 2012; Medina-Elizalde et al., 2010).

Deleted: (Medina-Elizalde et al., 2016b).

Deleted: (e.g., Frappier et al., 2014; Webster et al., 2007; Akers et al., 2016; Akers et al., 2019; James et al., 2025; Medina-Elizalde et al., 2010; Kennett et al., 2022).

Deleted: (e.g., Douglas et al., 2015).

Deleted: Kóopo

Deleted: Kóopo Cave is located in La Estrella, a small Maya community in the northeastern YP (Figure 1a). The cave lies approximately 30 km northeast of Chemax and 7 km southwest of Xcan, at 20°48'26.7"N, 87°44'15.8"W (Figure 1b). Initial documentation of Áaktun Kóopo Cave by the AJAU cave explorers in 2007 recorded numerous archaeological remains. Subsequent exploration in 2010 extended the surveyed passages to a total length of 1900 m and a depth of 21 m (Thomas, 2011), and more recent mapping indicates over 2100 m of horizontal passage (Tec, 2021) (Figure 1c). There are at least nine distinct water bodies within the cave, and their water levels fluctuate seasonally between the rainy and dry seasons, which occasionally results in localized flooding in some parts of the cave (Tec, 2021). Cave sediments typically consist of red clay (kankab) that ranges from dry to muddy conditions.

Áaktun Kóopo' Cave is developed within the low-relief Yucatán carbonate platform, which consists of thick Cretaceous and Tertiary shallow-marine limestones, forming a great limestone plain with a shallow water table and almost no surface rivers (Ward et al., 1995; Perry et al., 2009; Smart et al., 2006). The cave comprises more than 2 km of horizontal passages and at least nine water bodies (Figure 1b), with seasonally fluctuating water levels that can locally flood parts of the cave (Thomas, 2011; Tec, 2021). Cave sediments are dominated by red clay (*kankab*) that ranges from profound to muddy conditions. Archaeological evidence inside the cave includes Maya paintings, polychrome pottery, and skeletal remains of 23 individuals (juveniles and adults), dating to the Late Preclassic (–250 to 300 AD) and Early Classic (300–600 AD) periods (Gómez, 2020). The Maya also modified parts of the cave by constructing walls using limestone blocks, speleothems, and soil to create chambers (Tec, 2021). The presence of imported materials such as flint and obsidian (Gómez, 2020) suggests that members of the local elite performed mortuary and ritual practices in the cave. In addition to these archaeological features, Áaktun Kóopo' Cave is decorated with numerous speleothem features, including stalactites, stalagmites, flowstones, and draperies, making it an important site for both archaeological and paleoclimate research.

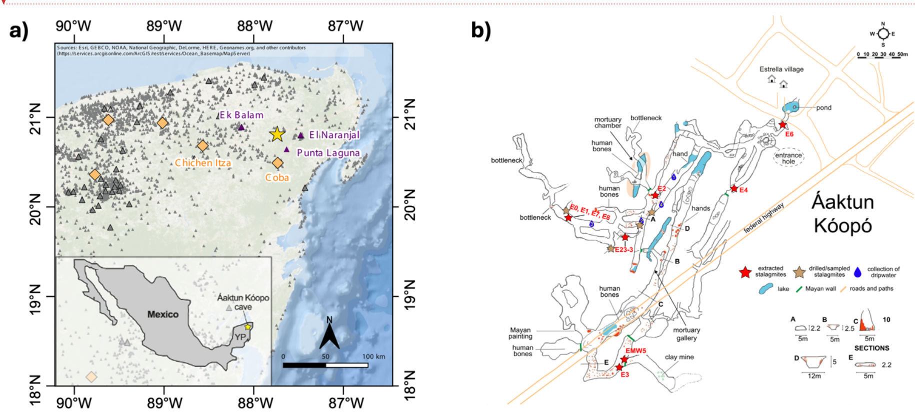

Figure 1: a) Location of the Áaktun Kóopo' Cave (yellow asterisk) in the northeastern Yucatán Peninsula, Mexico, relative to other Maya archaeological settlements in the area. Orange diamonds represent large settlements while large (small) triangles represent intermediate (smallest) ones, based on Witschey and Brown (2010). Well-known settlements are e.g., Coba, Punta Laguna, El Naranjal, and Ek Balam. b) Map of Áaktun Kóopo' Cave with sample locations. Red stars show locations of stalagmites that have been extracted from the cave, while brown stars represent locations where samples were drilled or scraped from stalagmites. Blue symbols mark sites of drip water collection. Map taken from Thomas (2011) and modified after Gómez (2020) and Tec (2021). Green lines indicate locations of Maya walls.

Formatted: Font color: Black, English (US)

Deleted: (Gómez, 2020).

Deleted: (Tec, 2021). The presence of imported materials such as flint and obsidian (Gómez, 2020)

Deleted: Kóopo

Deleted: formations

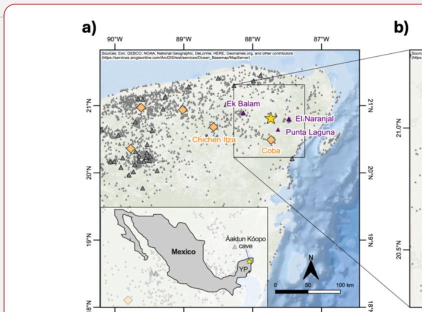

Deleted:

Deleted: 1:

Deleted: Kóopo

Deleted: b) Zoom-in showing the settlement density around Áaktun Kóopo Cave, with well-known settlements such as Coba, Punta Laguna, El Naranjal, and Ek Balam, all within 20–40 km distance, and the closest settlement, Xcan (encircled), less than 10 km to the northeast.

Deleted: Witschey and Brown (2010). c)

Deleted: Kóopo

Deleted: was

Deleted: Thomas (2011)

Deleted: Gómez (2020)

Deleted: Tec (2021).

2.2 Sample material

During three cave visits in 2018, 2022, and 2023, samples for ^{230}Th/U dating were collected from 15 different speleothems inside Áaktun Kóopo' Cave, including stalagmites, flowstones, and modern carbonate deposits. In addition to in-situ drill cores from various speleothems, ten stalagmites, ranging from 6.5 to 34 cm in length, were extracted completely for more detailed analysis (Figure S 1). For six of these stalagmites (E0, E1, E2, E7, E8, E23-3) their drip site was still actively dripping at the time of collection. Stalagmites E0, E1, E7, E8, and E23-3 were all collected from the same cave chamber in the northwestern part of the cave, with E0, E1, E7 and E8 even from the same two square metre area (Figure 1b). Interestingly, both E0 and E7 exhibited an L-shaped, or "double" formation (Figure S 1). This morphology occurs when a stalagmite falls over, and continued carbonate precipitation causes growth to proceed at a perpendicular angle to the original axis, resulting in the observed L-shape. Notably, E0 was not calcified to the ground but rather embedded in soft sediment, which may have contributed to its collapse. During the extraction, a third stalagmite (E0-A) was uncovered beneath 10 cm of sediment. Stalagmite E2 was collected from the central part of the cave, while stalagmite E4 was retrieved from the northeastern section, closer to the cave's entrance. Stalagmite E3 was collected from the southern portion, located in front of a large Maya wall, from which a small stalagmite (EMW5) detached and was collected as well. For the follow-up analyses, the stalagmites were cut along their presumed growth axis into slices.

Furthermore, we collected three drip water samples (EDW-1, EDW-2 and EDW-3) from different parts of the cave in 2022 (Figure 1b) to evaluate the R02i in drip water. EDW-3 consists of an integrated water sample collected from different drips (soda straws) with low drip rates within an area of about 1 m^2 within the chamber in the western part of the cave where most of the analysed stalagmites were extracted (Figure 1b). After drip water collection, the plastic bottles (125 ml) were immediately sealed with Parafilm for transportation and storage upon measurement. From the floor below the drip site EDW-1, we collected a small sample of what appeared to be modern carbonate precipitates.

2.3 Mineralogical Characterization of Stalagmites

2.3.1 XRD Measurements

Slices of stalagmites from Áaktun Kóopo' Cave revealed several changes in colour throughout their growth (Figure S 1), which may indicate changes in mineralogy or crystal fabrics. To investigate these variations and determine the mineralogical composition of the stalagmites (e.g., calcite vs. aragonite), nine samples were analysed from visually distinct sections of stalagmite E0-C for XRD analysis (Figure S 2a). Additionally, a sample was collected

Deleted: Kóopo

Deleted: (Figure S 1).

Deleted: E8

Deleted: a c. two square metre area

Deleted: (Figure 1c).

Deleted: (Figure S 1).

Deleted: (Figure 1c

Deleted: (Figure 1c).

Deleted: Kóopo

Deleted: (Figure S 1),

Deleted: (Figure S 2a).

from the bottom portion of stalagmite E1, where the fan-like crystal texture and silky gloss suggested aragonite as the dominant polymorph (Figure S 1 and S 2). Each sample consisted of approximately 1 g of carbonate powder that was drilled using a Proxxon machine equipped with a diamond-coated stainless-steel drill bit. XRD measurements were performed at the Institute of Earth Sciences, Heidelberg University, using a Bruker D8 ADVANCE Eco diffractometer. The measurements were conducted with the following parameters: Cu K radiation source, 30 kV voltage, 33 mA current, Ni filter, SSD160 detector. Samples were analysed in rotating sample holders over an angular range of 2θ from 5°to 70°, with increments of 0.019°and a counting time of 1 second per step. Peak positions and intensities were processed using Diffrac.Suite EVA software (Bruker).

Deleted: (Figure S 1

2.3.2 Thin section inspection

Thin sections have been used to study the crystal fabrics in further detail, i.e. the individual expression of mineral phases, direction, non-carbonate contamination and/or signs of dissolution (e.g., Frisia et al., 2002; Perrin et al., 2014). Thin sections were prepared from stalagmites E0-B, E0-C, E4, E8, and the upper section of E1. These sections were analysed under a polarized transmitted-light microscope (KEYENCE VHX-6000) at the Institute of Earth Sciences, Heidelberg University.

Deleted: (e.g., Frisia et al., 2002; Perrin et al., 2014).

2.4 Geochemistry

2.4.1 In-situ Strontium – Calcium analysis

Laser ablation ICP-MS analyses of selected stalagmites and for Sr/Ca ratios followed established protocols (Warken et al., 2021; Jochum et al., 2012; Schorndorf, 2024) and were performed using a 193 nm ArF excimer laser (NWR193UC by New Wave Research) coupled to an inductively coupled plasma quadrupole mass spectrometer (Thermo Fisher iCAP-Q) at the Institute of Environmental Physics, Heidelberg University. Line scans were conducted along the growth axis of the stalagmite slices using a rectangular spot size of 25×100 µm. The repetition rate was set to 20 Hz, with scan speeds of 5 µm s^{-1} for stalagmites E1 and E8, and 10 µm s^{-1} for stalagmite E23-3. To eliminate potential surface contamination, a pre-ablation step was performed along each scan path using a circular spot size of 150 µm at a scan speed of 100 µm s^{-1} and a repetition rate of 10 Hz. Background counts were measured with the laser in the off mode and subtracted from the raw data. Data processing involved an outlier correction using a floating 1.5 interquartile range (IQR). To account for matrix effects, blank-corrected count rates of ^{43}Ca and ^{88}Sr were normalized to the ^{44}Ca signal, which served as an internal standard for the total ablation efficiency. External calibration was performed using silicate glass NIST SRM 612, with reference values provided by Jochum et al. (2011). Drift corrections were applied through linear interpolation between two standard

Deleted: (Warken et al., 2021; Jochum et al., 2012; Schorndorf, 2024)

Deleted: External calibration was performed using silicate glass NIST SRM 612, with reference values provided by Jochum et al. (2011).

measurements taken before and after each ablation path. The resulting Sr/Ca elemental ratios are presented as mass concentration ratios.

2.4.2 Stable isotope analysis

For stalagmites E0-C, E1, and E23-3, approximately 50–90 µg of powdered samples was drilled using a Micromill (2010A Sherline) equipped with a micro milling cutter (TiSiN) of 500 µm in diameter. Most samples were analyzed for their stable isotope composition of oxygen ($\delta^{18}O$) and carbon ($\delta^{13}C$) at the Institute of Earth Sciences, Heidelberg University, using a ThermoFinnigan MAT253Plus gas source mass spectrometer equipped with a Thermo Fisher Scientific Kiel IV carbonate device. Quality control is based on the analysis of an in-house standard (Solnhofen limestone, $\delta^{13}C_{VPDB}$ = +1.38 ± 0.03‰ and $\delta^{18}O_{VPDB}$ = −4.59 ± 0.06‰) calibrated to the reference material IAEA-603 (calcite; $\delta^{13}C_{VPDB}$ = +2.46 ± 0.01‰ and $\delta^{18}O_{VPDB}$ = −2.37 ± 0.04‰). A part of the samples of E0-C was analysed at Elemtex Ltd., Cornwall, UK, using an isotope ratio mass spectrometer (IRMS) (Thermo Scientific Delta V) coupled with a Gasbench II). Here, quality control is performed using a Carrara marble standard ($\delta^{13}C$ = 2.10‰, $\delta^{18}O$ = − 2.01‰) and a second in-house calcite standard ($\delta^{13}C$ = 2.89‰, $\delta^{18}O$ = − 6.15‰), calibrated directly against NBS18 and NBS19.
External reproducibility at both labs is better than 0.04‰ for $\delta^{13}C_{VPDB}$ and 0.07‰ for $\delta^{18}O_{VPDB}$ at the 1σ confidence level, and all $\delta^{13}C$ and $\delta^{18}O$ values are reported relative to Vienna Pee Dee Belemnite (VPDB) standard.

2.5 Chronology

2.5.1 $^{230}Th/U$ Dating

A total of 157 samples from Áaktun Kóopo' speleothems as well as the three drip water samples were analysed using high-precision $^{230}Th/U$ dating at the Institute of Environmental Physics, Heidelberg University. For the analysis, small sample plates weighing approximately 100 mg were cut perpendicular to their growth direction using a diamond wire saw and subsequently sample leaching in weak acid, weighing, dissolution in ultra-clean nitric acid and spiking with our in-house triple-spike solution ('TriSpike', ^{233}U, ^{236}U and ^{229}Th) (Kerber et al., 2023). For drip water analysis, about 15 to 30 ml of sample was weighed and spiked with 'TriSpike', acidified with ultra-clean nitric acid, subsequently dried down and re-dissolved. Overall, the preparation involving sample leaching, dissolution, spiking, and wet column extraction chromatography using Eichrom UTEVA resin, followed established protocols (Wefing et al., 2017; Matos et al., 2015; Douville et al., 2010). Chemical blanks are regularly monitored and commonly below 0.4 fg for ^{234}U and 0.04 fg for ^{230}Th (Kerber et al., 2023; Kerber et al., 2025).

Deleted: subsamples from Áaktun Kóopo speleothems were analysed using high-precision $^{230}Th/U$ dating

Isotope measurements were performed with a multi-collector inductively coupled plasma source mass spectrometer (MC-ICP-MS, Thermo Fisher Neptune plus) using a semi-static multi-cup setting as described by Kerber et al. (2023). Mass spectrometry techniques and data treatment adhered to procedures are detailed in Kerber et al. (2023); (2025). Data analysis was performed using a Python-based GUI application (Kerber et al., 2025). Ages were calculated using the half-lives provided by Cheng et al. (2013) for ^{230}Th and ^{234}U as well as by Jaffey et al. (1971) for ^{238}U. All uncertainties are reported at the 2σ level, excluding errors associated with half-life values.

Deleted: at the Institute of Environmental Physics, Heidelberg University. Prior to the analysis, the stalagmites were cut along their presumed growth axis into slices. From these slices, small sample plates weighing approximately 100 mg were cut perpendicular to their growth direction using a diamond wire saw. The preparation involved sample leaching, dissolution, spiking, and wet column extraction chromatography using Eichrom UTEVA resin, following established protocols (Wefing et al., 2017; Matos et al., 2015; Douville et al., 2010). Isotope measurements were conducted using a semi-static multi-cup setting as described by Kerber et al. (2023). Mass spectrometry techniques and data treatment adhered to procedures detailed in Kerber et al. (2023); (2025). Data analysis was performed using a Python-based GUI application (Kerber et al., 2025). Ages were calculated using the half-lives provided by Cheng et al. (2013), and

2.5.2 Radiocarbon Dating

To constrain recent carbonate deposition, the tops of presumably modern speleothems were analysed using radiocarbon dating. Small calcite samples (10–20 mg) were cut from the tops of stalagmites E0-C, E1, and E8 using a diamond wire saw at the Institute of Environmental Physics, Heidelberg University. To avoid contamination by ambient air, the samples were leached in 4% hydrochloric acid prior to hydrolysis and graphitization. A detailed description of the sample preparation routine is provided in Therre et al. (2021). The resulting graphite–iron compounds were measured using a 200 kV tandem mini carbon dating system (MICADAS) accelerator mass spectrometer (AMS) at the Curt-Engelhorn Center for Archaeometry in Mannheim, Germany (Kromer et al., 2013; Synal et al., 2007). Details regarding long-term blank values and external standard reproducibility can be found in Beisel et al. (2025) and Therre et al. (2021).

Deleted: A detailed description of the sample preparation routine is provided in Therre et al. (2021). The resulting graphite–iron compounds were measured using a 200 kV tandem mini carbon dating system (MICADAS) accelerator mass spectrometer (AMS) at the Curt-Engelhorn Center for Archaeometry in Mannheim, Germany (Kromer et al., 2013; Synal et al., 2007). Details regarding long-term blank values and external standard reproducibility can be found in Beisel et al. (2025) and Therre et al. (2021).

2.5.3 Speleothem age-depth models

The age-depth models for selected stalagmites were constructed using a suite of established approaches: linear interpolation, linear regression, Bchron (Haslett and Parnell, 2008), Bacon (Blaauw and Christen, 2011; Blaauw et al., 2021), COPRA (Breitenbach et al., 2012), and StalAge (Scholz and Hoffmann, 2011). Model construction followed and extended the protocols of the Speleothem Isotopes Synthesis and Analysis (SISAL) working group (Roesch and Rehfeld, 2020), which is provided as a supplement to Comas-Bru et al. (2020); SISAL.AM. In case of identified hiatuses, the age-depth models were split at the depth of the growth interruption into separate sections. This approach improves model convergence and allows more methods to return successful chronologies, rather than including the hiatuses in the models. For each model, the median and the 2.5–97.5 % quantiles across the ensemble were extracted to define the central age estimate and its 95% uncertainty range at each depth. To derive the final chronology, all models that returned successful chronologies were included. At each depth, the composite chronology was calculated as the arithmetic mean of the selected models (equal weights):

Deleted: (Haslett and Parnell, 2008), Bacon (Blaauw and Christen, 2011; Blaauw et al., 2021), COPRA (Breitenbach et al., 2012), and StalAge (Scholz and Hoffmann, 2011).

Deleted: (Roesch and Rehfeld, 2020), which is provided as a supplement to Comas-Bru et al. (2020);

$$\mu_{final}(d) = \frac{1}{N}\sum^{N} M_i(d)$$

where $M_i(d)$ is the age of model i at depth d, and N is the number of selected models. The corresponding 95 % uncertainty was derived by combining (i) the between-model spread (standard error of model ages) and (ii) the mean within-model uncertainty (average 95 % half-widths) in quadrature:

$$\sigma_{final,95} = \sqrt{\sigma_{between}^2 + \overline{\sigma_{within}}^2}$$

Where geochemically defined annual cycles from Sr/Ca variations were identified, the resulting layer-count chronologies were treated as an independent constraint rather than being incorporated into the composite chronology. These were converted to absolute ages by anchoring the layer-count chronology either (i) to the year of stalagmite extraction, if continuous growth until collection can be assumed, or (ii) to the U-Th age with the smallest analytical uncertainty within the counted interval. For intervals in which seasonal variations were less pronounced or individual cycles were indistinct, a conservative uncertainty of ± 0.5 layers per 10 counted layers was assigned, reflecting the potential for missed or ambiguous cycles

3 Results

3.1 Speleothem Petrography

One XRD analysis of the bottom portion of stalagmite E1 verified the presence of aragonite, as initially suggested by its fan-like crystal texture and silky gloss (Figure S 2b). In contrast, all nine XRD measurements from different sections of stalagmite E0-C indicated the presence of pure calcite (Figure S 2a). Thin section analyses of stalagmites E0-B, E0-C, E1, E4 and E8 revealed only calcite phases. These primarily consisted of two fabrics: compact- and open-elongated calcite, with crystals exhibiting a length-to-width ratio greater than 6:1 (Frisia, 2015) (Figure S 3). Macroscopically, the compact elongated calcite phase appeared more translucent, while the open elongated fabric displayed a whitish appearance (Figure S 1). Growth interruptions (hiatuses) were macroscopically visible either as major flooding layers (Figure S 1) or as smaller detrital layers, typically near the tops of the stalagmites but occasionally occurring throughout their growth (Figure S 3). Under the microscope, these interruptions were characterized by clear rhombohedral crystal terminations and the presence of detrital minerals such as clay (Figure S 3). No evidence of aragonite-to-calcite recrystallization, such as preserved aragonite textures or "ghosts" of aragonite (Frisia et al., 2002; Perrin et al., 2014), was observed in any of the thin sections. Therefore, it is assumed

Commented [SN1]: Hier stimmt was mit der Formel nicht…die hochgestellte 2 ist verrutscht

Deleted: (Figure S 2b).

Deleted: (Figure S 2a).

Deleted: (Frisia, 2015) (Figure S 3).

Deleted: (Figure S 3).

Deleted: (Figure S 3).

Deleted: (Frisia et al., 2002; Perrin et al., 2014), that stalagmites E0-B, E0-C, E4, E8, and the upper portion of stalagmite E1 consist of primary calcite, predominantly in the form of compact or slightly open elongated fabrics.

3.2 Radiocarbon dating

A total of four ^{14}C measurements were performed on three different stalagmite tips (E0-C, E1, and E8), with one duplicate measurement taken from the E0-C sample (Table S 1). The measured ^{14}C activities ($a^{14}C_{meas}$) ranged from 97.54 ± 0.20 pmC to 94.95 ± 0.19 pmC. Assuming even only a minor contribution of "dead carbon" (<10%) to the carbonate in the stalagmite would result in $a^{14}C_{meas}$ values >100 pmC, which suggests modern growth (post-1950 AD) for the stalagmite tips.

3.3 $^{230}Th/U$ dating

$^{230}Th/U$ dating was performed on 157 samples from the Áaktun Kóopo' Cave speleothems (Table S 3). The uranium content of the analysed speleothems spans from 106 to 2237 ng g^{-1}. Measured $\delta^{234}U$ values time independently average 14 ± 8 ‰ which is close to secular radioactive equilibrium with minimal variation, mirroring the low activity ratios of the drip (Table S 3) as well as local ground water (Schorndorf et al., 2023). ^{232}Th concentrations are generally low with values <0.1 ng g^{-1}, resulting in ($^{230}Th/^{232}Th$) activity ratios >300, indicating minor residual initial Th influence. Overall, $^{230}Th/U$ dating suggests late Holocene speleothem growth for most studied stalagmites from Áaktun Kóopo' Cave, since most uncorrected ages cluster during the past c. 2.7 kyr (Table S 3). Notable exceptions are stalagmites E6 or E23-1 where uncorrected ages suggest deposition between 333 ± 13 to 264.1± 5.7 kyr and 74.90 ± 0.20 to 16.735 ± 0.061 kyr, respectively.

However, several samples show elevated ^{232}Th (up to 26.5 ng g^{-1}), young ages, lower uranium concentrations, or a combination of these factors. Consequently, measured $^{230}Th/U$ ages do not align stratigraphically, and many of the inversions are not resolved when using a bulk Earth detrital ($^{230}Th/^{232}Th$) activity ratio of ~0.8, typical for the upper continental crust (Taylor and Mclennan, 1985). Notably, the modern carbonate sample yielded an elevated ($^{230}Th/^{232}Th$) activity ratio of 6.57 ± 0.03, while ($^{230}Th/^{232}Th$) activity ratios in three drip water samples from the cave ranged from 1.659 ± 0.046 to 8.9 ± 1.0 (Table S 2), suggesting high levels of initial ^{230}Th in the system. Since using the drip water or modern carbonate ($^{230}Th/^{232}Th$) activity ratio for age correction does not yield satisfying results either, we infer that a more detailed inspection of the elevated initial ^{230}Th systematics is mandatory to obtain reliable chronologies.

Deleted: (Table S 1).

Deleted: speleothem sub-

Deleted: Kóopo

Deleted: (Table S 2).

Deleted: (Table S 2) as well as local ground water (Schorndorf et al., 2023).

Deleted: Àaktun Kóopo

Deleted: (Table S 2).

Deleted: (Taylor and Mclennan, 1985).

Deleted: (Table S 2),

3.4 Sr/Ca ratios

For stalagmites E1, E8, and E23-3, LA-ICP-MS analyses revealed pronounced oscillations in Sr/Ca ratios from 0.1 to 0.66 mg/g, permitting identification of strong geochemical cycles (Figure S 4). These cycles serve as a potential proxy for seasonal abundance changes of Sr relative to Ca and thus annual geochemical laminae (Warken et al., 2018; Huang et al., 2001). The interval between two successive Sr/Ca minima is here interpreted as representing one year. Annual cycles of strongly variable amplitude and distance were identified by plotting Sr/Ca ratios against the dft and manually counting the distance between successive Sr/Ca minima. The minima appeared as the best choice since those are sharper and more distinct than the broader maxima. This approach provides an independent means to refine age-depth models derived from ^{230}Th/U dating (Smith et al., 2009) and may ultimately allow for annual relative age precision of climate proxy data.

Deleted: (Figure S 4).

Deleted: (Warken et al., 2018; Huang et al., 2001).

Deleted: (Smith et al., 2009)

3.5 Stable isotope values

The stable isotopes of oxygen and carbon analyzed in stalagmites E0-C (Table S4), E1 (Table S5), and E23-3 (Table S6) yielded δ^{13}C values ranging between c. −7.9 ‰ and c. −12.4‰, while the range of δ^{18}O values is between c. −7.1‰ to c. −3.8 ‰. Notably, the lowest and highest δ^{13}C and δ^{18}O values in all three stalagmites are very similar, respectively.

4 Discussion

4.1 Determination of initial (^{230}Th/^{232}Th) ratios

^{230}Th/U dating of Áaktun Kóopo' Cave speleothems reveal a vast spread, including significant age inversions. Petrographic observations suggest no obvious recrystallization or diagenetic alteration; the stalagmites show well-preserved primary fabrics and display largely coherent U concentrations and δ^{234}U values along their growth axes. Therefore, we consider wide-spread post-depositional U remobilization to play a subordinate role for our dated material. There is, however, strong evidence for elevated initial ^{230}Th in the Áaktun Kóopo' cave system. Most age inversions are associated with elevated ^{232}Th concentrations and a relationship between (^{230}Th /^{238}U) and (^{232}Th /^{238}U) activity ratios, consistent with significant Th transport through the karst water, either associated to particles, colloids or chemical complexing agents (Ludwig, 2003). The resulting relationship follows a first order binary mixing, when activity ratios are plotted as Osmond type II isochrons (a). Modern carbonate and drip water samples yielded variable R02i of up to 8.9 ± 1.0, but even with these elevated ratios applied to correct for detrital Th contamination, many speleothem age inversions persist.

Deleted: Kóopo

Deleted: analyses exclude

Deleted: dissolution effects which could have affected

Deleted: quality of the ages.

Formatted: Font color: Black, English (US)

Formatted: Font color: Black, English (US)

Formatted: Font color: Black, English (US)

Deleted: Àaktun Kóopo

Formatted: Font color: Black, English (US)

Deleted: (Ludwig, 2003).

Deleted: (Figure 2a).

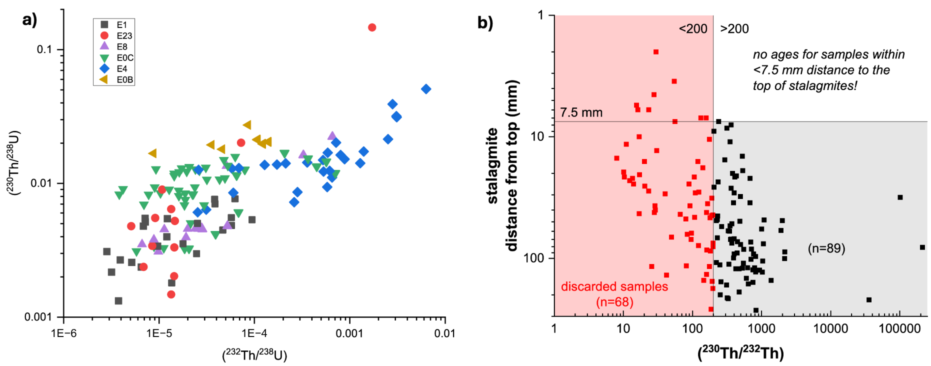

Figure 2. Activity ratios from various stalagmites in Áaktun Kóopo' Cave. a) Relationship between (^{230}Th/^{238}U) and (^{232}Th/^{238}U) activity ratios. The observed linear trend indicates significant detrital contamination. Different symbols and colors correspond to individual stalagmites. Both axes are plotted on a logarithmic scale. b) (^{230}Th/^{232}Th) activity ratios. Samples with (^{230}Th/^{232}Th) activity ratios <200 (n=68, red squares) were excluded from age-depth models due to significant initial Th contamination. Remaining samples (n=89, black squares) were included in age-depth models and further analysis. No samples with (^{230}Th/^{232}Th) ratios >200 were observed within 7.5 mm of the stalagmite tops, due to the young age of these carbonates and limited ^{230}Th ingrowth.

Consequently, higher R02i are necessary in cases to meet the stratigraphic constraint of increasing ages from top to bottom (Hellstrom, 2006). To estimate the range of R02i, different approaches are tested, including (i) isochrons and (ii) stratigraphic constraint. In addition, (iii) geochemical Sr/Ca cycles were used as annual layer counts to estimate relative age differences between Th/U ages and to independently test the other approaches (Domínguez-Villar et al., 2012; Nagra et al., 2017). Given the difficulty in accurately constraining R02i, all samples with (^{230}Th/^{232}Th) ratios <200 (n=68) were excluded from the age–depth modelling and from further chronological interpretation (b), because for such highly Th-contaminated samples the propagated age uncertainty is dominated by the initial Th correction and does not add meaningful information to the chronologies. This criterion also applies to all samples within 7.5 mm of the stalagmite tops, which are generally highly contaminated and have limited ^{230}Th ingrowth.

4.1.1 Comparison of different approaches

Dense sampling in some stalagmites allows for first-order linear two-endmember mixing regressions (Osmond type 1 – like 'isochrons'). In this study, such 'isochrons' are applied only to closely spaced, co-genetic subsamples and are interpreted as local, first-order estimates of R02i, similar to the approaches of Warken et al. (2020) or Stinnesbeck et al. (2020). The 'isochron' approach using ISOPLOT (Ludwig and Titterington, 1994; Ludwig, 2008;

Moved (insertion) [1]

Deleted: (Hellstrom, 2006).

Deleted: (Domínguez-Villar et al., 2012; Nagra et al., 2017). Given the difficulty in accurately constraining R02i, all samples with ratios <200 (n=68) were excluded from further discussion (Figure 2b), as they provide no meaningful chronological information due to the growing age uncertainty, when propagating the uncertainty of the correction model in the corrected ages. This criterion also applies to all samples within 7.5 mm of the stalagmite tops, as these were generally highly contaminated with limited ^{230}Th ingrowth.

Deleted: Dense sampling in some stalagmites allows for linear two-endmember mixing regressions (Osmond type 1 isochrons) using ISOPLOT (Ludwig and Titterington, 1994; Ludwig, 2008; Vermeesch, 2018), similar to the approaches of Warken et al. (2020) or Stinnesbeck et al. (2020). The isochron approach produced five successful isochrons

Vermeesch, 2018), produced five successful ‘isochrons’ from three stalagmites (E0-C, E4, E8), which yielded R02i ranging from 6.4 ± 2.4 to as large as 19 ± 10 (Figure S 5, Supplementary material S1.1). To apply stratigraphic constraints (e.g., Roy-Barman and Pons-Branchu, 2016; Hellstrom, 2006), we used samples with no detectable ^{232}Th as stratigraphic anchors, as their ages are unaffected by initial Th contamination and because those provide a steady growth pattern. In addition, we adopt the assumption that stalagmite tops with elevated ^{232}Th are younger than uncorrected ages below them, but older than the year of collection. From Stalagmite E0-C, 34 of 51 samples could be placed in stratigraphic order using individual R02i ranging from 11.5 to 49 (Figure 4b). In contrast, for other stalagmites, such as E0-B or E1, only single ages can be corrected using a stratigraphically derived ratio. Lastly, we exploit distinct cyclic variations in Sr/Ca ratios from LA-ICP-MS measurements (Figure S 4) to estimate relative age differences between ^{230}Th/U measurements, thus allowing to correct the ages and estimate R02i (James et al., 2025). For example, in stalagmite E23-3, in total 331 ± 17 Sr/Ca minima are counted from 0 to 84 mm dft. Assuming the topmost layer to correspond to 2022 AD (the year of collection), the R02i is estimated to 26 ± 7 to align the ^{230}Th/U ages with the layer-counted age model presuming Sr/Ca seasonal cycles within uncertainties of both methods. In contrast, in the upper section of stalagmite E8 (8.5–26 mm dft), ages could only be corrected with individual R02i ranging from 7 to 35.5 to match the Sr/Ca-based age-depth model. Overall, to correct stalagmite ages with the different approaches, R02i ranging from 4 to 68 are found (Table S 3). Notably, only one sample from stalagmite E1 requires a ratio as high as 68, while most other samples need ratios between 30 and 50 or lower. R02i <20 are only found for three ages via stratigraphic constraint and for nine ages by isochrons. Therefore, samples without specific estimates, are corrected by using the mean ratio of 35.5 ± 32.5 to account for the full range of possible initial Th corrections (Table S 3). Taken together, these independent approaches indicate that strongly elevated initial Th activity ratios are plausible and necessary at least in parts of the record to obtain stratigraphically consistent age models, even though the exact numerical values of R02i for individual, highly contaminated samples remain poorly constrained.

4.1.2 Elevated and variable initial (^{230}Th/^{232}Th) ratios in Áaktun Kóopo’ cave

Overall, our analysis shows, that significantly elevated and strongly variable R02i (up to 68) are required to correct stalagmite ages from Áaktun Kóopo’ Cave for initial Th contamination (Table S 3). These values greatly exceed the commonly assumed upper continental crust ratio of (^{230}Th/^{232}Th) ~ 0.8 (Taylor and Mclennan, 1985). However, they align with findings from other tropical sites (e.g., the Caribbean and Southeast Asia) where similarly high ratios have been reported (e.g., Beck et al., 2001; Richards and Dorale, 2003; Partin et al., 2007; Carolin et al., 2013; Arienzo et al., 2015; Hoffmann et al., 2010; Moseley et al., 2015; Ridley et al., 2015; Stinnesbeck et al.,

Deleted: (Figure S 5, Supplementary material S1.1). To apply stratigraphic constraints (e.g., Roy-Barman and Pons-Branchu, 2016; Hellstrom, 2006),

Deleted: (Figure 4b).

Deleted: (Figure S 4)

Deleted: (James et al., 2025).

Deleted: (Table S 2).

Deleted: (Table S 2).

Moved up [1]: **a) Relationship between (^{230}Th/^{238}U) and (^{232}Th/^{238}U) activity ratios. The observed linear trend indicates significant detrital contamination. Different symbols and colors correspond to individual stalagmites. Both axes are plotted on a logarithmic scale. b) (^{230}Th/^{232}Th) activity ratios. Samples with (^{230}Th/^{232}Th) activity ratios <200 (n=68, red squares) were excluded from age-depth models due to significant initial Th contamination. Remaining samples (n=89, black squares) were included in age-depth models and further analysis. No samples with (^{230}Th/^{232}Th) ratios >200 were observed within 7.5 mm of the stalagmite tops, due to the young age of these carbonates and limited ^{230}Th ingrowth.**

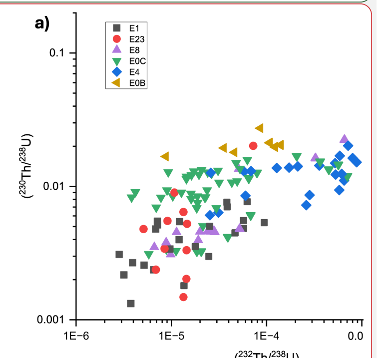

Deleted:
Figure 2. Activity ratios from various stalagmites in Áaktun Kóopo Cave.

Deleted: Àaktun Kóopo

Deleted: Kóopo

Deleted: (Table S 2).

Deleted: (Taylor and Mclennan, 1985).

Deleted: (e.g., Beck et al., 2001; Richards and Dorale, 2003; Partin et al., 2007; Carolin et al., 2013; Arienzo et al., 2015; Hoffmann et al., 2010; Moseley et al., 2015; Ridley et al., 2015; Stinnesbeck et al., 2020; Vieten et al., 2024a; Vieten et al., 2024b; Steidle et al., 2021; Warken et al., 2021; James et al., 2025).

2020; Vieten et al., 2024a; Vieten et al., 2024b; Steidle et al., 2021; Warken et al., 2021; James et al., 2025). Furthermore, our measurements demonstrate that this pronounced variability is largely unsystematic, occurring not only spatially across different stalagmites within the same cave, similar to findings in Larga Cave, Puerto Rico (Vieten et al., 2024b; Warken et al., 2020; Kerber et al., 2025), but also temporally within individual stalagmites. The vast spread of R02i may be attributed to the varying contributions of multiple Th reservoirs within the karst and epikarst environments (Li et al., 2022; Wortham et al., 2022; Huang et al., 2024). Rather than a single source, Th can be transported as a complex mixture of detrital particles (e.g., clay minerals, aluminosilicates, iron oxyhydroxides), colloidal phases, and organic complexes (Morton et al., 2001; Nascimento et al., 2019; Reiller et al., 2002; Richards and Dorale, 2003). In tropical environments with relatively young reef limestones as host rock, such as the YP, the rapid dissolution and varying mobilization of these different organic and inorganic fractions lead to highly variable initial Th isotopic signatures. This dynamic reflects the observations from various aquatic systems, where the (^{230}Th/^{232}Th) activity ratio has been shown to vary by orders of magnitude (Scott, 1968; Hubert et al., 2006; Hirose et al., 2012; Töchterle et al., 2022; Moore and Sackett, 1964; Moore, 1981). Consequently, highly elevated and time-variable R02i should be regarded as the rule rather than the exception in such settings, fundamentally questioning the applicability of a static 'bulk earth' value for age corrections. In such settings, initial Th corrections are best treated as approximations with explicit uncertainty, constrained where possible by multiple, independent estimates of R02i.

Because we do not find any systematic behaviour that would allow to predict R02i a priori, developing accurate age models remains challenging. Initial Th corrections are particularly critical for younger speleothems (less than a few thousand years old), as even small uncertainties in the R02i can significantly influence age models. While monitoring ZAC and drip water provides a baseline for estimating R02i (Wortham et al., 2022; Li et al., 2022), this approach often fails to capture long-term temporal variability. In Áaktun Kóopo' Cave, for example, the (^{230}Th/^{232}Th) activity ratio from supposedly modern carbonate and drip-water samples remain far below the highest estimated ratios (up to 68) required to align stalagmite ages with the sedimentary sequence. Therefore, to reduce the uncertainty of corrected ages in similar karst settings, it is strongly recommended to employ a combination of independent validation methods. Integrating ^{230}Th/U dating with radiocarbon or other radiometric dating methods (Akers et al., 2019; Huang et al., 2024; Sengupta et al., 2025) or annual layer counting (e.g., Warken et al., 2025; Domínguez-Villar et al., 2012; James et al., 2025; Faraji et al., 2021; Nagra et al., 2017) provides a more robust framework to constrain these erratic detrital inputs and secure reliable chronologies.

Deleted: (Vieten et al., 2024b; Warken et al., 2020; Kerber et al., 2025) ,

Deleted: (Li et al., 2022; Wortham et al., 2022; Huang et al., 2024).

Deleted: (Morton et al., 2001; Nascimento et al., 2019; Reiller et al., 2002; Richards and Dorale, 2003).

Deleted: (Scott, 1968; Hubert et al., 2006; Hirose et al., 2012; Töchterle et al., 2022; Moore and Sackett, 1964; Moore, 1981).

Deleted: , even assuming simple binary (linear) mixing.

Deleted: (Wortham et al., 2022; Li et al., 2022),

Deleted: Kóopo

Deleted: (Akers et al., 2019; Huang et al., 2024; Sengupta et al., 2025) or annual layer counting (e.g., Warken et al., 2025; Domínguez-Villar et al., 2012; James et al., 2025; Faraji et al., 2021; Nagra et al., 2017)

4.2 The Áaktun Kóopo' Chronology

The finally corrected ages of speleothems from Áaktun Kóopo' Cave range from as old as 353 ± 7 kyr to as young as 0.13 ± 0.015 kyr (Table S 3). Five older samples indicate speleothem growth during earlier glacial and interglacial periods, but most samples (84 out of 89) are younger than 3 kyr (Figure 3). Even though most ^{230}Th/U samples with low (^{230}Th/^{232}Th) activity ratios <200 were rejected, radiocarbon measurements on speleothem tops (E1, E0-C, E8) as well as seasonal Sr/Ca chronologies (E1, E8, E23-3) suggest carbonate deposition within the last 130 years, likely continuing up to the present (Supplementary material S1.1). Overall, the stalagmites from Áaktun Kóopo' Cave provide a robust basis for paleoclimatic and paleoenvironmental reconstructions over the late Holocene.

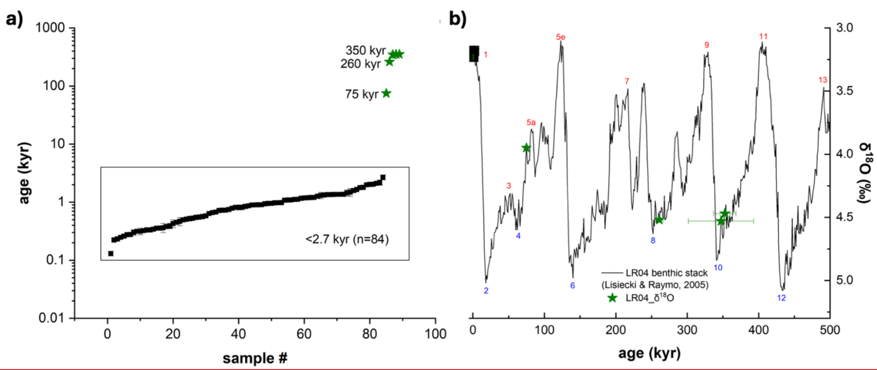

Figure 3 a) Distribution of speleothem samples according to their corrected ages on a logarithmic scale. Most samples are younger than 2.7 kyr, with some carbonate deposition at~75 kyr, 260 kyr, and 350 kyr. (b) ^{230}Th/U ages plotted against the LR04 benthic δ^{18}O stack (Lisiecki and Raymo, 2005), highlighting deposition during earlier glacial and interglacial periods, with marine isotope stages shown in blue and red.

4.2.1 Late Holocene speleothem growth history

Figure 4 shows the individual age-depth models constructed for stalagmites E0-B, E0-C, E1, E4, E8, and E23-3, as described in detail in the Methods section and Supplementary material S1.1. Although some of the analysed stalagmites exhibit decade-long growth interruptions, their chronologies overlap and suggest continuous carbonate deposition in Áaktun Kóopo' Cave over the last 2.7 kyr with mean growth rates of 200–300 µm a^{-1} (Figure 5).

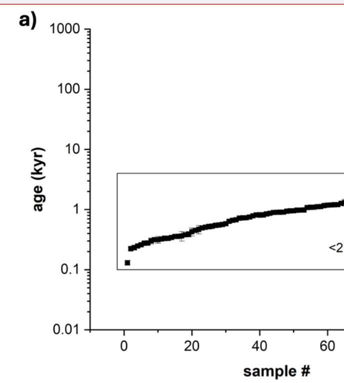

Deleted: Figure 3

Deleted: (Lisiecki and Raymo, 2005),

Deleted: <#>The Àaktun Kóopo Chronology
The finally corrected ages of speleothems from Àaktun Kóopo Cave range from as old as 353 ± 7 kyr to as young as 0.13 ± 0.015 kyr (Table S 2). Five older samples indicate speleothem growth during earlier glacial and interglacial periods, but most samples (84 out of 89) are younger than 3 kyr (Figure 3). Even though most ^{230}Th/U samples with low (^{230}Th/^{232}Th) activity ratios <200 were rejected, radiocarbon measurements on speleothem tops (E1, E0-C, E8) as well as seasonal Sr/Ca chronologies (E1, E8, E23-3) suggest carbonate deposition within the last 130 years, likely continuing up to the present (Supplementary material S1.1). Overall, the stalagmites from Àaktun Kóopo Cave provide a robust basis for paleoclimatic and paleoenvironmental reconstructions over the late Holocene.

Deleted: Figure 4

Deleted: S1.1.

Deleted: Àaktun Kóopo

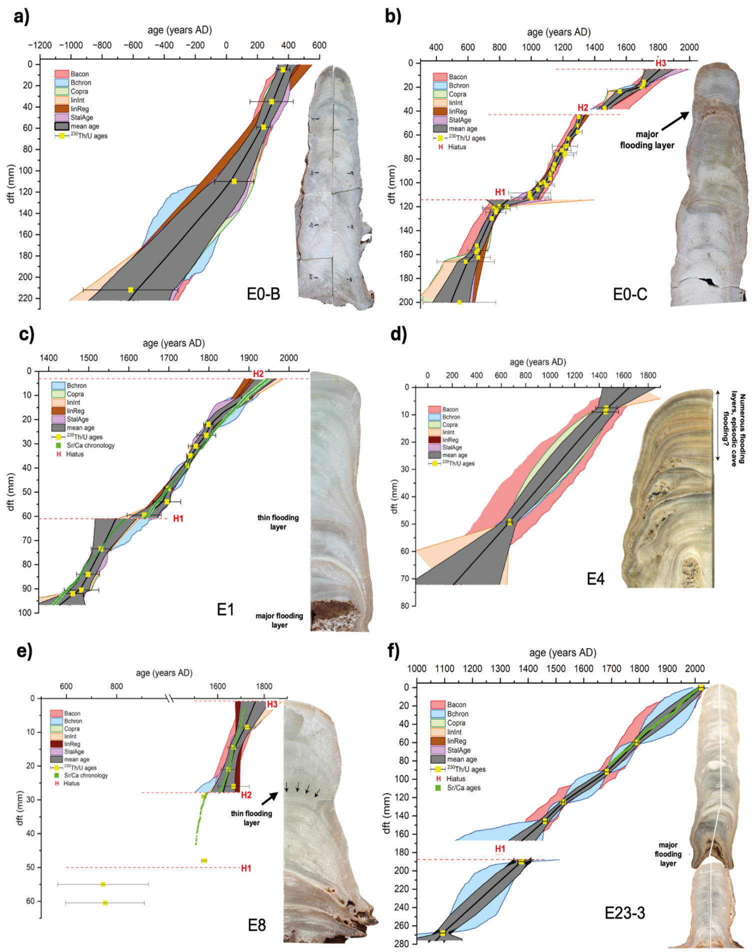

Figure 4 Age-depth models for Áaktun Kóopo' Cave stalagmites E0-B (a), E0-C (b), E1 (c), E4 (d), E8 (e) and E23-3 (f), generated using Bacon, Bchron, Copra, linInt, linReg, and StalAge, respectively. The final composite age-depth model is shown in black with its corresponding 95 % uncertainty band in grey, representing the arithmetic mean of the six model chronologies (equal weights). The ^{230}Th/U ages used in the models are indicated along with identified growth hiatuses and major flooding layers (E0-C, E1, E4,

Moved (insertion) [2]

E8, E23-3). A scan of each stalagmite is shown on the right of each plot. Speleothem scans are at the same vertical scale as the y-axis (dft) values.

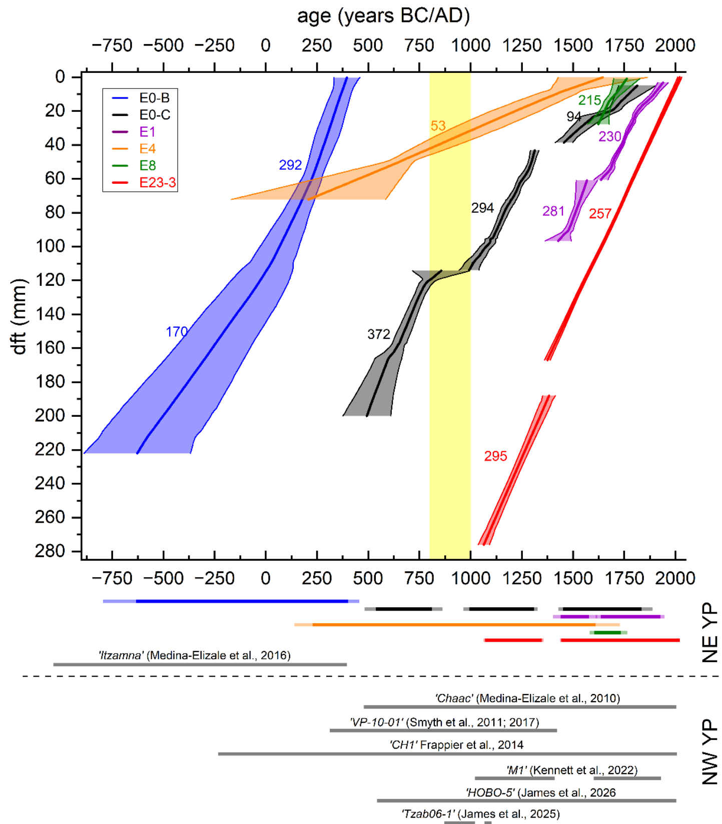

Figure 5 Mean age-depth models for stalagmites E0-B, E0-C, E1, E4, E8, and E23-3 from Áaktun Kóopo' Cave. Numbers indicate the average growth rates (in μm a^{-1}) during different growth periods. The coloured horizontal bars at the bottom illustrate the overlapping growth periods of the stalagmites over the last 2.7 kyr, highlighting intervals of simultaneous growth across multiple stalagmites. Lighter shades within the bars reflect the associated age uncertainties. Grey bars indicate periods covered by other published stalagmite records from the northern Yucatán Peninsula (YP). Notably, while most records are from the northwestern YP (Kennett et al., 2022; Medina-Elizalde et al., 2010; James et al., 2025; Frappier et al., 2014; Medina-Elizalde et al., 2016a; James

Formatted: Font color: Text 1

Moved (insertion) [3]

Deleted: (Figure 5).

et al., 2026), there is presently a marked absence of stalagmite proxy records from the northeastern YP for the last 1600 years, with only one record covering an earlier period between 1037 BC and 397 AD (Medina-Elizalde et al., 2016b).

While E0-B covers the oldest growth period (633 ± 161 BC to 403 ± 54 AD, Figure 4a), the growth of its "sibling" E0-C can be divided into three periods separated by hiatuses: (1) 538 ± 56 AD to 811 ± 52 AD; (2) 994 ± 29 AD to 1311 ± 15 AD; and (3) 1451 ± 22 AD to 1835 ± 53 AD (Figure 4b). The last millennium is also covered by several speleothems (Figure 5), with E1 growing from 1440 ± 39 AD to 1577 ± 42 AD and between1635 ± 24 AD to 1926 ± 20 AD (Figure 4c). Stalagmite E4 grew from approximately 228 ± 88 AD to 1611 ± 118 AD, even though high initial Th contamination led to the rejection of 24 of 28 samples (Figure 4d). Similar challenges arose for the chronology of E8, where growth could be tightly constrained for the latest part (1605 ± 24 AD to 1733 ± 33 AD, Figure 4e). Lastly, the growth history of stalagmite E23-3 can be divided into two periods, with the older part covering 1070 ± 7 AD to 1347 ± 9 AD, and the upper part spanning 1441 ± 5 AD to the year of collection in 2022 AD (Figure 4f).

Figure 5 compares the late Holocene Áaktun Kóopo' Cave growth history with periods covered by other published stalagmite records from the northern YP. Notably, while most records are from the northwestern or central YP (Kennett et al., 2022; Medina-Elizalde et al., 2010; James et al., 2025; Frappier et al., 2014; Medina-Elizalde et al., 2016a; James et al., 2026) there is a marked absence of stalagmite proxy records from the northeastern YP for the last 1600 years, with only one record covering an earlier period between 1037 BC and 397 AD (Medina-Elizalde et al., 2016b). Given the known regional heterogeneity in past hydroclimate reconstructions and projected trends, the Áaktun Kóopo' Cave record thus fills an important gap in the region (Douglas et al., 2016; Obrist-Farner et al., 2023; Steinman et al., 2022).

4.2.2 Origin of flooding layers and other growth interruptions

While precise ^{230}Th/U dating establishes the absolute chronological framework for these stalagmites, the numerous growth interruptions (hiatuses) observed throughout their growth histories provide an additional, independent means to cross-validate these highly corrected age models. Detectable either as macroscopic millimeter- to centimeter-thick mud layers or via microscopic thin-section analysis, these hiatuses indicate discrete environmental events that simultaneously affected multiple stalagmites within the cave (Figure 4).

One prominent flooding layer (~ 1 cm thick) appears in stalagmites E0-C, E1, and E23-3, which were all collected from the same cave area at a similar elevation. This layer likely represents a single event around 1400 AD. By comparing the ^{230}Th/U dates across the stalagmites, the timing can be constrained between ~1350 AD and ~1430 AD. The latest confirmed carbonate precipitation prior to the event is recorded by stalagmite E23-3, which yielded

Deleted: Figure 4a

Deleted: (Figure 4b).

Deleted: (Figure 5),

Deleted: (Figure 4c

Deleted: (Figure 4d).

Deleted: Figure 4e).

Deleted: (Figure 4f

Deleted: Figure 5

Deleted: Àaktun Kóopo

Deleted: YP (Kennett et al., 2022; Medina-Elizalde et al., 2010; James et al., 2025; Frappier et al., 2014; Medina-Elizalde et al., 2016a; James, 2024)

Deleted: (Medina-Elizalde et al., 2016b).

Deleted: Àaktun Kóopo

Deleted: (Douglas et al., 2016; Obrist-Farner et al., 2023; Steinman et al., 2022).

Deleted: ¶ ... [1]

Formatted: Font color: Text 1

Deleted: (Figure 4).

Deleted: representing

a ^{230}Th/U age of 1347 ± 9 AD. Following the flood, stalagmite E1's growth resumed directly upon the detrital substrate at 1428 ± 40 AD. The sediment sequence of Sullivan et al. (2025) from Cenote Muyil c. 80 km south of Áaktun Kóopo' cave recorded a period of intense hurricane activity between 1285 to 1420 AD in the area, which suggests that a major storm event may have caused the flooding of the cave during that time. Indeed, historical records report a major hurricane ("hurricane of the four winds") that impacted the area in 1464 AD (Sullivan et al., 2025; Masson and Lope, 2014), which is however not fully consistent with our date, suggesting another extreme event caused the mud layer in Áaktun Kóopo' Cave. Thinner layers (0.5–1 mm) in stalagmites E1 and E8, which also stems from the same area in the cave, correspond to a shorter interruption that may have lasted only months to years. The timing can be precisely dated to 1624 ± 24 AD within the continuous age models of stalagmite E8, perfectly aligning with a brief hiatus observed in E1 between ~1590 AD and ~1630 AD. In addition to detecting and dating single extreme events that may have impacted the environment and the people living in the area, such markers could serve as key stratigraphic tie-points, analogous to ash layers in marine sediments or ice cores, for anchoring proxy records and refining chronologies (Warken et al., 2025). Fine laminations (alternating carbonate and mud/clay) of stalagmite E4 even suggest recurrent flooding in the part of the cave near the entrance. While the current efforts limit a more precise dating of the individual layers, future studies could deliver a more detailed history of local flooding (Frappier et al., 2014; Denniston and Luetscher, 2017; Gonzalez-Lemos et al., 2015). Although many hiatuses coincide with clear flooding layers, other interruptions could reflect periods of reduced effective moisture due to reduced precipitation and/or enhanced evapotranspiration, or other processes. For example, the special morphology of Áaktun Kóopo' Cave (Figure 1b) makes it conceivable, that a sufficiently high-water table sealed cave ventilation in some sections of the cave, leading to elevated cave CO_2. Because Áaktun Kóopo' Cave was visited and modified by the Maya, at least during the Late Preclassic (–250 to 300 AD) and Early Classic (300–600 AD) periods (Gómez, 2020), human influences speleothem development can also not be ruled out. Deforestation and agricultural practices above the cave, for example, may have altered soil cover and infiltration pathways, thereby influenced recharge and ultimately affected speleothem formation. Likewise, cave use and ritual activities might have modified the cave's microclimate (e.g., CO_2 concentration, humidity, temperature) or sedimentological conditions in ways that impacted speleothem formation, although such influences remain speculative. Disentangling natural hydrological variability from potential anthropogenic influences on speleothem formation remains a challenging task and requires a comprehensive multi-proxy approach that explores all aspects of speleothem formation, aimed at separating climatic from human-induced signals.

Deleted: The sediment sequence of Sullivan et al. (2025) from Cenote Muyil c. 80 km south of Àaktun Kóopo

Deleted: (Sullivan et al., 2025; Masson and Lope, 2014),

Deleted: Àaktun Kóopo

Deleted: (Warken et al., 2025).

Deleted: (Frappier et al., 2014; Denniston and Luetscher, 2017; Gonzalez-Lemos et al., 2015).

Deleted: Àaktun Kóopo Cave (Figure 1c

Deleted: Kóopo

Deleted: (Gómez, 2020), human influences on

4.3 Age model uncertainties and algorithm comparison

4.3.1 Evaluation of the chronologies

Evaluating the diverse performance of the applied age-depth modelling algorithms reinforces the necessity of our ensemble approach. Consistent with Comas-Bru et al. (2020), no single algorithm universally outperformed the others across all speleothems, as the underlying statistical assumptions of each model respond differently to variations in growth rates and dating resolution. This methodological variability becomes especially evident when comparing the models against independent layer-counting chronologies: while the Bacon model closely matched the visual layer counts for stalagmite E23-3, Bchron and linear interpolation provided the tightest fits for different sections of E8. Furthermore, the individual algorithms diverged significantly in their chronological treatment of extreme events, such as the major flooding layers and resulting hiatuses. The chosen algorithm significantly affects not only the estimated duration of an event, but also its absolute timing. For instance, the first hiatus in stalagmite E0-C (at 40 mm depth) has an estimated duration ranging from 96 (+58/–55) years (linear regression) to 174 (+85/–88) years (Bacon). Consequently, the absolute timing of the growth interruption shifts across models: Bchron dates the onset of the hiatus to 1302 (+25/–4) AD, whereas linear regression places it almost four decades later at 1341 (+26/–25) AD. Constructing a composite "mean" age model is therefore justified, relying on any single algorithm risks either artificially over-smoothing or over-estimating the timing and duration of discrete environmental events.

Deleted: Consistent with Comas-Bru et al. (2020),

4.3.2 Validation of age models via stable isotope comparison

To further assess the robustness of our age models, we compared the independent stable oxygen ($\delta^{18}O$) and carbon ($\delta^{13}C$) isotope records of stalagmites E0-C, E1, and E23-3 for their overlapping growth periods. The chronology of stalagmite E23-3 is considered the most reliable anchor for the last 400 years. It is constrained by continuous counting of seasonal Sr/Ca cycles and anchored to the year of extraction (2022 AD), resulting in a cumulative counting error of ± 17 year at 1691 AD. When plotting the stable isotope time series using the individually established $^{230}Th/U$ age-depth models, the records already show an apparent coherence in both $\delta^{18}O$ and $\delta^{13}C$ values over the past 600 years (Figure 6a). Despite being fed by different drip sites within the same cave chamber, the stalagmites capture nearly identical multi-decadal to centennial-scale geochemical patterns. This coherence suggests that the individual proxy records are driven by a common external forcing, such as regional hydroclimate variability affecting cave recharge and prior calcite precipitation (PCP), rather than localized kinetic or drip-specific effects (Skiba and Fohlmeister, 2023; Baker et al., 2019; Treble et al., 2022). However, the individual chronologies appear to be shifted relative to each other, reflected in the weak or insignificant correlations between the stable

Deleted: (Figure 6a).

Deleted: (Skiba and Fohlmeister, 2023; Baker et al., 2019; Treble et al., 2022).

isotope records. For example, the largest significant coefficient of 0.2 ($p<0.01$) occurs for the $\delta^{18}O$ records of E23-3 and E1. To precisely align the time series, a wiggle-matching procedure was performed using QAnalySeries software (Kotov and Pälike, 2018; Pälike, 2024), similar to the approach of Huang et al. (2024). The upper section of the E1 $\delta^{18}O$ record (3–61 mm dft) was tuned to the E23-3 reference record using 10 tie points, while the upper section of E0-C (5–38.6 mm dft) was subsequently matched to E1 using 11 tie points. As a result, the maximum shift of E1 with respect to E23-3 is c. 20 years directly after the thin flooding layer around 1620 AD, while the other sections are only corrected by <7 years. The chronology of E0-C requires larger shifts by around 25-70 years with respect to E23-3. Overall, the resulting adjustments required to align these independent records fall entirely within the calculated 95% uncertainty ranges of their respective $^{230}Th/U$ age-depth models (Figure 6b). After the synchronization, the $\delta^{18}O$ ($\delta^{13}C$) record of E1 exhibits a correlation of 0.62 (0.61) with E23-3 and 0.42 (0.51) with E0-C ($p<0.01$, respectively), demonstrating a striking coherence between the stalagmite records. The successful replication of stable isotope patterns across three distinct stalagmites and the tuning required to synchronize them strongly validate our geochronological approach. It demonstrates that the strategies used to correct for elevated and highly variable initial ^{230}Th contamination, specifically the integration of $^{230}Th/U$ dating with seasonal trace-element layer counting and stratigraphic constraints, yield robust and accurate chronologies suitable for high-resolution paleoclimate reconstruction on the YP.

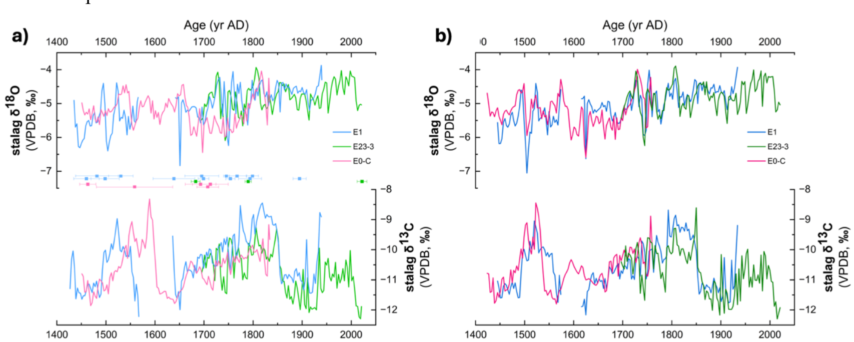

Figure 6. Stable oxygen ($\delta^{18}O$) and carbon ($\delta^{13}C$) records of speleothems E1, E23-3 and E0-C for the period from 1400 to 2022 AD binned to three-year averages, respectively. In panel a), the records are plotted on their original age scale. In addition, the respective $^{230}Th/U$ ages are shown to indicate the uncertainty in the respective chronologies. Panel b) shows the $\delta^{18}O$ and $\delta^{13}C$ records on the composite timescales, demonstrating a remarkable agreement. Note that the overlap between E23-3 and E0-C is too short to calculate meaningful correlation coefficients.

Deleted: (Kotov and Pälike, 2018; Pälike), similar to the approach of Huang et al. (2024).

Moved down [4]: **Stable oxygen ($\delta^{18}O$) and carbon ($\delta^{13}C$) records of speleothems E1, E23-3 and E0-C for the period from 1400 to 2022 AD binned to three-year averages, respectively. In panel a), the records are plotted on their original age scale. In addition, the respective $^{230}Th/U$ ages are shown to indicate the uncertainty in the respective chronologies. Panel b) shows the $\delta^{18}O$ and $\delta^{13}C$ records on the composite timescales, demonstrating a remarkable agreement. Note that the overlap between E23-3 and E0-C is too short to calculate meaningful correlation coefficients.**

Deleted: (Figure 6b).

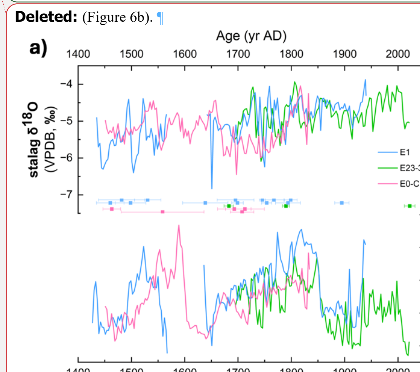

Figure 6.

Moved (insertion) [4]

5 Conclusions

Reconstructing reliable paleoclimate records from speleothems requires precise chronologies, which are frequently compromised by variations of initial Th contamination through time in tropical karst environments. While low-Th speleothems with simple initial ratios would be preferable, such material is not always available at sites of high archaeological and paleoclimate interest, so working with variable Th-contaminated samples is sometimes unavoidable if any chronological information is to be obtained.

In this study, we generated robust age-depth models for multiple late Holocene stalagmites from Áaktun Kóopo' Cave, Yucatán, spanning the past 2.7 kyr. ^{230}Th/U dating revealed significant and highly variable initial Th contamination, with initial (^{230}Th/^{232}Th) activity ratios ranging unpredictably between 4 and 68. These values vastly exceed standard bulk earth corrections and demonstrate substantial spatial and temporal variability within the cave system. This indicates that static initial Th corrections are insufficient in such settings, and modern drip-water or ZAC monitoring may not capture the full range of initial ^{230}Th variability. Considering the vast number of other studies suggesting high and variable R02i ratios in (sub-)tropical caves, we expect that this could be also a characteristic of other, comparable cave systems. To determine R02i and resolve chronological inversions, we successfully employed a multi-method approach, combining isochron methods, stratigraphic constraints, and relative seasonal layer counting (Sr/Ca). We note, however, that R02i constrained by local 'isochrons' assuming binary-mixing relationships should be regarded as helpful local, first-order approximations to delimit the plausible range of initial Th activity ratios, rather than as exact descriptions of the underlying Th sources.

Furthermore, our analysis highlights that different age-depth algorithms (e.g., Bacon, Bchron, copRa, StalAge, Linear Regression) may yield different results, particularly when handling growth discontinuities. This can affect both the estimated duration and the absolute timing of hiatus or other events; thus, the integration of multiple constraints can yield more reliable chronologies.

Ultimately, the improved chronologies and accompanying coherent proxy records from Áaktun Kóopo' Cave now provide a robust foundational framework for future high-resolution reconstructions of hydroclimate and environmental change throughout the timeline of Maya cultural evolution on the YP, e.g., how long-term trends and short-term extreme events, such as the identified flood layers, are related and how they may have intersected with phases of cultural change.

Deleted: highly

Deleted: Koopo

Deleted: To

Deleted: Our

Deleted: this comprehensive chronological approach tackles

Deleted: complexities of initial Th in

Deleted: Kóopo

Deleted: on the YP, providing

Deleted: proxy

Deleted: . The resulting stable isotope climate proxy records show outstanding coherence for the past 600 years.

6 Data availability

All data is available in the supplementary material.

7 Supplement link

The link to the supplement will be included by Copernicus, if applicable.

8 Author contributions

NS: Conceptualization, Formal analysis, Investigation, Validation, Visualization, Writing (original draft preparation), Writing (review and editing)

SW: Conceptualization, Formal analysis, Funding acquisition, Investigation, Supervision, Visualization, Writing (review and editing)

RE: Data curation, Formal analysis, Methodology

ASM, JAO, FTP, CE, MJG: Resources

Deleted: ASM: Investigation, Formal analysis, Data curation

FK: Methodology, Resources, Data curation

DH: Formal analysis, Funding acquisition, Data curation

WS: Funding acquisition, Resources, Supervision

NF: Conceptualization, Funding acquisition, Investigation, Methodology, Resources, Supervision, Writing (review and editing)

9 Competing interests

A coauthor (Norbert Frank) is editor of Geochronology.

10 Disclaimer

Will be added by copernicus

Deleted: Copernicus.

11 Acknowledgements

We thank Julia Becker for helping with sample collection, and Antonia Wantzen and Alexander Slawik for supporting the sample preparation. We acknowledge support for stable isotope analysis by Stefan Rheinberger, Bernd Knape, Markus Greule, Alexa Fischer and Johannes Thommes. Steffen Therre and Ronny Friedrich are thanked for their help with ^{14}C sample preparation and analysis, and Ilse Glass for XRD analysis.

Lastly, we dedicate this work to René Eichstädter, who passed away in 2025 after a long and very serious illness. René supported our team every day for more than 12 years with great enthusiasm and knowledge. His expertise in the mass spectrometry laboratory was invaluable, and he was a fantastic colleague, especially when we were doing field work. His commitment to his work was always very important to him and he would have loved to come back. We wish him a peaceful journey.

12 Financial support

This research has been supported by the Deutsche Forschungsgemeinschaft (grant nos. 247825108, 256561558, 497323584, and 512385350).

13 Review statement

The review statement will be added by Copernicus Publications listing the handling editor as well as all contributing referees according to their status anonymous or identified.

14 References

Akers, P. D., Brook, G. A., Railsback, L. B., Liang, F. Y., Iannone, G., Webster, J. W., Reeder, P. P., Cheng, H., and Edwards, R. L.: An extended and higher-resolution record of climate and land use from stalagmite MC01 from Macal Chasm, Belize, revealing connections between major dry events, overall climate variability, and Maya sociopolitical changes, Palaeogeography Palaeoclimatology Palaeoecology, 459, 268-288, 10.1016/j.palaeo.2016.07.007, 2016.

Akers, P. D., Brook, G. A., Railsback, L. B., Cherkinksy, A., Liang, F., Ebert, C. E., Hoggarth, J. A., Awe, J. J., Cheng, H., and Edwards, R. L.: Integrating U-Th, 14C, and 210Pb methods to produce a chronologically reliable isotope record for the Belize River Valley Maya from a low-uranium stalagmite, The Holocene, 29, 1234-1248, 10.1177/0959683619838047, 2019.

Arienzo, M. M., Swart, P. K., Pourmand, A., Broad, K., Clement, A. C., Murphy, L. N., Vonhof, H. B., and Kakuk, B.: Bahamian speleothem reveals temperature decrease associated with Heinrich stadials, Earth and Planetary Science Letters, 430, 377-386, 10.1016/j.epsl.2015.08.035, 2015.

Baker, A., Hartmann, A., Duan, W., Hankin, S., Comas-Bru, L., Cuthbert, M. O., Treble, P. C., Banner, J., Genty, D., and Baldini, L. M.: Global analysis reveals climatic controls on the oxygen isotope composition of cave drip water, Nature Communications, 10, 2984, 2019.

Deleted:

Formatted: Not Highlight

Deleted: Akers, P. D., Brook, G. A., Railsback, L. B., Liang, F. Y., Iannone, G., Webster, J. W., Reeder, P. P., Cheng, H., and Edwards, R. L.: An extended and higher-resolution record of climate and land use from stalagmite MC01 from Macal Chasm, Belize, revealing connections between major dry events, overall climate variability, and Maya sociopolitical changes, Palaeogeography Palaeoclimatology Palaeoecology, 459, 268-288, 10.1016/j.palaeo.2016.07.007, 2016.¶
Akers, P. D., Brook, G. A., Railsback, L. B., Cherkinksy, A., Liang, F., Ebert, C. E., Hoggarth, J. A., Awe, J. J., Cheng, H., and Edwards, R. L.: Integrating U-Th, 14C, and 210Pb methods to produce a chronologically reliable isotope record for the Belize River Valley Maya from a low-uranium stalagmite, The Holocene, 29, 1234-1248, 10.1177/0959683619838047, 2019.¶
Arienzo, M. M., Swart, P. K., Pourmand, A., Broad, K., Clement, A. C., Murphy, L. N., Vonhof, H. B., and Kakuk, B.: Bahamian speleothem reveals temperature decrease associated with Heinrich stadials, Earth and Planetary Science Letters, 430, 377-386, 10.1016/j.epsl.2015.08.035, 2015.¶
Baker, A., Hartmann, A., Duan, W., Hankin, S., Comas-Bru, L., Cuthbert, M. O., Treble, P. C., Banner, J., Genty, D., and Baldini, L. M.: Global analysis reveals climatic controls on the oxygen isotope composition of cave drip water, Nature Communications, 10, 2984, 2019.¶
Beck, J. W., Richards, D. A., Edwards, R. L., Silverman, B. W., Smart, P. L., Donahue, D. J., Hererra-Osterheld, S., Burr, G. S., Calsoyas, L., Jull, A. J., and Biddulph, D.: Extremely large variations of atmospheric 14C concentration during the last glacial period, Science, 292, 2453-2458, 10.1126/science.1056649, 2001.¶
Beisel, E., Therre, S., Wienberg, C., Friedrich, R., and Frank, N.: Status report of the Heidelberg Radiocarbon Laboratory: Precision and application in Mauritanian cold-water corals over the last 30,000 years, Radiocarbon, 67, 450-460, 2025.¶
Blaauw, M. and Christen, J. A.: Flexible paleoclimate age-depth models using an autoregressive gamma process, 2011.¶
Blaauw, M., Christen, J. A., Lopez, M. A. A., Vazquez, J. E., Belding, T., Theiler, J., Gough, B., Karney, C., Rcpp, L., and Blaauw, M. M.: Package 'rbacon', R package documentation, 2021.¶
Breitenbach, S. F., Rehfeld, K., Goswami, B., Baldini, J., Ridley, H., Kennett, D., Prufer, K., Aquino, V., Asmerom, Y., and Polyak, V.: Constructing proxy records from age models (COPRA), Climate of the Past, 8, 1765-1779, 2012.¶
Carolin, S. A., Cobb, K. M., Adkins, J. F., Clark, B., Conroy, J. L., Lejau, S., Malang, J., and Tuen, A. A.: Varied response of western Pacific hydrology to climate forcings over the last glacial period, Science, 340, 1564-1566, 2013.¶
Cheng, H., Edwards, R. L., Shen, C.-C., Polyak, V. J., Asmerom, Y., Woodhead, J., Hellstrom, J., Wang, Y., Kong, X., Spötl, C., and others: Improvements in 230Th dating, 230Th and 234U half-life values, and U--Th isotopic measurements by multi-collector inductively coupled plasma mass spectrometry, Earth and Planetary Science Letters, 371, 82-91, 2013.¶
Comas-Bru, L., Rehfeld, K., Roesch, C., Amirnezhad-Mozhdehi, S., Harrison, S. P., Atsawawaranunt, K., Ahmad, S. M., Ait Brahim, Y., Baker, A., Bosomworth, M., Breitenbach, S. F. M., Burstyn, Y., Columbu, A., Deininger, M., Demény, A., Dixon, B., Fohlmeister, J., Hatvani, I. G., Hu, J., Kaushal, N., Kern, Z., Labuhn, I., Lechleitner, F. A., Lorrey, A., Martrat, B., Novello, V. F., Oster, J., Pérez-Mejías, C., Scholz, D., Scroxton, N., Sinha, N., Ward, B. M., Warken, S., and Zhang, H.: SISALv2: A comprehensive speleothem isotope da ... [2]

Beck, J. W., Richards, D. A., Edwards, R. L., Silverman, B. W., Smart, P. L., Donahue, D. J., Hererra-Osterheld, S., Burr, G. S., Calsoyas, L., Jull, A. J., and Biddulph, D.: Extremely large variations of atmospheric 14C concentration during the last glacial period, Science, 292, 2453-2458, 10.1126/science.1056649, 2001.

Beisel, E., Therre, S., Wienberg, C., Friedrich, R., and Frank, N.: Status report of the Heidelberg Radiocarbon Laboratory: Precision and application in Mauritanian cold-water corals over the last 30,000 years, Radiocarbon, 67, 450-460, 2025.

Blaauw, M. and Christen, J. A.: Flexible paleoclimate age-depth models using an autoregressive gamma process, 2011.

Blaauw, M., Christen, J. A., Lopez, M. A. A., Vazquez, J. E., Belding, T., Theiler, J., Gough, B., Karney, C., Rcpp, L., and Blaauw, M. M.: Package ‘rbacon’, R package documentation, 2021.

Breitenbach, S. F., Rehfeld, K., Goswami, B., Baldini, J., Ridley, H., Kennett, D., Prufer, K., Aquino, V., Asmerom, Y., and Polyak, V.: Constructing proxy records from age models (COPRA), Climate of the Past, 8, 1765-1779, 2012.

Carolin, S. A., Cobb, K. M., Adkins, J. F., Clark, B., Conroy, J. L., Lejau, S., Malang, J., and Tuen, A. A.: Varied response of western Pacific hydrology to climate forcings over the last glacial period, Science, 340, 1564-1566, 2013.

Cheng, H., Edwards, R. L., Shen, C.-C., Polyak, V. J., Asmerom, Y., Woodhead, J., Hellstrom, J., Wang, Y., Kong, X., Spötl, C., and others: Improvements in 230Th dating, 230Th and 234U half-life values, and U--Th isotopic measurements by multi-collector inductively coupled plasma mass spectrometry, Earth and Planetary Science Letters, 371, 82-91, 2013.

Comas-Bru, L., Rehfeld, K., Roesch, C., Amirnezhad-Mozhdehi, S., Harrison, S. P., Atsawawaranunt, K., Ahmad, S. M., Ait Brahim, Y., Baker, A., Bosomworth, M., Breitenbach, S. F. M., Burstyn, Y., Columbu, A., Deininger, M., Demény, A., Dixon, B., Fohlmeister, J., Hatvani, I. G., Hu, J., Kaushal, N., Kern, Z., Labuhn, I., Lechleitner, F. A., Lorrey, A., Martrat, B., Novello, V. F., Oster, J., Pérez-Mejías, C., Scholz, D., Scroxton, N., Sinha, N., Ward, B. M., Warken, S., and Zhang, H.: SISALv2: A comprehensive speleothem isotope database with multiple age-depth models, Earth Syst. Sci. Data Discuss., 2020, 1-47, 10.5194/essd-2020-39, 2020.

Denniston, R. F. and Luetscher, M.: Speleothems as high-resolution paleoflood archives, Quaternary Science Reviews, 170, 1-13, 2017.

Domínguez-Villar, D., Baker, A., Fairchild, I. J., and Edwards, R. L.: A method to anchor floating chronologies in annually laminated speleothems with U–Th dates, Quaternary Geochronology, 14, 57-66, 10.1016/j.quageo.2012.04.019, 2012.

Douglas, P. M., Pagani, M., Canuto, M. A., Brenner, M., Hodell, D. A., Eglinton, T. I., and Curtis, J. H.: Drought, agricultural adaptation, and sociopolitical collapse in the Maya Lowlands, Proc Natl Acad Sci U S A, 112, 5607-5612, 10.1073/pnas.1419133112, 2015.

Douglas, P. M. J., Demarest, A. A., Brenner, M., and Canuto, M. A.: Impacts of Climate Change on the Collapse of Lowland Maya Civilization, Annual Review of Earth and Planetary Sciences, Vol 44, 44, 613-645, 10.1146/annurev-earth-060115-012512, 2016.

Douville, E., Sallé, E., Frank, N., Eisele, M., Pons-Branchu, E., and Ayrault, S.: Rapid and accurate U–Th dating of ancient carbonates using inductively coupled plasma-quadrupole mass spectrometry, Chemical Geology, 272, 1-11, 10.1016/j.chemgeo.2010.01.007, 2010.

Fairchild, I. J. and Baker, A.: Speleothem science: from process to past environments, John Wiley & Sons2012.

Faraji, M., Frisia, S., Hua, Q., Borsato, A., and Markowska, M.: Accurate chronological construction for two young stalagmites from the tropical South Pacific, Quaternary Geochronology, 74, 101415, 2023.

Faraji, M., Borsato, A., Frisia, S., Hellstrom, J. C., Lorrey, A., Hartland, A., Greig, A., and Mattey, D. P.: Accurate dating of stalagmites from low seasonal contrast tropical Pacific climate using Sr 2D maps, fabrics and annual hydrological cycles, Scientific Reports, 11, 2178, 10.1038/s41598-021-81941-x, 2021.

Fensterer, C., Scholz, D., Hoffmann, D., Mangini, A., and Pajón, J. M.: 230Th/U-dating of a late Holocene low uranium speleothem from Cuba, IOP Conference Series: Earth and Environmental Science, 9, 012015, 10.1088/1755-1315/9/1/012015, 2010.

Frank, N., Mangini, A., and Korfmann, M.: 230Th/U dating of the Trojan 'water quarries', Archaeometry, 44, 305-314, 2002.

Frank, N., Turpin, L., Cabioch, G., Blamart, D., Tressens-Fedou, M., Colin, C., and Jean-Baptiste, P.: Open system U-series ages of corals from a subsiding reef in New Caledonia: Implications for sea level changes, and subsidence rate, Earth and Planetary Science Letters, 249, 274-289, 10.1016/j.epsl.2006.07.029, 2006.

Frappier, A. B., Pyburn, J., Pinkey-Drobnis, A. D., Wang, X., Corbett, D. R., and Dahlin, B. H.: Two millennia of tropical cyclone-induced mud layers in a northern Yucatán stalagmite: Multiple overlapping climatic hazards during the Maya Terminal Classic "megadroughts", Geophysical Research Letters, 41, 5148-5157, 2014.

Frisia, S.: Microstratigraphic logging of calcite fabrics in speleothems as tool for palaeoclimate studies, International Journal of Speleology, 44, 1-1, 2015.

Frisia, S., Borsato, A., Fairchild, I. J., McDermott, F., and Selmo, E. M.: Aragonite-calcite relationships in speleothems (Grotte de Clamouse, France): Environment, fabrics, and carbonate geochemistry, Journal of Sedimentary Research, 72, 687-699, 2002.

Gómez, M. J.: Práctica Mortuoria Maya Prehispánica En Una Cueva En
El Oriente De Yucatán: Áaktun Kóopo, Master, Escuela Nacional de Antropología e Historia (ENAH), Ciudad de México, 2020.

Gonzalez-Lemos, S., Müller, W., Pisonero, J., Cheng, H., Edwards, R. L., and Stoll, H. M.: Holocene flood frequency reconstruction from speleothems in northern Spain, Quaternary Science Reviews, 127, 129-140, 2015.

Haslett, J. and Parnell, A.: A simple monotone process with application to radiocarbon-dated depth chronologies, Journal of the Royal Statistical Society: Series C (Applied Statistics), 57, 399-418, 2008.

Hellstrom, J.: U–Th dating of speleothems with high initial 230Th using stratigraphical constraint, Quaternary Geochronology, 1, 289-295, 10.1016/j.quageo.2007.01.004, 2006.

Hirose, K., Kikawada, Y., and Igarashi, Y.: Temporal variation and provenance of thorium deposition observed at Tsukuba, Japan, Journal of environmental radioactivity, 108, 24-28, 2012.

Hoffmann, D. L., Beck, J. W., Richards, D. A., Smart, P. L., Singarayer, J. S., Ketchmark, T., and Hawkesworth, C. J.: Towards radiocarbon calibration beyond 28ka using speleothems from the Bahamas, Earth and Planetary Science Letters, 289, 1-10, 10.1016/j.epsl.2009.10.004, 2010.

Hu, C., Henderson, G. M., Huang, J., Xie, S., Sun, Y., and Johnson, K. R.: Quantification of Holocene Asian monsoon rainfall from spatially separated cave records, Earth and Planetary Science Letters, 266, 221-232, 2008.

Huang, S., Cai, Y., Cheng, H., Xue, G., Cheng, X., He, M., Li, R., Ma, L., Wei, Y., Lu, Y., Yang, L., and Edwards, R. L.: An integrated study of constraining the initial 230Th of a stalagmite and its implications, Quaternary Geochronology, 80, 101497, https://doi.org/10.1016/j.quageo.2024.101497, 2024.

Huang, Y., Fairchild, I. J., Borsato, A., Frisia, S., Cassidy, N. J., McDermott, F., and Hawkesworth, C. J.: Seasonal variations in Sr, Mg and P in modern speleothems (Grotta di Ernesto, Italy), Chemical Geology, 175, 429-448, 2001.

Hubert, A., Bourdon, B., Pili, E., and Meynadier, L.: Transport of radionuclides in an unconfined chalk aquifer inferred from U-series disequilibria, Geochimica et Cosmochimica Acta, 70, 5437-5454, 2006.

Ivanovich, M. and Harmon, R.: Uranium series disequilibrium. Applications to environmental problems. Clarendon, 1992.

Jaffey, A., Flynn, K., Glendenin, L., Bentley, W. t., and Essling, A.: Precision measurement of half-lives and specific activities of U 235 and U 238, Physical review C, 4, 1889, 1971.

James, D. H., Bradbury, H. J., Carolin, S. A., Breitenbach, S. F., Cheng, H., Orland, I. J., Curtis, J. H., Hartland, A., Gallup, C., and Kwiecien, O.: Pronounced drought and wet periods during the Maya Terminal Classic period reconstructed using stalagmite calcium isotopes, Earth and Planetary Science Letters, 691, 120226, 2026.

James, D. H., Carolin, S. A., Breitenbach, S. F., Hoggarth, J. A., Lases-Hernández, F., Endsley, E. A., Curtis, J. H., Gallup, C. D., Milbrath, S., and Nicolson, J.: Classic Maya response to multiyear seasonal droughts in Northwest Yucatán, Mexico, Science advances, 11, eadw7661, 2025.

Jochum, K. P., Scholz, D., Stoll, B., Weis, U., Wilson, S. A., Yang, Q., Schwalb, A., Börner, N., Jacob, D. E., and Andreae, M. O.: Accurate trace element analysis of speleothems and biogenic calcium carbonates by LA-ICP-MS, Chemical Geology, 318-319, 31-44, 10.1016/j.chemgeo.2012.05.009, 2012.

Jochum, K. P., Weis, U., Stoll, B., Kuzmin, D., Yang, Q., Raczek, I., Jacob, D. E., Stracke, A., Birbaum, K., Frick, D. A., Günther, D., and Enzweiler, J.: Determination of Reference Values for NIST SRM 610-617 Glasses Following ISO Guidelines, Geostandards and Geoanalytical Research, 35, 397-429, 10.1111/j.1751-908X.2011.00120.x, 2011.

Kaufman, A.: An evaluation of several methods for determining 230ThU ages in impure carbonates, Geochimica et Cosmochimica Acta, 57, 2303-2317, 1993.

Kennett, D. J., Breitenbach, S. F., Aquino, V. V., Asmerom, Y., Awe, J., Baldini, J. U., Bartlein, P., Culleton, B. J., Ebert, C., Jazwa, C., Macri, M. J., Marwan, N., Polyak, V., Prufer, K. M., Ridley, H. E., Sodemann, H., Winterhalder, B., and Haug, G. H.: Development and disintegration of Maya political systems in response to climate change, Science, 338, 788-791, 10.1126/science.1226299, 2012.

Kennett, D. J., Masson, M., Lope, C. P., Serafin, S., George, R. J., Spencer, T. C., Hoggarth, J. A., Culleton, B. J., Harper, T. K., Prufer, K. M., Milbrath, S., Russell, B. W., González, E. U., McCool, W. C., Aquino, V. V., Paris, E. H., Curtis, J. H., Marwan, N., Zhang, M., Asmerom, Y., Polyak, V. J., Carolin, S. A., James, D. H., Mason, A. J., Henderson, G. M., Brenner, M., Baldini, J. U. L., Breitenbach, S. F. M., and Hodell, D. A.: Drought-Induced Civil Conflict Among the Ancient Maya, Nature Communications, 13, 3911, 10.1038/s41467-022-31522-x, 2022.

Kerber, I. K., Kontor, F., Mielke, A., Warken, S., and Frank, N.: "U–Th Analysis"–open-source software dedicated to MC-ICP-MS U-series data treatment and evaluation, Geochronology, 7, 1-13, 2025.

Kerber, I. K., Arps, J., Eichstädter, R., Kontor, F., Dornick, C., Schröder-Ritzrau, A., Babu, A., Warken, S., and Frank, N.: Simultaneous U and Th isotope measurements for U-series dating using MCICPMS, Nuclear Instruments and Methods in

Physics Research Section B: Beam Interactions with Materials and Atoms, 539, 169-178, https://doi.org/10.1016/j.nimb.2023.04.003, 2023.

Koltai, G., Scholger, R., Knipping, M., Wang, J., Cheng, H., Frisia, S., Borsato, A., Braunhofer, D., and Spötl, C.: Ancient speleothem giant preserved in a high-Alpine cave (Dolomites, N Italy): Rare insights into the Neogene, Palaeogeography, Palaeoclimatology, Palaeoecology, 113619, 2026.

Kotov, S. and Pälike, H.: QAnalySeries-a cross-platform time series tuning and analysis tool, AGU Fall Meeting Abstracts, PP53D-1230,

Kromer, B., Lindauer, S., Synal, H.-A., and Wacker, L.: MAMS–a new AMS facility at the Curt-Engelhorn-Centre for Achaeometry, Mannheim, Germany, Nuclear instruments and methods in physics research Section B: beam interactions with materials and atoms, 294, 11-13, 2013.

Lases-Hernandez, F., Medina-Elizalde, M., Burns, S., and DeCesare, M.: Long-term monitoring of drip water and groundwater stable isotopic variability in the Yucatán Peninsula: Implications for recharge and speleothem rainfall reconstruction, Geochimica et Cosmochimica Acta, 246, 41-59, 2019.

Li, T.-Y., Wang, X., Chen, C.-J., Tan, M., and Wu, Y.: Testing the initial 230Th/232Th for “Known Age Carbonate” and its significance for 230Th dating and paleoclimate research, Quaternary International, 607, 113-119, 2022.

Lisiecki, L. E. and Raymo, M. E.: A Pliocene-Pleistocene stack of 57 globally distributed benthic δ18O records, Paleoceanography, 20, 2005.

Ludwig, K.: Mathematical–statistical treatment of data and errors for 230Th/U geochronology, Reviews in Mineralogy and Geochemistry, 52, 631-656, 2003.

Ludwig, K.: Isoplot version 4.15: a geochronological toolkit for microsoft Excel, Berkeley Geochronology Center, Special Publication, 247-270, 2008.

Ludwig, K. R. and Titterington, D. M.: Calculation of (230)Th/U Isochrons, Ages, and Errors, Geochimica Et Cosmochimica Acta, 58, 5031-5042, Doi 10.1016/0016-7037(94)90229-1, 1994.

Masson, M. and Lope, C. P.: Kukulcan's realm: Urban life at Ancient Mayapán, University Press of Colorado2014.

Matos, L., Mienis, F., Wienberg, C., Frank, N., Kwiatkowski, C., Groeneveld, J., Thil, F., Abrantes, F., Cunha, M. R., and Hebbeln, D.: Interglacial occurrence of cold-water corals off Cape Lookout (NW Atlantic): First evidence of the Gulf Stream influence, Deep-Sea Research Part I-Oceanographic Research Papers, 105, 158-170, 10.1016/j.dsr.2015.09.003, 2015.

Medici, G., Marianelli, D., Cornacchia, I., Gori, F., and Brandano, M.: Multi-disciplinary approach to paleokarst occurrence in the Eocene–Oligocene succession of the Apulia Carbonate Platform (Salento, Italy), Facies, 72, 17, 2026.

Medina-Elizalde, M., Polanco-Martínez, J. M., Lases-Hernández, F., Bradley, R., and Burns, S.: Testing the “tropical storm” hypothesis of Yucatan Peninsula climate variability during the Maya Terminal Classic Period, Quaternary Research, 86, 111-119, 2016a.

Medina-Elizalde, M., Burns, S. J., Polanco-Martinez, J. M., Beach, T., Lases-Hernandez, F., Shen, C. C., and Wang, H. C.: High-resolution speleothem record of precipitation from the Yucatan Peninsula spanning the Maya Preclassic Period, Global and Planetary Change, 138, 93-102, 10.1016/j.gloplacha.2015.10.003, 2016b.

Medina-Elizalde, M., Burns, S. J., Lea, D. W., Asmerom, Y., von Gunten, L., Polyak, V., Vuille, M., and Karmalkar, A.: High resolution stalagmite climate record from the Yucatán Peninsula spanning the Maya terminal classic period, Earth and Planetary Science Letters, 298, 255-262, 10.1016/j.epsl.2010.08.016, 2010.

Moore, W. S.: The thorium isotope content of ocean water, Earth and Planetary Science Letters, 53, 419-426, 1981.

Moore, W. S. and Sackett, W. M.: Uranium and thorium series inequilibrium in sea water, Journal of Geophysical Research, 69, 5401-5405, 1964.

Morton, L., Evans, C., Harbottle, G., and Estes, G.: Pedogenic fractionation and bioavailability of uranium and thorium in naturally radioactive spodosols, Soil Science Society of America Journal, 65, 1197-1203, 2001.

Moseley, G. E., Richards, D. A., Smart, P. L., Standish, C. D., Hoffmann, D. L., ten Hove, H., and Vinn, O.: Early–middle Holocene relative sea-level oscillation events recorded in a submerged speleothem from the Yucatán Peninsula, Mexico, The Holocene, 25, 1511-1521, 2015.

Moseley, G. E., Edwards, R. L., Wendt, K. A., Cheng, H., Dublyansky, Y., Lu, Y., Boch, R., and Spotl, C.: Reconciliation of the Devils Hole climate record with orbital forcing, Science, 351, 165-168, 10.1126/science.aad4132, 2016.

Nagra, G., Treble, P. C., Andersen, M. S., Bajo, P., Hellstrom, J., and Baker, A.: Dating stalagmites in mediterranean climates using annual trace element cycles, Scientific reports, 7, 1-12, 2017.

Nascimento, R. C., da Silva, Y. J. A. B., do Nascimento, C. W. A., da Silva, Y. J. A. B., da Silva, R. J. A. B., and Collins, A. L.: Thorium content in soil, water and sediment samples and fluvial sediment-associated transport in a catchment system with a semiarid-coastal interface, Brazil, Environmental Science and Pollution Research, 26, 33532-33540, 2019.

Obrist-Farner, J., Steinman, B. A., Stansell, N. D., and Maurer, J.: Incoherency in Central American hydroclimate proxy records spanning the last millennium, Paleoceanography and Paleoclimatology, 38, e2022PA004445, 2023.

Pälike, H.: QAnalySeries [dataset], https://doi.org/10.5281/zenodo.10892222, 2024.

Partin, J. W., Cobb, K. M., Adkins, J. F., Clark, B., and Fernandez, D. P.: Millennial-scale trends in west Pacific warm pool hydrology since the Last Glacial Maximum, Nature, 449, 452-455, 10.1038/nature06164, 2007.

Perrin, C., Prestimonaco, L., Servelle, G., Tilhac, R., Maury, M., and Cabrol, P.: Aragonite–calcite speleothems: identifying original and diagenetic features, Journal of Sedimentary Research, 84, 245-269, 2014.

Perry, E., Paytan, A., Pedersen, B., and Velazquez-Oliman, G.: Groundwater geochemistry of the Yucatan Peninsula, Mexico: Constraints on stratigraphy and hydrogeology, Journal of hydrology, 367, 27-40, 2009.

Reiller, P., Moulin, V., Casanova, F., and Dautel, C.: Retention behaviour of humic substances onto mineral surfaces and consequences upon thorium (IV) mobility: case of iron oxides, Applied Geochemistry, 17, 1551-1562, 2002.

Richards, D. A. and Dorale, J. A.: Uranium-series chronology and environmental applications of speleothems, Uranium-Series Geochemistry, 52, 407-460, Doi 10.2113/0520407, 2003.

Ridley, H. E., Asmerom, Y., Baldini, J. U. L., Breitenbach, S. F. M., Aquino, V. V., Prufer, K. M., Culleton, B. J., Polyak, V., Lechleitner, F. A., Kennett, D. J., Zhang, M. H., Marwan, N., Macpherson, C. G., Baldini, L. M., Xiao, T. Y., Peterkin, J. L., Awe, J., and Haug, G. H.: Aerosol forcing of the position of the intertropical convergence zone since AD 1550, Nature Geoscience, 8, 195-200, 10.1038/Ngeo2353, 2015.

Rivera-Collazo, I., Winter, A., Scholz, D., Mangini, A., Miller, T., Kushnir, Y., and Black, D.: Human adaptation strategies to abrupt climate change in Puerto Rico ca. 3.5 ka, The Holocene, 25, 627-640, 10.1177/0959683614565951, 2015.

Roesch, C. and Rehfeld, K.: AUTOMATISING CONSTRUCTION AND EVALUATION OF AGE-DEPTH MODELS FOR HUNDREDS OF SPELEOTHEMS, 2020.

Romero, D. and Alfaro, E. J.: Spatiotemporal variability of the rainy season in the Yucatan Peninsula, International Journal of Climatology, 44, 2561-2574, https://doi.org/10.1002/joc.8468, 2024.

Roy-Barman, M. and Pons-Branchu, E.: Improved U–Th dating of carbonates with high initial 230Th using stratigraphical and coevality constraints, Quaternary Geochronology, 32, 29-39, 10.1016/j.quageo.2015.12.002, 2016.

Scholz, D. and Hoffmann, D.: 230Th/U-dating of fossil corals and speleothems, Quat. Sci. J, 57, 52, 2008.

Scholz, D. and Hoffmann, D. L.: StalAge – An algorithm designed for construction of speleothem age models, Quaternary Geochronology, 6, 369-382, 10.1016/j.quageo.2011.02.002, 2011.

Schorndorf, N.: Soil-Sensitive Proxies in Northeast Yucatán Speleothems Since the Classic Maya Period, 2024.

Schorndorf, N., Frank, N., Ritter, S. M., Warken, S. F., Scholz, C., Keppler, F., Scholz, D., Weber, M., Aviles Olguin, J., and Stinnesbeck, W.: Mid-to late Holocene sea-level rise recorded in Hells Bells 234U/238U ratio and geochemical composition, Scientific Reports, 13, 10011, 2023.

Scott, M. R.: Thorium and uranium concentrations and isotope ratios in river sediments, Earth and Planetary Science Letters, 4, 245-252, 1968.

Sengupta, D., Dutt, S., Warken, S. F., Singam, A., Frank, N., Sagwal, S., and Maurya, S.: Climate-change induced human migration and socio-political changes in eastern India during the Meghalayan age, Palaeogeography, Palaeoclimatology, Palaeoecology, 667, 112873, 2025.

Skiba, V. and Fohlmeister, J.: Contemporaneously growing speleothems and their value to decipher in-cave processes–A modelling approach, Geochimica et Cosmochimica Acta, 348, 381-396, 2023.

Smart, P. L., Beddows, P. A., Coke, J., Doerr, S., Smith, S., and Whitaker, F. F.: Cave development on the Caribbean coast of the Yucatan Peninsula, Quintana Roo, Mexico, in: Perspectives on Karst Geomorphology, Hydrology, and Geochemistry - A Tribute Volume to Derek C. Ford and William B. White, edited by: Harmon, R. S., and Wicks, C. M., Geological Society of America, 105–128, https://doi.org/10.1130/2006.2404(10), 2006.

Smith, C. L., Fairchild, I. J., Spotl, C., Frisia, S., Borsato, A., Moreton, S. G., and Wynn, P. M.: Chronology building using objective identification of annual signals in trace element profiles of stalagmites, Quaternary Geochronology, 4, 11-21, 10.1016/j.quageo.2008.06.005, 2009.

Spötl, C., Mangini, A., Frank, N., Eichstädter, R., and Burns, S. J.: Start of the last interglacial period at 135 ka: Evidence from a high Alpine speleothem, Geology, 30, 815-818, Doi 10.1130/0091-7613(2002)030<0815:Sotlip>2.0.Co;2, 2002.

Steidle, S. D., Warken, S. F., Schorndorf, N., Förstel, J., Schröder-Ritzrau, A., Moseley, G. E., Spötl, C., Aviles, J., Stinnesbeck, W., and Frank, N.: Reconstruction of Middle to Late Quaternary sea level using submerged speleothems from the northeastern Yucatán Peninsula, Journal of Quaternary Science, 10.1002/jqs.3365, 2021.

Steinman, B. A., Stansell, N. D., Mann, M. E., Cooke, C. A., Abbott, M. B., Vuille, M., Bird, B. W., Lachniet, M. S., and Fernandez, A.: Interhemispheric antiphasing of neotropical precipitation during the past millennium, Proceedings of the National Academy of Sciences, 119, e2120015119, 2022.

Stinnesbeck, W., Rennie, S. R., Avilés Olguín, J., Stinnesbeck, S. R., Gonzalez, S., Frank, N., Warken, S., Schorndorf, N., Krengel, T., and Velázquez Morlet, A.: New evidence for an early settlement of the Yucatán Peninsula, Mexico: The Chan Hol 3 woman and her meaning for the Peopling of the Americas, Plos one, 15, e0227984, 2020.

Sullivan, R. M., van Hengstum, P. J., Wallace, E. J., Coats, S., Donnelly, J. P., Korty, R., Little, S. N., Maas Vargas, M. G., Mejia-Ortiz, L., and Reinhardt, E. G.: Yucatan hurricane activity highlights Common Era tropical cyclone dipole, Geophysical Research Letters, 52, e2024GL113940, 2025.

Synal, H. A., Stocker, M., and Suter, M.: MICADAS: A new compact radiocarbon AMS system, Nuclear Instruments & Methods in Physics Research Section B-Beam Interactions with Materials and Atoms, 259, 7-13, 10.1016/j.nimb.2007.01.138, 2007.

Taylor, S. R. and McLennan, S. M.: The continental crust: its composition and evolution, 1985.

Tec, F.: Centro de Interpretación Biocultural en Áaktun Kóopo, una
Caverna del Complejo Santa Rita, Yucatán, México, Master, Universidad Autónoma de Yucatán, 2021.

Therre, S., Pross, L., Friedrich, R., Trussel, M., and Frank, N.: Heidelberg Radiocarbon Lab - Establishing a New Carbon Dioxide Extraction Line for Carbonate Samples, Radiocarbon, 63, 915-924, 2021.

Thomas, C.: Las Cuevas de Yucatán: No. 1 La Región de Valladolid, 2011.

Töchterle, P., Steidle, S. D., Edwards, R. L., Dublyansky, Y., Spötl, C., Li, X., Gunn, J., and Moseley, G. E.: 230 Th⁄U isochron dating of cryogenic cave carbonates, Geochronology, 4, 617-627, 2022.

Treble, P. C., Baker, A., Abram, N. J., Hellstrom, J. C., Crawford, J., Gagan, M. K., Borsato, A., Griffiths, A. D., Bajo, P., and Markowska, M.: Ubiquitous karst hydrological control on speleothem oxygen isotope variability in a global study, Communications Earth & Environment, 3, 29, 2022.

Vermeesch, P.: IsoplotR: a free and open toolbox for geochronology, Geoscience Frontiers, 9, 1479-1493, doi: 10.1016/j.gsf.2018.04.001, 2018.

Vieten, R., Warken, S. F., Winter, A., Scholz, D., Zanchettin, D., Black, D., and Lachniet, M.: A Sequence of Abrupt Climate Fluctuations in the Northern Caribbean related to the 8.2 ka event, The Holocene, 34, 325-337, 10.1177/09596836231211874, 2024a.

Vieten, R., Warken, S. F., Zanchettin, D., Winter, A., Scholz, D., Black, D., Koltai, G., and Spötl, C.: Northeastern Caribbean rainfall variability linked to solar and volcanic forcing, Paleoceanography and Paleoclimatology, 39, e2023PA004720, 2024b.

Ward, W. C., Keller, G., Stinnesbeck, W., and Adatte, T.: Yucatan Subsurface Stratigraphy - Implications and Constraints for the Chicxulub Impact, Geology, 23, 873–876, https://doi.org/10.1130/0091-7613(1995)023<0873:Ynssia>2.3.Co;2, 1995.

Warken, S., Schorndorf, N., Stinnesbeck, W., Hennhoefer, D., Stinnesbeck, S., Förstel, J., Steidle, S., Olguin, J. A., and Frank, N.: Solar Forcing of Early Holocene Droughts on the Yucatán Peninsula, Scientific Reports, 11 (13885), 10.1038/s41598-021-93417-z, 2021.

Warken, S., Vieten, R., Winter, A., Spötl, C., Miller, T., Jochum, K., Schröder-Ritzrau, A., Mangini, A., and Scholz, D.: Persistent link between Caribbean precipitation and Atlantic Ocean circulation during the Last Glacial revealed by a speleothem record from Puerto Rico, 10.1002/essoar.10502676.1, 2020.

Warken, S. F., Schmitt, A. K., Scholz, D., Hertwig, A., Weber, M., Mertz-Kraus, R., Reinig, F., Esper, J., and Sigl, M.: Discovery of Laacher See eruption in speleothem record synchronizes Greenland and central European Late Glacial climate change, Science Advances, 11, eadt4057, 2025.

Warken, S. F., Fohlmeister, J., Schröder-Ritzrau, A., Constantin, S., Spotl, C., Gerdes, A., Esper, J., Frank, N., Arps, J., Terente, M., Riechelmann, D. F. C., Mangini, A., and Scholz, D.: Reconstruction of late Holocene autumn/winter precipitation variability in SW Romania from a high-resolution speleothem trace element record, Earth and Planetary Science Letters, 499, 122-133, 10.1016/j.epsl.2018.07.027, 2018.

Webster, J. W., Brook, G. A., Railsback, L. B., Cheng, H., Edwards, R. L., Alexander, C., and Reeder, P. P.: Stalagmite evidence from Belize indicating significant droughts at the time of Preclassic Abandonment, the Maya Hiatus, and the Classic Maya collapse, Palaeogeography Palaeoclimatology Palaeoecology, 250, 1-17, 10.1016/j.palaeo.2007.02.022, 2007.

Wefing, A.-M., Arps, J., Blaser, P., Wienberg, C., Hebbeln, D., and Frank, N.: High precision U-series dating of scleractinian cold-water corals using an automated chromatographic U and Th extraction, Chemical Geology, 475, 140-148, 10.1016/j.chemgeo.2017.10.036, 2017.

Wendt, K. A., Li, X., and Edwards, R. L.: Uranium–thorium dating of speleothems, Elements: An International Magazine of Mineralogy, Geochemistry, and Petrology, 17, 87-92, 2021.

Wenz, S., Scholz, D., Sürmelihindi, G., Passchier, C. W., Jochum, K. P., and Andreae, M. O.: 230Th/U-dating of carbonate deposits from ancient aqueducts, Quaternary Geochronology, 32, 40-52, 10.1016/j.quageo.2015.12.001, 2016.

Witschey, W. R. and Brown, C. T.: The electronic atlas of ancient Maya sites, Mayagis. smv. org, 2010.

Wortham, B. E., Banner, J. L., James, E. W., Edwards, R. L., and Loewy, S.: Application of cave monitoring to constrain the value and source of detrital 230Th/232Th in speleothem calcite: Implications for U-series geochronology of speleothems, Palaeogeography, Palaeoclimatology, Palaeoecology, 596, 110978, https://doi.org/10.1016/j.palaeo.2022.110978, 2022.

Supplementary material

S1 Supplementary text

S1.1 Speleothem Age depth models

S1.1.1 Stalagmite E0-B

Eight samples from stalagmite E0-B were analyzed for $^{230}Th/U$ dating (Table S 3). The uranium content ranged from 476 to 555 ng g^{-1}. Three samples were rejected due to low ($^{230}Th/^{232}Th$) activity ratios (<200). Of the remaining five, one was corrected using a stratigraphically derived ($^{230}Th/^{232}Th$) ratio of 43.75 ± 24.25, while the other four used a mean ratio of 35.5 ± 32.5. The obtained age models for stalagmite E0-B exhibit overall mean uncertainties ranging from 117 to 224 years. The Bchron algorithm provides the tightest confidence intervals and thus aligns most closely with the weighted mean chronology. Based on the weighted mean of the used age models, stalagmite E0-B grew from 633 ± 161 BC to 403 ± 54 AD (Figure 4a). The growth rate in the lower part of the stalagmite (222–110 mm dft) was slightly lower at 170 µm a^{-1} compared to the upper section (110–0 mm dft), where it increased to 292 µm a^{-1}.

S1.1.2 Stalagmite E0-C

A total of 51 samples from stalagmite E0-C were analysed for $^{230}Th/U$ dating (Table S 3). The uranium content ranged between 355 and 1324 ng g^{-1}. 11 samples were rejected due to low ($^{230}Th/^{232}Th$) activity ratios (<200). The remaining 40 samples were corrected using individual ($^{230}Th/^{232}Th$) ratios between 7 to 49, derived from both isochron techniques and stratigraphic constraints. One sample, taken at 81.5 mm dft, remained unordered chronologically and was excluded. As a result, the modelled chronologies for stalagmite E0-C display relatively low mean uncertainties across its three distinct growth phases, ranging overall from 33 to 69 years. Across all phases, the Bchron algorithm yields the tightest uncertainty intervals. Growth in E0-C was interrupted by two distinct hiatuses, and it is notable that the modelled durations of these gaps vary substantially depending on the algorithm's assumptions: the first hiatus (at ~40 mm depth) spans from 95 (+58/–55) years (Linear Regression) to 179 (+85/–88) years (Bacon), while the second hiatus (at ~114 mm depth) ranges from 175 (+80/−513) years (StalAge) to 196 years (+93 / −93 years) years (Linear Regression). Based on the weighted mean of the used age models, the growth of E0-C can be divided into three periods separated by hiatuses: (1) 538 ± 56 AD to 811 ± 52 AD; (2) 994 ± 29 AD to 1311 ± 15 AD; and (3) 1451 ± 22 AD to 1835 ± 53 AD (Figure 4b). The average growth rates were 372 µm a^{-1}, 294 µm a^{-1}, and 94 µm a^{-1} for these periods, respectively. Due to a hiatus near the top, no age model is provided for the uppermost 5 mm. However, radiocarbon measurements from the top of the stalagmite indicate modern growth for this growth layers (post-1950 AD, Table S 1).

S1.1.3 Stalagmite E1

A total of 25 samples from stalagmite E1 were analysed for ^{230}Th/U dating (Table S 3). The uranium content ranged from 1202 to 2237 ng g^{-1}. Twelve samples were excluded due to low (^{230}Th/^{232}Th) activity ratios (<200). Of the remaining 13 samples, one was corrected using a stratigraphically derived ratio of 49 ± 19. The other 12 were corrected with a mean ratio of 35.5 ± 32.5. The overall uncertainties for the stalagmite E1 age models range between 25 and 45 years. Over the entire dataset, StalAge provided the most tightly constrained uncertainty intervals. Stalagmite E1 comprises two distinct growth phases separated by a relatively brief hiatus at roughly 61 mm depth. The absolute timing of this interruption in stalagmite E1 spans from 1591 (+46/–35) AD to 1631 (+40/–65) AD according to Bacon, whereas Bchron shifts the onset of the event earlier, dating it from 1557 (+107/–27) AD to 1636 (+21/–34) AD. The estimated duration of this hiatus varies slightly depending on the modelling approach, ranging from 41 (+80/−116) years (Linear Interpolation) to 79 (+34/−136) years (Bchron).

On average, stalagmite E1 grew from 1440 ± 39 AD to approximately 1577 ± 42 AD, with a growth rate of 281 µm a^{-1} (Figure 4c). Growth resumed around 1635 ± 24 AD and continued until approximately 1926 ± 20 AD at ~3 mm dft, with a growth rate of ~230 µm a^{-1}. It was also possible to count individual growth years based on seasonal Sr/Ca variations obtained through LA-ICP-MS measurements. For the section between 3 and 61 mm dft, 311 ± 16 Sr/Ca cycles were counted, while for the lower portion between 61 and 96 mm dft, a total of 182 ± 9 cycles were counted. To test the reliability of the detritus-corrected ^{230}Th/U ages, the Sr/Ca-based age-depth model for the section between 3 and 61 mm dft was anchored to the ^{230}Th/U age at 39 mm dft, which contained no measurable ^{232}Th and thus required no detrital Th correction (Figure 4c). For the lower section, the Sr/Ca-based age-depth model was anchored to the bottommost ^{230}Th/U age, corresponding to the highest (^{230}Th/^{232}Th) activity ratio in this section, minimizing detrital Th correction influence. With a mean absolute deviation of just 9–10 years, both models align perfectly when considering the uncertainties of the ^{230}Th/U-based and Sr/Ca-based age-depth models. No age model is provided for the top section due to a hiatus at 3 mm dft. However, radiocarbon measurements from the top of the stalagmite indicate modern growth (post-1950 AD, Table S 1).

S1.1.4 Stalagmite E4

A total of 28 samples from stalagmite E4 were analyzed for ^{230}Th/U dating (Table S 3). The uranium content ranged from 604 to 1740 ng g^{-1}. Most samples (n=24) were excluded due to high ^{232}Th concentrations of up to 26.5 ng g^{-1}, resulting in (^{230}Th/^{232}Th) activity ratios below 200. One isochron, constructed from three samples, yielded an initial (^{230}Th/^{232}Th) activity ratio of 8.2 ± 1.3, with a probability of fit >0.05 and an MSWD of 0.0001 (Figure S 5d) (Vermeesch, 2018). Two of these samples were corrected using this isochron-derived ratio (8.2 ± 1.3), while the remaining two samples from the top part of the stalagmite were corrected with a mean ratio of 35.5 ± 32.5. As a result, the modelled chronologies for stalagmite E4 display a relatively large spread in mean uncertainties, ranging from 67 years to over 314 years. On average, stalagmite E4 grew from approximately 228 ± 88 AD to 1611 ± 118 AD, with an average growth rate of 53 µm a^{-1}, assuming uninterrupted and constant growth (Figure 4d).

S1.1.5 Stalagmite E8

A total of 15 samples from stalagmite E8 were analyzed for ^{230}Th/U dating (Table S 3). The uranium content ranged from 524 to 1368 ng g^{-1}. Seven samples were excluded due to low (^{230}Th/^{232}Th) activity ratios (<200). One isochron, derived from four samples with a probability of fit >0.05 and an MSWD of 0.016, yielded an initial (^{230}Th/^{232}Th) activity ratio of 6.4 ± 2.4 (Figure S 5e) (Vermeesch, 2018). Between 3 and 43 mm dft, individual growth years were counted based on seasonal Sr/Ca variations obtained through LA-ICP-MS measurements. Three distinct growth phases were identified in stalagmite E8:

1. Lower Section (65–50 mm dft): Due to only two samples with overlapping ages, no age-depth model was constructed for this section. However, ^{230}Th/U ages at 60.5 and 55 mm dft suggest some growth between 565 and 927 AD (Figure 4e).
2. Middle Section (50–27.9 mm dft): Following a hiatus at 50 mm dft, growth resumed. The sample at 29 mm dft, corrected with the isochron-derived ratio (6.4 ± 2.4), yielded an age of 1541 ± 9 AD. However, the uncorrected age at 42 mm dft (1533 ± 9 AD) was inconsistent with the 40 ± 2 Sr/Ca layers counted between 29 and 42 mm dft. As a result, no definitive age model was constructed for this section.
3. Upper Section (27.9–0.8 mm dft): After a minor growth interruption at 27.9 mm dft, growth continued until 0.8 mm dft. The layer-counted age-depth model was anchored to the ^{230}Th/U age at 14.5 mm dft, corrected with a broad (^{230}Th/^{232}Th) ratio of 35.5 ± 32.5, as this sample was least affected by detrital Th. Ages for the remaining samples (8.5–26 mm dft) were corrected with individual (^{230}Th/^{232}Th) ratios ranging from 7 to 35.5 to match the Sr/Ca-based age-depth model. Considering the uncertainties of the anchor age and Sr/Ca layer counting (± 0.5

layers per 10 counted layers). As a result, the modelled chronologies for the last growth phase of stalagmite E8 display highly constrained mean uncertainties across all methods, ranging narrowly from 24 to 42 years. Overall, speleothem E8 deposition can be constrained to around 1605 ± 24 AD and continued at an average rate of 215 µm a^{-1} until 1733 ± 33 AD, when growth ceased at 0.8 mm dft.

No seasonal Sr/Ca layers were visible in the topmost 0.8 mm, making it impossible to determine the time span covered by this section. However, radiocarbon measurements from the top of the stalagmite indicate modern growth (post-1950 AD, Table S 1).

S1.1.6 Stalagmite E23-3

A total of eight samples from stalagmite E23-3 were analyzed for ^{230}Th/U dating (Table S 3). The uranium content ranged between 1134 and 1501 ng g^{-1}. All samples exhibited low ^{232}Th concentrations (<0.06 ng g^{1}), resulting in (^{230}Th/^{232}Th) activity ratios >200, except for the two topmost ones, due to their young age. The uncorrected ages were in stratigraphic order. As with stalagmites E1 and E8, individual growth years were determined based on seasonal Sr/Ca variations. From 0 to 84 mm dft, a total of 331 ± 17 layers were counted. Assuming the topmost layer corresponds to 2022 AD (the year of collection), the layer at 84 mm depth was deposited around 1691 ± 17 AD. This information was used to estimate detrital thorium contributions to the ^{230}Th/U ages, leading to the selection of an (^{230}Th/^{232}Th) activity ratio of 26 ± 7 to align the ^{230}Th/U ages with the layer-counted model within uncertainties. For the final age-depth model, an artificial sample at the stalagmite top with an age of 2022 AD was included. As a result, the modelled chronologies for stalagmite E23-3 display small mean uncertainties, ranging from roughly 11 to 61 years. Because this specific stalagmite exhibited a highly constant, stable growth rate throughout its formation, the Linear Regression algorithm proved as robust approach. When comparing the models to the available layer counting chronology, the Bacon algorithm provided the closest match to the visual layer counts, with a mean absolute deviation of just 6.6 years. Consequently, the growth history of stalagmite E23-3 is divided into two periods, separated by a growth interruption at 167 mm dft (Figure 4f).

1. Older Part (188–167 mm dft): Two ^{230}Th/U ages indicate growth from 1070 ± 7 AD to 1347 ± 9 AD, with an average growth rate of 283 µm a^{-1}.
2. Upper Part (167–0 mm dft): Spanning 1441 ± 5 AD to 2022 AD (assuming continuous growth), this period is represented by five ^{230}Th/U ages, including the artificial age of 2022 AD at the top. The average growth rate is 269 µm a^{-1}, similar to the older portion.

S2 Supplementary Figures

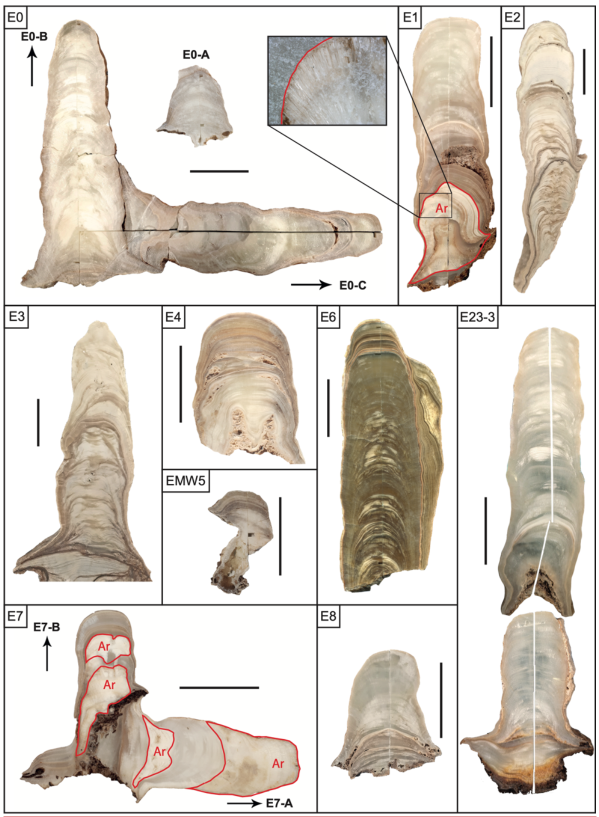

Figure S 1 Scans of slices from ten stalagmites recovered from Áaktun Kóopo' Cave during field trips in 2018 and 2023. The black scale bar represents 5 cm in all images. Red outlines indicate macroscopically identifiable aragonite phases in stalagmites E1 and E7. The inset of stalagmite E1 shows millimeter-long aragonite crystals adjacent to a more compact calcite phase.

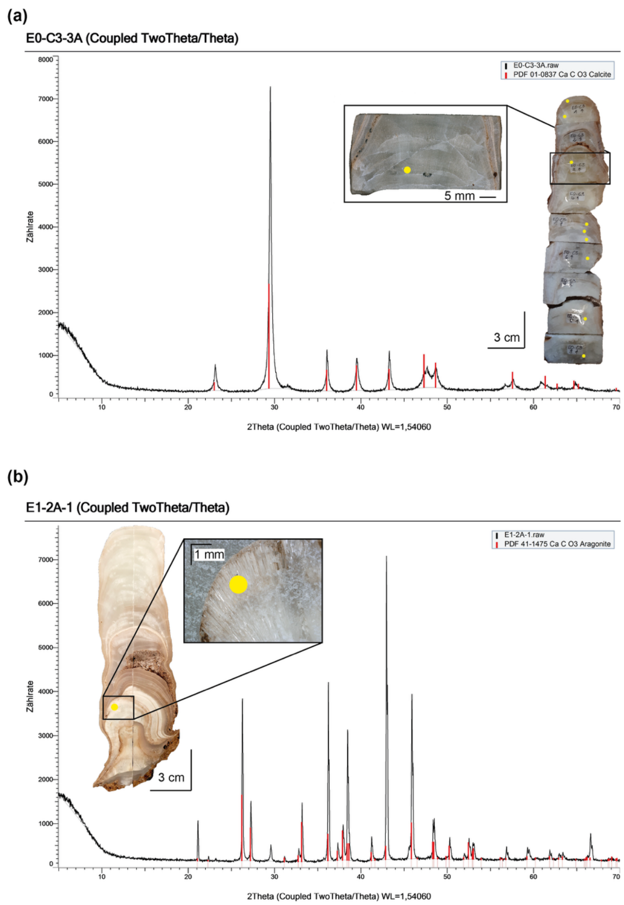

Figure S 2 (a) X-ray diffraction (XRD) pattern showing the characteristic diffraction peaks (2θ) of calcite for a sample from stalagmite E0-C. The image on the right displays the remaining stalagmite cubes from the thin section preparation, from which sample powder was drilled for XRD analysis (yellow dots). The inset indicates the location of the sample corresponding to the presented diffraction pattern. All eight additional samples analyzed from stalagmite E0-C exhibited the same calcite pattern and are therefore not shown. (b) XRD pattern showing the characteristic diffraction peaks (2θ) of aragonite for a sample from the bottom part of stalagmite E1 (yellow dot on the scan). The presence of millimeter-sized needle-like crystals with a silky luster suggested an aragonitic phase, which was confirmed by XRD analysis. Peak positions and intensity data were analyzed using Diffrac.Suite EVA software (Bruker).

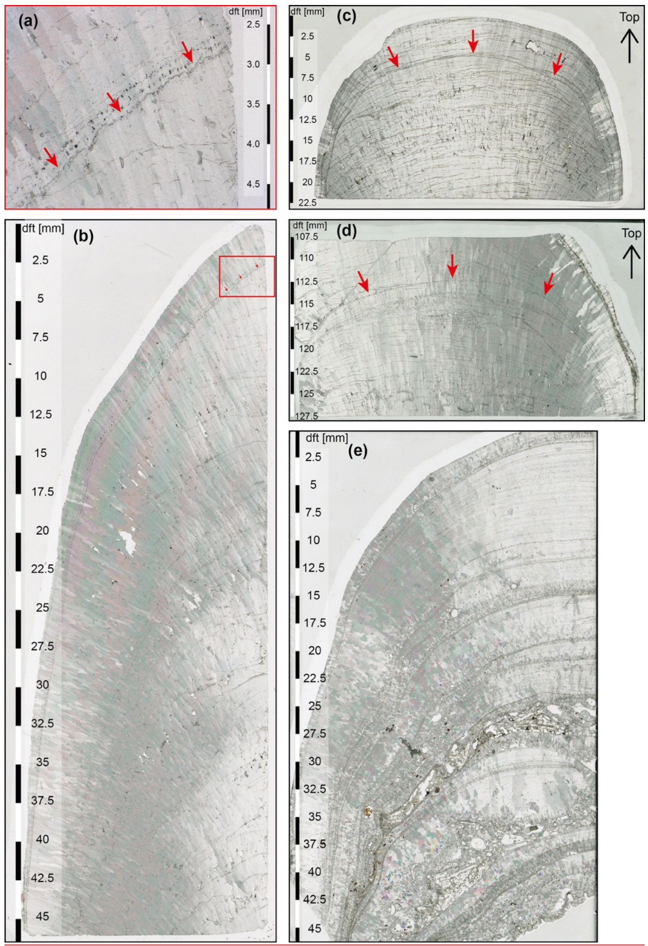

Figure S 3 Thin section photographs of stalagmites E0-C, E1 and E4 from Áaktun Kóopo' Cave. (a) Zoom-in of the top part of stalagmite E1. Red arrows highlight the hiatus at 2.8 mm distance from top (dft). (b) Top part of stalagmite E1, consisting mostly of compact elongated calcite and to some minor extent of open elongated calcite. The red square near the top indicates the zoom-in image shown in (a). (c) Top of stalagmite E0-C consisting of both compact and elongated columnar calcite. Red arrows highlight the hiatus at 5 mm dft. (d) Another hiatus occurring around 113 mm dft in stalagmite E0-C, indicated by rhombohedral crystal terminations (red arrows). (e) Top part of stalagmite E4 showing many growth interruptions as indicated by the layering. Some of these layers consist of detrital material, likely indicating recurrent flooding of the stalagmite.

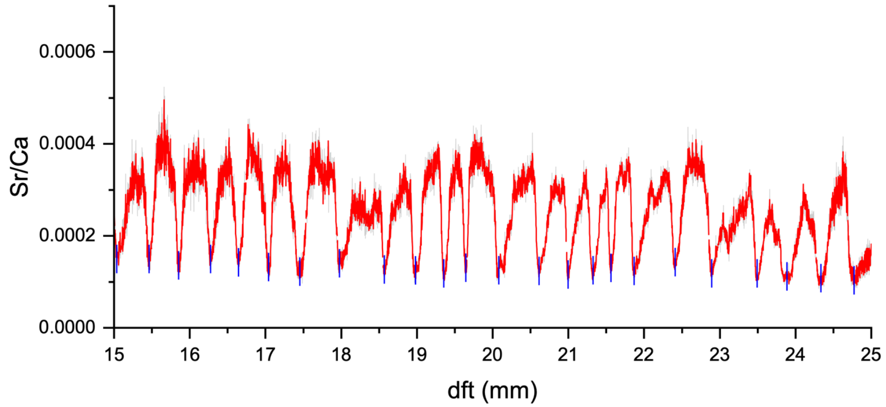

Figure S 4 The counting of seasonal Sr/Ca cycles in stalagmites from Áaktun Kóopo' Cave is exemplarily shown for the section between 25 and 15 mm dft of stalagmite E23-3. The Sr/Ca ratios are shown in light grey, with a moving average of 30 in red. The counted Sr/Ca minima (blue vertical bars) in this section correspond to 24 ± 1 years, assuming a counting error of 0.5 layers per 10 counted layers. More details to the origin of the seasonal cycles can be found in Schorndorf (2024).

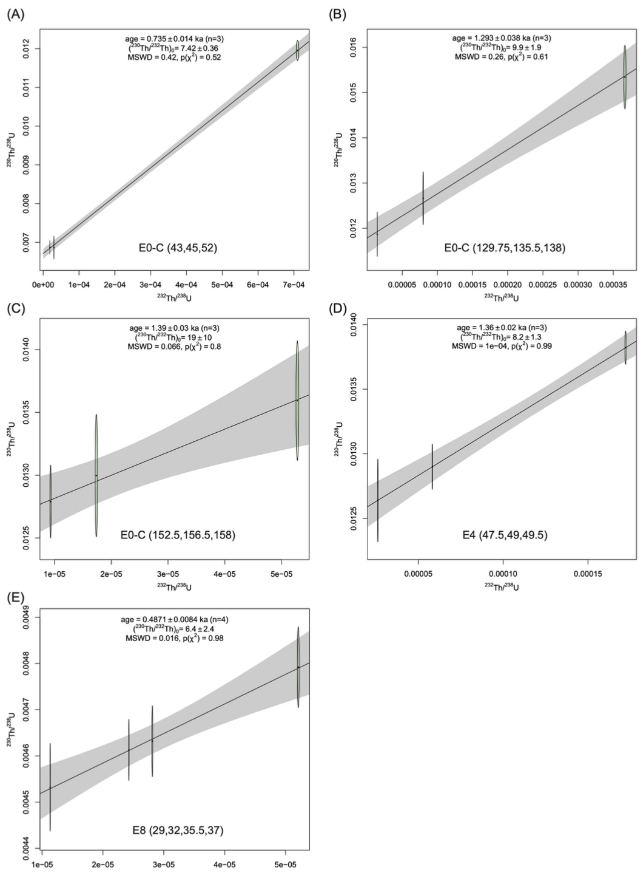

Figure S 5 Five isochrons from three different stalagmites (E0-C, E4, and E8), with fit probabilities >0.05 and mean squared weighted deviation (MSWD) values <1, were derived using ISOPLOT software (Vermeesch, 2018). (a–c) Isochrons from stalagmite E0-C. (d) Isochron from stalagmite E4. (e) Isochron from stalagmite E8. The numbers in brackets next to the stalagmite's name indicate the distance in millimeters (mm) from the top of the stalagmite of the samples that comprise the individual isochrons.

S3 Supplementary Tables

Table S 1 Radiocarbon (^{14}C) measurement results for the tops of stalagmites E0-C, E1, and E8, including a duplicate analysis for E1. Uncertainties in age (yr) and percent modern carbon (pmC) are reported at 1σ.

MAMS	Hd lab-nr.	Label	^{14}C counts	^{12}C (ta)	$^{14}C/^{12}C$ (10^{-12})	$^{13}C/^{12}C$ (%)	pmc	± pmc	^{14}C age (yr)	± (yr)	$\delta^{13}C$ (‰)
52703	HD21-111	E1-Top a	463833	15.2	1.0345	1.0488	95.19	0.19	396	16	-9.0
52704	HD21-114	E1-Top b	490034	16.1	1.0342	1.0499	94.95	0.19	416	16	-8.0
52705	HD21-113	E0-C-Top	476207	15.2	1.0598	1.0487	97.54	0.2	200	16	-9.1
52706	HD21-112	E8-Top	485338	15.5	1.062	1.05	97.49	0.2	204	16	-7.9

Table S 2 $^{230}Th/U$ dating results of drip water from Áaktun Kóopo' Cave. Errors are reported as 2σ analytical uncertainties.

Sample Label	Lab. No.	^{238}U (ng/g)	±2σ	^{232}Th (ng/g)	±2σ	$^{230}Th/^{238}U$ (Act. Ratio)	±2σ	$^{230}Th/^{232}Th$ (Act. Ratio)	±2σ	$\delta^{234}U$ (‰)	±2σ	uncorr. Age (ka)	±2σ
MULTIPLE DRIP SITES	11567	3.27463	0.00019	0.00046562	0.00000082	0.000281	0.000034	6.04	0.74	5.66	0.96	0.0304	0.0037
EDW1	11568	2.34939	0.00019	0.017490	0.000027	0.00404	0.00011	1.659	0.046	7.5	2.2	0.4382	0.012
EDW2	11569	1.57120	0.00013	0.00023727	0.00000059	0.000443	0.000050	8.9	1.0	12.5	1.7	0.0477	0.0055

'able S 3 ^{230}Th/U data of speleothems from Áaktun Kóopo' Cave. Errors are 2σ analytical errors. Corrected ^{230}Th ages assume variable (^{230}Th/^{232}Th) activity ratios ranging between 4 and 68. Those atios have been estimated by using different approaches, such as isochron techniques (i), stratigraphic constrain (s), zero-age carbonate (zac) or layer counting (lc). For samples for which the initial ^{230}Th/^{232}Th) activity ratio couldn't be estimated, a mean value (m) of 35.5±32.5 was used to account for the high range. For samples with (^{230}Th/^{232}Th) < 200, corrected ages are not reported, because age ncertainties are dominated by initial Th correction and do not constrain the chronologies. The corresponding initial (^{230}Th/^{232}Th) ratios are shown only to illustrate the range of initial Th contamination nd should not be treated to calculate ages for individual samples.

Sample Label	Lab. No.	dft (mm)	^{238}U (ng/g)	±2σ	^{232}Th (ng/g)	±2σ	^{230}Th/^{238}U (Act. Ratio)	±2σ	^{230}Th/ ^{232}Th (Act. Ratio)	±2σ	δ^{234}U (‰)	±2σ	uncorr. Age (ka)	±2σ	corr.age (ka)	±2σ	corr.age (a AD)	±2σ	$\delta^{234}U_{ini}$ (‰)	±2σ	(^{230}Th/^{232}Th) initial	Error	Method
E0-A-49	9602	49	645.397	0.035	0.01935	0.00017	0.01952	0.00031	1997	36	38.6	1.5	2.068	0.033	2.032	0.046	-14	46	38.9	1.5	35.5	32.5	m
E0-A-8	9603	8	530.436	0.035	0.07321	0.0004	0.0163	0.00035	362.8	8	38.2	1.6	1.725	0.037	1.56	0.16	461	159	38.4	1.7	35.5	32.5	m
E0-B-5	9553	5	476.15	0.045			0.01525	0.00039			19.3	2.5	1.643	0.043	1.643	0.043	375	43	19.4	2.5	35.5	32.5	m
E0-B-35	11221	35	529.677	0.084	0.0746	0.0012	0.01801	0.00064	392	15	18.7	2.3	1.945	0.072	1.73	0.14	292	137	18.8	2.3	43.75	24.25	s,m
E0-B-59	9756	59	479.457	0.039	0.01293	0.00017	0.01675	0.00031	1909	44	16.2	1.9	1.812	0.035	1.778	0.047	240	47	16.3	1.9	35.5	32.5	m
E0-B-85,5	10986	85.5	560.886	0.042	0.20982	0.00078	0.01977	0.00029	161.3	2.5	16.9	1.7	2.141	0.032							15	12	s,m
E0-B-110	11222	110	591.414	0.031	0.06447	0.00029	0.01943	0.00019	547	5.8	15.3	1.5	2.107	0.021	1.97	0.13	50	131	15.4	1.5	35.5	32.5	m
E0-B-152	9755	152	655.593	0.061	0.28205	0.0008	0.02041	0.00033	145.5	2.4	14.6	1.9	2.215	0.036							16	13	s,m
E0-B-177	10987	177	601.345	0.047	0.19689	0.0006	0.02123	0.00027	197.6	2.6	20.4	1.4	2.292	0.03							23.5	20.5	s,m
E0-B-212	9552	212	549.821	0.047	0.14486	0.00074	0.0273	0.00045	317.9	5.5	18.5	3	2.962	0.05	2.63	0.31	-616	308	18.6	3	35.5	32.5	m
E0-C-TOP	10521	2	926.114	0.05	1.2732	0.0028	0.01338	0.00015	29.73	0.34	19.2	1.2	1.441	0.016							26	3.7	s
E0-C-7	9555	7	769.553	0.047	0.04864	0.00018	0.00326	0.0001	158.1	4.9	13.6	1.2	0.352	0.011							36.5	31.5	s,m
E0-C-10,5	11232	10.5	935.652	0.059	0.05312	0.00035	0.00326	0.00013	175.9	7	11.9	1.1	0.352	0.014							36.25	31.75	s,m
E0-C-15,5	11233	15.5	1165.767	0.056	0.04018	0.00017	0.00329	0.000073	293.3	6.7	10.68	0.79	0.3556	0.0079	0.308	0.036	1713	36	10.69	0.79	39	29	s,m
E0-C-19	10973	19	1186.315	0.046	0.02106	0.00011	0.003113	0.000064	536	11	12.82	0.67	0.3357	0.0069	0.314	0.022	1708	22	12.83	0.67	35.5	32.5	m
E0-C-20	12136	20	1014.64	0.39	0.02751	0.000081	0.003377	0.000037	380.6	4.4	13.53	0.38	0.3639	0.0057	0.33	0.031	1693	31	13.54	0.38	35.5	32.5	m
E0-C-21,5	11234	21.5	832.906	0.044	0.10012	0.00027	0.004181	0.000079	106.7	2	11.05	0.63	0.4519	0.0087							35.5	32.5	m
E0-C-23.5	10520	23.5	804.089	0.053	0.05268	0.00018	0.005042	0.000099	234.8	4.7	14.4	1.1	0.543	0.011	0.462	0.074	1559	74	14.4	1.1	35.5	32.5	m
E0-C-24,5	11235	24.5	838.226	0.042	0.17535	0.00052	0.00608	0.00013	89.4	2	11.7	1.2	0.658	0.015							35.5	32.5	m
E0-C-37,5	9759	37.5	1105.866	0.073			0.00507	0.00014			13.3	1.1	0.547	0.015	0.555	0.017	1463	17	13.4	1.1	35.5	32.5	m
E0-C-43	11236	43	774.849	0.044	1.6817	0.0035	0.01195	0.00011	17	0.2	14.9	1.1	1.292	0.012							7.42	0.36	i
E0-C-45	9758	45	843.683	0.055	0.07688	0.00042	0.00687	0.00012	231.6	4.2	11.4	1	0.743	0.013	0.719	0.013	1299	13	11.4	1	7.42	0.36	i
E0-C-52	10974	52	980.159	0.049	0.05544	0.00016	0.006874	0.000073	371.4	4.1	10.55	0.85	0.7443	0.0078	0.73	0.008	1292	8	10.57	0.85	7.42	0.36	i
E0-C-57,5	11220	57.5	1076.86	0.3	0.022908	0.00008	0.006964	0.000083	1002	12	11.51	0.77	0.7533	0.009	0.727	0.026	1294	26	11.54	0.77	35.5	32.5	m
E0-C-63	10519	63	1113.238	0.066			0.007233	0.000076			11.42	0.61	0.7826	0.0082	0.785	0.009	1235	9	11.44	0.61	35.5	32.5	m
E0-C-69	10975	69	1050.387	0.06	0.06055	0.00016	0.007541	0.000082	399.8	4.5	10.3	0.66	0.817	0.009	0.794	0.02	1228	20	10.33	0.66	11.5	8.5	s,m
E0-C-69,5	12137	69.5	920.76	0.3	0.06441	0.00025	0.00831	0.00012	363.3	5.3	12.52	0.67	0.898	0.013	0.811	0.085	1212	85	12.55	0.67	35.5	32.5	m
E0-C-73	11237	73	933.81	0.043	0.05407	0.00016	0.008442	0.000099	448.9	5.5	12.77	0.67	0.913	0.011	0.828	0.054	1193	54	12.8	0.67	41.5	26.5	s,m
E0-C-75	11062	75	922.315	0.044	0.06312	0.00027	0.008285	0.000095	369.8	4.5	12.92	0.89	0.896	0.01	0.806	0.076	1215	76	12.95	0.9	37	31	s,m
E0-C-76	12138	76	921.68	0.2	0.021804	0.000085	0.008253	0.000084	1063	12	12.48	0.42	0.893	0.01	0.86	0.026	1163	26	12.51	0.42	39	29	s,m
E0-C-77	11238	77	994.05	0.05	0.04919	0.0002	0.008065	0.000091	498.6	5.9	11.6	1.1	0.873	0.01	0.811	0.057	1210	57	11.7	1.1	35.5	32.5	m
E0-C-81.5	10518	81.5	1087.077	0.068	0.00013409	0.00000072	0.008675	0.000085	213749	2386	12.5	1	0.9383	0.0093	0.938	0.009	1082	9	12.5	1	35.5	32.5	m
E0-C-84,5	11239	84.5	1231.992	0.064	0.06069	0.00029	0.00885	0.00013	549.9	8.4	12.16	0.82	0.957	0.014	0.875	0.037	1146	37	12.19	0.82	47.5	20.5	s,m
E0-C-88,5	11266	88.5	1273.923	0.072	0.015025	0.000091	0.00829	0.00012	2168	34	10.2	1.2	0.898	0.013	0.883	0.019	1138	19	10.3	1.2	35.5	32.5	m
E0-C-92.5	10517	92.5	1323.557	0.064			0.008327	0.000079			12.94	0.93	0.9001	0.0085	0.904	0.009	1116	9	12.97	0.93	35.5	32.5	m
E0-C-96,5	11267	96.5	1195.955	0.079	0.03813	0.00022	0.00846	0.00015	817	15	10.2	1.5	0.917	0.016	0.903	0.019	1118	19	10.2	1.5	12.5	9.5	s,m
E0-C-99,5	11063	99.5	1185.693	0.063	0.08613	0.0003	0.00937	0.00011	393.4	4.6	12	1	1.014	0.012	0.941	0.048	1080	48	12	1	28.5	19	s
E0-C-100,5	12139	100.5	1041.81	0.23	0.013372	0.000048	0.009084	0.000086	2160	22	13.25	0.59	0.982	0.01	0.966	0.018	1057	18	13.28	0.59	35.5	32.5	m
E0-C-102	11240	102	1099.32	0.072	0.04319	0.00029	0.009	0.00016	703	13	11.2	1.1	0.975	0.017	0.925	0.05	1096	50	11.2	1.1	35.5	32.5	m
E0-C-105,5	10976	105.5	1131.861	0.057	0.03114	0.0001	0.009367	0.000079	1041.3	9.4	12.27	0.63	1.0137	0.0085	0.979	0.033	1042	33	12.31	0.63	35.5	32.5	m
E0-C-108,5	11241	108.5	1112.965	0.066	0.16815	0.00048	0.01095	0.00014	222.9	2.9	13.4	1.2	1.184	0.015	1.03	0.14	990	140	13.5	1.2	28.75	25.75	s,m
E0-C-112	11268	112	1021.202	0.066	0.09948	0.00054	0.01068	0.00025	336.7	8.1	14.9	2.4	1.154	0.027	1.03	0.11	989	114	15	2.4	35.5	32.5	m
E0-C-113	10516	113	1117.696	0.06	0.14679	0.00022	0.01073	0.0001	249.1	2.4	13.53	0.7	1.161	0.011	1.02	0.13	1000	128	13.57	0.7	30.5	27.5	s,m
E0-C-115,5	11269	115.5	523.807	0.035	0.33368	0.00078	0.01689	0.00025	81.6	1.2	17.5	1.7	1.825	0.028							33.25	8.25	s

SAMPLE LABEL	Lab. No.	dft (mm)	^{238}U (ng/g)	±2σ	^{232}Th (ng/g)	±2σ	$^{230}Th/^{238}U$ (act. Ratio)	±2σ	$^{230}Th/^{232}Th$ (act. Ratio)	±2σ	$\delta^{234}U$ (‰)	±2σ	uncorr. Age (ka)	±2σ	corr.age (ka)	±2σ	corr.age (a ad)	±2σ	$\delta^{234}U_{Ini}$ (‰)	±2σ	($^{230}Th/^{232}Th$) initial	Error	Method
E0-C-116,75	11270	116.75	490.803	0.028	0.09853	0.00034	0.0115	0.00026	176.8	4	16.3	2	1.241	0.028							26	23	s,m
E0-C-117	10977	117	526.817	0.032	0.9144	0.0024	0.01455	0.00032	25.6	0.6	16.1	1.7	1.572	0.035							8	3	s,m
E0-C-119,5	11271	119.5	481.611	0.025	0.02899	0.00016	0.01225	0.00018	626.7	9.8	14.1	1.3	1.325	0.02	1.224	0.049	797	49	14.2	1.3	47.5	20.5	s,m
E0-C-120	9757	120	410.434	0.036	0.01817	0.00018	0.01137	0.00033	790	24	15.5	2.2	1.228	0.037	1.173	0.065	845	65	15.5	2.2	35.5	32.5	m
E0-C-120,75	12140	120.75	416.21	0.12	0.03035	0.00012	0.01276	0.00021	529.3	8.9	16.6	1	1.377	0.023	1.265	0.065	758	65	16.6	1	44	24	s,m
E0-C-122	11272	122	354.898	0.022	0.02883	0.00014	0.01249	0.0002	471.5	7.8	12.5	1.9	1.354	0.022	1.241	0.087	780	87	12.5	1.9	39.25	28.75	s,m
E0-C-122	12141	122	366.19	0.18	0.03441	0.00015	0.01315	0.00031	424	10	14.8	1.8	1.423	0.034	1.261	0.073	762	73	14.8	1.8	48.75	19.25	s,m
E0-C-124,75	12142	124.75	550.69	0.15	0.02739	0.00013	0.01215	0.00016	747	10	18.3	1.3	1.309	0.017	1.247	0.057	776	57	18.3	1.3	35.5	32.5	m
E0-C-129,75	11273	129.75	636.94	0.04	0.02816	0.00011	0.01187	0.0002	823	14	11.8	1.8	1.287	0.022	1.271	0.022	750	22	11.9	1.8	9.9	1.9	i
E0-C-135,5	12143	135.5	587.65	0.23	0.14321	0.00041	0.01266	0.00024	159.7	3.1	16.8	1.5	1.366	0.026							9.9	1.9	i
E0-C-138	12144	138	528.94	0.2	0.5926	0.0011	0.01534	0.00029	42.1	0.8	16.6	1.2	1.658	0.032							9.9	1.9	i
E0-C-152,5	11274	152.5	572.494	0.026	0.01628	0.000079	0.01279	0.00012	1380	14	14.2	1.2	1.384	0.013	1.365	0.017	656	17	14.2	1.2	19	10	i
E0-C-156,5	12145	156.5	560.93	0.16	0.09047	0.00018	0.01359	0.00019	259.2	3.7	16.15	0.92	1.469	0.021	1.361	0.06	662	60	16.21	0.92	19	10	i
E0-C-158	11275	158	598.252	0.036	0.03174	0.00016	0.013	0.0002	752	12	15.5	1.5	1.405	0.022	1.369	0.029	652	29	15.5	1.5	19	10	i
E0-C-162,5	10978	162.5	632.411	0.032	0.04017	0.00011	0.0133	0.00016	641.2	8.1	16.8	1.2	1.435	0.018	1.356	0.075	665	75	16.9	1.2	35.5	32.5	m
E0-C-166	11064	166	371.477	0.02	0.05432	0.00021	0.01499	0.00022	312.5	4.8	18	2.1	1.618	0.024	1.44	0.17	586	165	18	2.1	35.5	32.5	m
E0-C-200	9554	200	544.975	0.045	0.10513	0.00051	0.01585	0.00029	251.4	4.8	17.4	1.9	1.712	0.032	1.47	0.22	547	220	17.5	1.9	35.5	32.5	m
E1-TOP	10979	1	1771.328	0.089	0.51392	0.0009	0.005344	0.000057	56.5	0.6	9.23	0.63	0.5789	0.0061							52.1	4.1	s
E1-3,5	11223	3.5	1836.087	0.078	0.07911	0.00025	0.000765	0.000038	54.5	2.7	8.11	0.84	0.0828	0.0041							27	24	s,m
E1-7	11224	7	1743.306	0.097	0.07268	0.00023	0.001802	0.000037	132.3	2.8	8.49	0.61	0.195	0.0041							51	17	s,m
E1 - 11	11946	11	2237.344	0.088	0.02562	0.00011	0.00132	0.000025	350.9	6.9	10.01	0.66	0.1426	0.0039	0.128	0.013	1895	13	10.01	0.66	35.5	32.5	m
E1 - 16	11947	16	1551.859	0.055	0.11735	0.00037	0.002977	0.000046	120.2	1.9	10.22	0.63	0.3218	0.0053							50	18	s,m
E1-22	11225	22	1797.401	0.091	0.017469	0.000063	0.00217	0.000041	681	13	10.62	0.62	0.2343	0.0044	0.222	0.012	1799	12	10.63	0.62	35.5	32.5	m
E1 - 26,5	11948	26.5	1543.853	0.055	0.03103	0.0001	0.002362	0.000045	361.8	7	13.87	0.65	0.2544	0.0067	0.229	0.024	1794	24	13.88	0.65	35.5	32.5	m
E1 - 31	11949	31	1930.797	0.049	0.03077	0.00012	0.002563	0.00004	493.9	7.9	15.09	0.58	0.2757	0.0059	0.256	0.019	1767	19	15.1	0.58	35.5	32.5	m
E1-35	11058	35	1473.198	0.075	0.017711	0.000075	0.002671	0.000045	679	12	12.47	0.67	0.288	0.0049	0.267	0.009	1754	9	12.48	0.67	49	19	s,m
E1 - 39	11950	39	1745.56	0.077			0.002577	0.000051			14.7	0.9	0.2773	0.0059	0.2773	0.0059	1746	6	14.7	0.9			
E1 - 44	11951	44	1728.205	0.06	0.09521	0.00033	0.003532	0.000046	197.6	2.7	13.11	0.56	0.3808	0.0051							38.5	14.5	s
E1-48,5	11226	48.5	1726.966	0.083	0.014962	0.000064	0.003087	0.000042	1087	16	12.61	0.5	0.333	0.0046	0.322	0.011	1699	11	12.63	0.5	35.5	32.5	m
E1 - 54	11952	54	1715.401	0.08	0.05117	0.00015	0.003389	0.000043	350	4.5	14.25	0.82	0.3649	0.0066	0.328	0.034	1695	34	14.26	0.82	35.5	32.5	m
E1-59,5	10980	59.5	1523.231	0.082	0.05646	0.00013	0.003989	0.000042	329.3	3.5	17.06	0.49	0.4285	0.0046	0.382	0.043	1639	43	17.08	0.49	35.5	32.5	m
E1-62	11059	62	1313.74	0.58	0.2305	0.0022	0.00555	0.00015	96.8	2.7	15.95	0.95	0.597	0.016							35.75	16.25	s
E1-63,5	11674	63.5	1354.252	0.055	0.23936	0.00027	0.004845	0.000053	84.1	0.9	16.03	0.41	0.5213	0.0057							23.25	16.25	s
E1 - 70	11953	70	1242.043	0.079	0.17828	0.00051	0.004473	0.000065	95.9	1.4	17.71	0.85	0.4803	0.0071							21.5	18.5	s,m
E1-73,5	11227	73.5	1735.97	0.088	0.03627	0.00015	0.004784	0.00006	698	9.3	12.19	0.57	0.5166	0.0065	0.491	0.025	1531	25	12.2	0.57	35.5	32.5	m
E1-75	11060	75	1202.21	0.061	0.14117	0.00039	0.007591	0.000087	198.3	2.3	14.89	0.93	0.819	0.01							68	0	s
E1-78,5	11061	78.5	1512.197	0.095	0.2912	0.0011	0.00765	0.00019	122	3.1	13.4	1.2	0.827	0.021							55.25	12.75	s,m
E1-80,5	11675	80.5	1434.68	0.046	0.11122	0.00014	0.005014	0.000043	198.3	1.7	14.43	0.4	0.5403	0.0046							35.5	32.5	m
E1 - 84	11954	84	1541.23	0.065	0.03422	0.0002	0.00514	0.00013	714	18	17.58	0.71	0.552	0.014	0.525	0.029	1498	29	17.6	0.71	35.5	32.5	m
E1 - 87	11955	87	1515.484	0.076	0.18074	0.00061	0.00702	0.00017	181.7	4.5	15.28	0.69	0.756	0.02							54	14	s,m
E1-90,5	11228	90.5	1621.764	0.089	0.06072	0.00023	0.005437	0.000056	443.5	4.9	14.58	0.66	0.5859	0.0061	0.539	0.043	1482	43	14.6	0.66	35.5	32.5	m
E1-92	10981	92	1695.43	0.1	0.03719	0.00012	0.005474	0.000061	764.8	8.8	18.04	0.58	0.5879	0.0065	0.561	0.026	1460	26	18.07	0.58	35.5	32.5	m
E2-6	9629	6	762.897	0.072	0.09972	0.00059	0.00099	0.00014	23.3	3.3	10.6	1.5	0.107	0.015							35.5	32.5	m
E2-262,5	9628	262.5	509.779	0.044	0.17169	0.00059	0.02049	0.00034	186.6	3.1	7.4	2.2	2.241	0.037							35.5	32.5	m
E3-5,5	9631	5.5	970.698	0.076	0.26381	0.00074	0.00137	0.00011	15.5	1.3	7.2	1.6	0.149	0.012							9.2	6.2	s,m
E3-2B-22	12146	22	633.16	0.15	0.33474	0.00071	0.002339	0.000054	13.6	0.3	8.23	0.66	0.2532	0.0068							8.1	5.1	s,m
E3-2B-70	12147	70	575.55	0.17	0.025897	0.000091	0.005241	0.00009	356.8	6.2	5.01	0.74	0.57	0.01	0.513	0.054	1510	54	5.01	0.74	35.5	32.5	m
E3-2B-130	12148	130	325.44	0.24	0.012097	0.000081	0.01255	0.0003	1028	25	9.1	1.6	1.365	0.033	1.318	0.053	705	53	9.1	1.6	35.5	32.5	m
E3-2B-155	12149	155	440.53	0.24	0.09521	0.00031	0.01379	0.00017	193.2	2.5	10.7	0.94	1.498	0.018							35.5	32.5	m
E3-215	9630	215	331.193	0.042	0.06848	0.00068	0.02208	0.00063	328	10	17.8	4.1	2.391	0.07	2.13	0.25	-116	247	17.9	4.1	35.5	32.5	m

SAMPLE LABEL	Lab. No.	dft (mm)	^{238}U (ng/g)	±2σ	^{232}Th (ng/g)	±2σ	^{230}Th/^{238}U (act. Ratio)	±2σ	^{230}Th/ ^{232}Th (act. Ratio)	±2σ	δ^{234}U (‰)	±2σ	uncorr. Age (ka)	±2σ	corr.age (ka)	±2σ	corr.age (a ad)	±2σ	δ^{234}U$_{Ini}$ (‰)	±2σ	(^{230}Th/^{232}Th) initial	Error	Method
E4-TOP	11051	1	1126.134	0.061	8.657	0.018	0.02142	0.00017	8.53	0.07	8.2	1.1	2.342	0.019							7.3	1.2	s
E4-4,5	11141	4.5	1065.393	0.077	0.8496	0.0025	0.007237	0.000087	27.74	0.34	9.4	1	0.785	0.01							15.9	11.7	s
E4-6	9550	6	1140.565	0.067	2.0224	0.0046	0.0094	0.00016	16.23	0.28	7.63	0.86	1.022	0.018							10.9	5.2	s
E4-7,5	11142	7.5	1237.376	0.072	0.09626	0.00022	0.006081	0.000065	239	2.6	8.49	0.77	0.6595	0.0071	0.562	0.088	1459	88	8.5	0.77	35.5	32.5	m
E4-9	11143	9	1254.572	0.06	0.11964	0.00025	0.006362	0.000081	204.2	2.6	7.7	1	0.6906	0.009	0.57	0.11	1450	108	7.7	1	35.5	32.5	m
E4-10	11052	10	1153.243	0.076	2.2986	0.0042	0.01109	0.00011	17.01	0.18	8.27	0.89	1.206	0.013							10	6.5	s
E4-11,5	11144	11.5	1130.282	0.068	4.456	0.012	0.01418	0.00016	11.03	0.13	10.4	1	1.541	0.018							7.65	3.3	s
E4-13	11145	13	1202.259	0.092	1.0409	0.0025	0.00861	0.00012	30.51	0.44	12.5	1.6	0.931	0.014							9.15	6.15	s,m
E4-15	11146	15	1365.197	0.079	26.473	0.059	0.05088	0.00024	8.065	0.042	11.23	0.81	5.629	0.027							7.36	0.64	s
E4-16	11147	16	1473.913	0.079	2.7839	0.0056	0.012427	0.000097	20.2	0.16	6.54	0.68	1.355	0.011							13.15	6.85	s
E4-18	10982	18	1740.17	0.11	0.32014	0.00065	0.0085	0.000095	141.6	1.6	7.03	0.63	0.924	0.011							35.5	32.5	m
E4-19,5	11152	19.5	1645.78	0.1	15.62	0.046	0.0313	0.00019	10.095	0.067	9.46	0.81	3.435	0.021							7.45	1.3	s
E4-20,5	11153	20.5	1326.155	0.062	3.5764	0.0088	0.015155	0.000099	17.21	0.12	8.9	0.81	1.65	0.011							7.8	4.7	s
E4-21,5	11154	21.5	997.112	0.055	9.369	0.022	0.0318	0.00016	10.328	0.057	8.62	0.77	3.493	0.018							7.7	1.3	s
E4-23	11155	23	869.915	0.041	3.7221	0.0092	0.01734	0.00014	12.4	0.11	7.4	1.1	1.893	0.016							6.5	2.9	s
E4-24,5	11156	24.5	885.362	0.052	7.593	0.019	0.03917	0.00024	13.99	0.092	8.9	1.1	4.318	0.027							11	1.5	s
E4-25,5	11157	25.5	740.474	0.038	1.8107	0.0033	0.01629	0.00015	20.41	0.19	8.5	1	1.776	0.016							10	5.1	s
E4-28	10983	28	853.239	0.055	1.3851	0.0022	0.01227	0.00014	23.17	0.27	9	1.2	1.334	0.016							9.1	6.1	s,m
E4-29,5	11158	29.5	823.449	0.034	0.8976	0.0023	0.01432	0.00013	40.12	0.39	8.15	0.69	1.56	0.015							16.5	11.8	s
E4-37	11053	37	744.671	0.032	1.1892	0.003	0.01494	0.00015	28.59	0.3	5.9	0.9	1.631	0.017							12.5	8.1	s
E4-40	11054	40	659.002	0.036	1.1814	0.0021	0.01697	0.00014	28.94	0.24	6.7	1	1.853	0.015							14.6	7.2	s
E4-42	11148	42	623.639	0.033	1.3714	0.0026	0.02015	0.00017	28.07	0.25	7.1	1.3	2.204	0.019							16.3	5.8	s
E4-43,5	11149	43.5	666.473	0.04	0.4339	0.0011	0.01411	0.00014	66.58	0.67	9	1.2	1.536	0.015							26.6	19.9	s
E4-44,5	11150	44.5	604.009	0.039	0.12745	0.00029	0.01301	0.00011	189.6	1.7	5.2	1.4	1.421	0.012							36.5	31.5	s,m
E4-46	11161	46	659.711	0.029	0.2563	0.00057	0.01376	0.00013	107.8	1.1	5.1	1.1	1.503	0.015							26	17	s
E4-47,5	11160	47.5	635.883	0.024	0.33454	0.00067	0.01382	0.0001	80.42	0.63	6.43	0.89	1.508	0.012							8.2	1.3	i
E4-49	11159	49	715.499	0.04	0.12728	0.00031	0.0129	0.00014	221.8	2.5	8	1.2	1.405	0.016	1.353	0.018	668	18	8	1.2	8.2	1.3	i
E4-49,5	9551	49.5	671.6	0.054	0.05352	0.00033	0.01264	0.00026	487	10	10.4	1.5	1.373	0.028	1.349	0.028	669	28	10.5	1.5	8.2	1.3	i
EMW5-28,5	9686	28.5	377.813	0.035	0.17431	0.00056	0.018491	0.000376	123.4	2.5	11.8	2.2	2.011	0.041							35.5	32.5	m
E6-7,5	9752	7.5	877.43	0.39			0.9110	0.0034			2.0	2.7	261.0	5.5	261.0	5.5	-258952	5496	4.1	5.7	35.5	32.5	m
E6-31,5	9751	31.5	106.068	0.071			0.981	0.013			17.1	2.7	347	46	347	46	-345265	45665	45.7	8.4	35.5	32.5	m
E6-220	9750	220	320.176	0.098	0.02666	0.00063	0.9788	0.0052	36054	867	14.1	2.2	353	16	353	16	-350578	15754	38.2	6.3	35.5	32.5	m
E7-B-21,5	9754	21.5	887.647	0.091	0.07604	0.00073	0.011399	0.000197	411.1	8.1	39	1.8	1.203	0.021	1.1	0.1	920	96	39.2	1.8	35.5	32.5	m
E8-TOP	10984	0	1221.09	0.068	2.4599	0.0046	0.022375	0.000184	34.05	0.29	9.93	0.91	2.443	0.021							31.6	2.3	s
E8-8,5	11340	8.5	1176.211	0.049	0.03538	0.00011	0.003085	0.000044	313.7	4.5	12.64	0.83	0.3327	0.0047	0.295	0.035	1726	35	12.65	0.84	35.5	32.5	m
E8-14,5	11229	14.5	948.936	0.046	0.01924	0.000081	0.003505	0.000068	527	10	12.04	0.68	0.3783	0.0074	0.353	0.024	1668	24	12.05	0.68	35.5	32.5	m
E8-21	11341	21	1082.946	0.042	0.029229	0.000079	0.003795	0.000072	430.5	8.3	14.15	0.56	0.4088	0.0078	0.375	0.031	1646	31	14.17	0.56	35.5	32.5	m
E8-26	11055	26	882.458	0.054	0.0518	0.00018	0.003951	0.000089	205.6	4.7	12.98	0.87	0.426	0.01	0.353	0.07	1668	70	12.99	0.87	35.5	32.5	m
E8-29	11056	29	1026.913	0.053	0.03556	0.00011	0.004532	0.000078	399.8	7	15.3	0.92	0.4878	0.0084	0.48	0.009	1541	9	15.32	0.92	6.4	2.4	i
E8-32	11676	32	1116.095	0.039	0.08274	0.00015	0.004613	0.000054	190.5	2.3	13.5	0.82	0.4974	0.006							6.4	2.4	i
E8-35,5	11677	35.5	1058.437	0.055	0.09093	0.00023	0.004632	0.000063	165.4	2.3	15.77	0.79	0.4984	0.0068							6.4	2.4	i
E8-37	11342	37	1100.165	0.064	0.17512	0.00047	0.004792	0.000072	92.1	1.4	15.35	0.74	0.5158	0.0077							6.4	2.4	i
E8-42	11678	42	1341.937	0.056	0.11717	0.00041	0.00455	0.000079	159.9	2.8	16.2	1	0.4894	0.0085							4	1	s,m
E8-46,5	11679	46.5	1367.938	0.07	0.10724	0.00031	0.004584	0.000078	178.9	3.1	15.3	0.76	0.4935	0.0085							5.25	2.25	s,m
E8-48	10985	48	1310.124	0.077	0.08031	0.00027	0.004577	0.00008	228.5	4.1	14.73	0.95	0.4929	0.0087	0.48	0.011	1542	11	14.75	0.95	6.25	3.25	s,m
E8-55	11231	55	596.551	0.027	0.09265	0.00034	0.013494	0.000194	264.7	3.9	7.5	1	1.47	0.022	1.27	0.18	746	181	7.5	1	35.5	32.5	m
E8-60,5	11057	60.5	523.577	0.04	0.06993	0.00029	0.013166	0.000207	301.7	4.9	7.1	1.4	1.435	0.023	1.27	0.15	754	148	7.1	1.4	35.5	32.5	m
E8-67	9633	67	597.658	0.057	0.598	0.0015	0.016261	0.000334	50	1	9.9	1.9	1.77	0.036							35.5	32.5	m

SAMPLE LABEL	Lab. No.	dft (mm)	^{238}U (ng/g)	±2σ	^{232}Th (ng/g)	±2σ	$^{230}Th/^{238}U$ (act. Ratio)	±2σ	$^{230}Th/^{232}Th$ (act. Ratio)	±2σ	$\delta^{234}U$ (‰)	±2σ	uncorr. Age (ka)	±2σ	corr.age (ka)	±2σ	corr.age (a ad)	±2σ	$\delta^{234}U_{Ini}$ (‰)	±2σ	$(^{230}Th/^{232}Th)$ initial	Error	Method
E-23-1-B	12454	0	874.48	0.32	0.05694	0.00094	0.509867	0.000888	24283	405	23.79	0.55	74.9	0.2	74.82	0.21	-72799	206	29.38	0.68	35.5	32.5	m
E-23-1-T	12459	0	680.29	0.34	3.624	0.0057	0.146284	0.00048	85.25	0.31	27.53	0.85	16.735	0.061							35.5	32.5	m
E-23-2-B	12455	0	535.299	0.038	0.12051	0.00025	0.020089	0.000121	276.7	1.8	22.22	0.53	2.164	0.013	1.88	0.26	138	259	22.34	0.53	35.5	32.5	m
E-23-2-T	12460	0	899.094	0.033	0.04017	0.00014	0.002021	0.000032	140.2	2.3	15.01	0.35	0.2173	0.0034							35.5	32.5	m
E-23-3B-7,5	12464	7.5	1309.574	0.061	0.04209	0.00013	0.000583	0.000023	55.9	2.2	21.77	0.63	0.0622	0.0025							26	7	lc
E-23-3B-29	12465	29	1133.958	0.091	0.04686	0.00014	0.001476	0.000049	110.1	3.7	22.6	0.73	0.1575	0.0052							26	7	lc
E-23-3B-60	12825	60	1264.36	0.59	0.027192	0.000093	0.002369	0.000036	344.2	5.4	19.63	0.55	0.2537	0.0053	0.234	0.006	1790	6	19.64	0.55	26	7	lc
E-23-3B-92	12824	92	1261.47	0.39	0.03349	0.00016	0.003411	0.000058	400.8	7.1	20.16	0.4	0.3652	0.0078	0.341	0.009	1683	9	20.18	0.4	26	7	lc
E-23-3B-125	12467	125	1422.348	0.065	0.022633	0.000066	0.00479	0.000034	937.1	7.1	20.72	0.47	0.513	0.0036	0.499	0.005	1526	5	20.74	0.47	26	7	lc
E-23-3B-146	12468	146	1501.446	0.054	0.04257	0.00011	0.005505	0.000045	603.5	5.2	21.12	0.48	0.5895	0.0049	0.564	0.008	1460	8	21.16	0.48	26	7	lc
E-23-3A-190	12462	190	1273.973	0.078	0.05294	0.00015	0.00641	0.000083	476.4	6.3	21.85	0.68	0.6861	0.0089	0.648	0.013	1376	13	21.89	0.68	26	7	lc
E-23-3A-268	12463	268	1362.189	0.058	0.0454	0.00012	0.008981	0.000061	830.7	6.1	23.47	0.39	0.961	0.0066	0.931	0.011	1093	11	23.54	0.39	26	7	lc
Estrella loc.5	11705	-	925.727	0.048	4.7348	0.0073	0.983	0.0017	593.3	1.4	15.76	0.62	358.3	5.3	351.9	8.1	-349878	8085	42.6	1.9	35.5	32.5	m
Estrella drip Site 1	11706	-	1325.237	0.06	24.42	0.043	0.03924	0.00017	6.571	0.03	3.11	0.65	4.352	0.02	0.01	1.38	2016	1378	3.11	0.65	6.5	3.25	zac

Table S 4 Stable isotope data of speleothem E0-C. The age of each sample corresponds to the chronology discussed in the main text.

Sample ID	Lab	dft [cm]	Age [a BP]	Age [a AD]	Age error [a]	δ13C [‰ VPDB]	δ18O [‰ VPDB]
E0-C-704	Institute of Earth Sciences, Heidelberg University	0.3				-10.40	-4.80
E0-C-703	Institute of Earth Sciences, Heidelberg University	0.4				-11.33	-4.98
E0-C-702	Institute of Earth Sciences, Heidelberg University	0.5				-11.04	-4.72
E0-C-700	Institute of Earth Sciences, Heidelberg University	0.7				-11.91	-5.16
E0-C-699	Institute of Earth Sciences, Heidelberg University	0.8				-10.49	-4.98
E0-C-698	Institute of Earth Sciences, Heidelberg University	0.9				-11.57	-5.28
E0-C-697	Institute of Earth Sciences, Heidelberg University	1				-11.47	-5.34
E0-C-696	Institute of Earth Sciences, Heidelberg University	1.1				-11.63	-5.46
E0-C-695	Institute of Earth Sciences, Heidelberg University	1.2				-12.23	-5.39
E0-C-694	Institute of Earth Sciences, Heidelberg University	1.3				-11.73	-5.17
E0-C-693	Institute of Earth Sciences, Heidelberg University	1.4				-12.55	-5.33
E0-C-692	Institute of Earth Sciences, Heidelberg University	1.5				-11.93	-4.96
E0-C-691	Institute of Earth Sciences, Heidelberg University	1.6				-11.33	-4.38
E0-C-689	Institute of Earth Sciences, Heidelberg University	1.8				-11.19	-4.12
E0-C-688	Institute of Earth Sciences, Heidelberg University	1.9				-10.86	-4.19
E0-C-687	Institute of Earth Sciences, Heidelberg University	2				-11.31	-4.05
E0-C-686	Institute of Earth Sciences, Heidelberg University	2.1				-12.09	-4.26
E0-C-685	Institute of Earth Sciences, Heidelberg University	2.2				-11.51	-4.34
E0-C-684	Institute of Earth Sciences, Heidelberg University	2.3				-11.26	-4.16
E0-C-683	Institute of Earth Sciences, Heidelberg University	2.4				-11.38	-4.24
E0-C-682	Institute of Earth Sciences, Heidelberg University	2.5				-11.69	-4.33
E0-C-681	Institute of Earth Sciences, Heidelberg University	2.6				-12.02	-4.25
E0-C-679	Institute of Earth Sciences, Heidelberg University	2.8				-11.88	-4.50
E0-C-678	Institute of Earth Sciences, Heidelberg University	2.9				-11.53	-4.43
E0-C-677	Institute of Earth Sciences, Heidelberg University	3				-11.24	-4.37
E0-C-676	Institute of Earth Sciences, Heidelberg University	3.1				-11.10	-4.30
E0-C-674	Institute of Earth Sciences, Heidelberg University	3.3				-12.61	-4.56
E0-C-673	Institute of Earth Sciences, Heidelberg University	3.4				-12.75	-4.55
E0-C-672	Institute of Earth Sciences, Heidelberg University	3.5				-11.88	-4.51
E0-C-671	Institute of Earth Sciences, Heidelberg University	3.6				-11.61	-4.37
E0-C-670	Institute of Earth Sciences, Heidelberg University	3.7				-11.31	-4.40
E0-C-669	Institute of Earth Sciences, Heidelberg University	3.8				-11.00	-4.15
E0-C-668	Institute of Earth Sciences, Heidelberg University	3.9				-10.51	-4.07
E0-C-667	Institute of Earth Sciences, Heidelberg University	4				-11.06	-4.11
E0-C-666	Institute of Earth Sciences, Heidelberg University	4.1				-11.20	-4.14
E0-C-665	Institute of Earth Sciences, Heidelberg University	4.2				-11.60	-4.17
E0-C-664	Institute of Earth Sciences, Heidelberg University	4.3				-10.14	-4.03
E0-C-663	Institute of Earth Sciences, Heidelberg University	4.4				-9.06	-3.83
E0-C-662	Institute of Earth Sciences, Heidelberg University	4.5				-9.39	-4.01
E0-C-661	Institute of Earth Sciences, Heidelberg University	4.6				-10.44	-4.27
E0-C-660	Institute of Earth Sciences, Heidelberg University	4.7				-10.14	-4.39
E0-C-659	Institute of Earth Sciences, Heidelberg University	4.8				-9.25	-4.70
E0-C-658	Institute of Earth Sciences, Heidelberg University	4.9				-8.84	-4.84
E0-C-657	Institute of Earth Sciences, Heidelberg University	5				-9.08	-4.72
E0-C-656	Institute of Earth Sciences, Heidelberg University	5.1	115.77	1834.23	52.83	-9.84	-5.13
E0-C-655	Institute of Earth Sciences, Heidelberg University	5.2	116.91	1833.09	52.58	-8.93	-4.26
E0-C-654	Institute of Earth Sciences, Heidelberg University	5.3	117.90	1832.10	52.40	-9.07	-4.24
E0-C-653	Institute of Earth Sciences, Heidelberg University	5.4	118.90	1831.10	52.26	-10.09	-4.37
E0-C-652	Institute of Earth Sciences, Heidelberg University	5.5	119.83	1830.17	52.16	-10.93	-5.20
E0-C-651	Institute of Earth Sciences, Heidelberg University	5.6	120.92	1829.08	52.06	-10.88	-5.63
E0-C-649	Institute of Earth Sciences, Heidelberg University	5.8	123.01	1826.99	51.90	-10.84	-5.70
E0-C-648	Institute of Earth Sciences, Heidelberg University	5.9	124.07	1825.93	51.90	-10.82	-4.99
E0-C-647	Institute of Earth Sciences, Heidelberg University	6	125.18	1824.82	51.76	-10.11	-4.82
E0-C-624	Elemtex Ltd., Cornwall	6.1	126.55	1823.45	51.36	-10.45	-4.80
E0-C-623	Elemtex Ltd., Cornwall	6.35	129.39	1820.61	50.79	-9.59	-4.32
E0-C-622	Elemtex Ltd., Cornwall	6.6	131.92	1818.08	50.30	-9.79	-4.13
E0-C-621	Elemtex Ltd., Cornwall	6.85	134.61	1815.39	49.86	-10.38	-3.91
E0-C-620	Institute of Earth Sciences, Heidelberg University	7.1	137.58	1812.42	49.37	-10.40	-4.65
E0-C-619	Elemtex Ltd., Cornwall	7.35	140.20	1809.80	48.86	-10.03	-4.32
E0-C-618	Institute of Earth Sciences, Heidelberg University	7.6	142.70	1807.30	48.52	-9.98	-4.77
E0-C-617	Elemtex Ltd., Cornwall	7.85	145.23	1804.77	48.20	-10.08	-4.57
E0-C-616	Institute of Earth Sciences, Heidelberg University	8.1	147.64	1802.36	47.82	-10.14	-4.93
E0-C-615	Elemtex Ltd., Cornwall	8.35	150.27	1799.73	47.18	-9.74	-4.48
E0-C-614	Institute of Earth Sciences, Heidelberg University	8.6	152.63	1797.37	46.73	-10.08	-5.23
E0-C-613	Elemtex Ltd., Cornwall	8.85	155.08	1794.92	46.16	-9.82	-4.69
E0-C-612	Institute of Earth Sciences, Heidelberg University	9.1	157.86	1792.14	45.68	-10.01	-5.35
E0-C-611	Elemtex Ltd., Cornwall	9.35	160.54	1789.46	45.17	-10.19	-4.90
E0-C-610	Institute of Earth Sciences, Heidelberg University	9.6	163.19	1786.81	44.69	-10.29	-5.56
E0-C-609	Elemtex Ltd., Cornwall	9.85	165.79	1784.21	44.28	-10.25	-5.08
E0-C-608	Institute of Earth Sciences, Heidelberg University	10.1	168.48	1781.52	43.84	-10.33	-5.66
E0-C-607	Elemtex Ltd., Cornwall	10.35	171.25	1778.75	43.02	-10.19	-5.34
E0-C-606	Institute of Earth Sciences, Heidelberg University	10.6	173.78	1776.22	42.46	-10.31	-5.56
E0-C-605	Elemtex Ltd., Cornwall	10.85	176.59	1773.41	41.68	-9.99	-5.04
E0-C-604	Institute of Earth Sciences, Heidelberg University	11.1	179.28	1770.72	40.94	-10.82	-5.87

Formatted: Left: 1.38 cm, Right: 0.78 cm, Top: 1.27 cm, Bottom: 1.27 cm, Width: 20.99 cm, Height: 29.7 cm

E0-C-603	Elemtex Ltd., Cornwall	11.35	181.82	1768.18	40.29	-10.09	-5.43
E0-C-602	Institute of Earth Sciences, Heidelberg University	11.6	184.37	1765.63	39.74	-10.22	-5.78
E0-C-601	Elemtex Ltd., Cornwall	11.85	186.96	1763.04	39.16	-10.42	-5.29
E0-C-600	Institute of Earth Sciences, Heidelberg University	12.1	189.38	1760.62	38.66	-10.21	-5.86
E0-C-599	Elemtex Ltd., Cornwall	12.35	191.75	1758.25	37.94	-10.23	-5.73
E0-C-598	Institute of Earth Sciences, Heidelberg University	12.6	194.38	1755.62	37.13	-10.85	-6.00
E0-C-597	Elemtex Ltd., Cornwall	12.85	196.88	1753.12	36.29	-10.81	-5.63
E0-C-596	Institute of Earth Sciences, Heidelberg University	13.1	199.24	1750.76	35.67	-10.50	-5.82
E0-C-595	Elemtex Ltd., Cornwall	13.35	201.64	1748.36	35.06	-10.01	-5.34
E0-C-594	Institute of Earth Sciences, Heidelberg University	13.6	203.93	1746.07	34.25	-10.47	-5.84
E0-C-593	Elemtex Ltd., Cornwall	13.85	206.19	1743.81	33.53	-10.18	-6.09
E0-C-592	Institute of Earth Sciences, Heidelberg University	14.1	208.57	1741.43	32.60	-10.54	-5.96
E0-C-591	Elemtex Ltd., Cornwall	14.35	210.80	1739.20	31.64	-10.27	-5.36
E0-C-590	Institute of Earth Sciences, Heidelberg University	14.6	213.16	1736.84	30.45	-10.45	-5.94
E0-C-589	Elemtex Ltd., Cornwall	14.85	215.35	1734.65	29.41	-10.77	-5.78
E0-C-588	Institute of Earth Sciences, Heidelberg University	15.1	217.61	1732.39	28.39	-10.42	-5.89
E0-C-587	Elemtex Ltd., Cornwall	15.35	220.09	1729.91	27.00	-10.37	-5.69
E0-C-586	Institute of Earth Sciences, Heidelberg University	15.6	222.37	1727.63	25.68	-10.46	-5.83
E0-C-585	Elemtex Ltd., Cornwall	15.85	224.26	1725.74	24.72	-10.68	-5.16
E0-C-584	Institute of Earth Sciences, Heidelberg University	16.1	226.35	1723.65	23.51	-10.29	-5.58
E0-C-583	Elemtex Ltd., Cornwall	16.35	228.34	1721.66	22.53	-10.66	-5.10
E0-C-582	Institute of Earth Sciences, Heidelberg University	16.6	230.33	1719.67	21.67	-11.22	-5.88
E0-C-581	Elemtex Ltd., Cornwall	16.85	232.57	1717.43	20.33	-11.39	-5.60
E0-C-580	Institute of Earth Sciences, Heidelberg University	17.1	234.44	1715.56	19.60	-11.40	-6.06
E0-C-579	Elemtex Ltd., Cornwall	17.35	236.25	1713.75	19.14	-10.94	-5.49
E0-C-578	Institute of Earth Sciences, Heidelberg University	17.6	237.65	1712.35	19.72	-11.14	-6.07
E0-C-577	Elemtex Ltd., Cornwall	17.85	239.19	1710.81	20.65	-10.78	-5.19
E0-C-576	Institute of Earth Sciences, Heidelberg University	18.1	241.10	1708.90	21.34	-10.89	-5.65
E0-C-575	Elemtex Ltd., Cornwall	18.35	243.46	1706.54	21.71	-11.17	-5.35
E0-C-574	Institute of Earth Sciences, Heidelberg University	18.6	246.17	1703.83	21.94	-11.12	-5.67
E0-C-573	Elemtex Ltd., Cornwall	18.85	248.97	1701.03	22.21	-10.98	-5.20
E0-C-572	Institute of Earth Sciences, Heidelberg University	19.1	252.41	1697.59	21.99	-10.99	-6.62
E0-C-571	Elemtex Ltd., Cornwall	19.35	257.89	1692.11	21.50	-10.52	-4.99
E0-C-570	Institute of Earth Sciences, Heidelberg University	19.6	264.70	1685.30	22.58	-10.79	-5.98
E0-C-569	Elemtex Ltd., Cornwall	19.85	270.92	1679.08	24.51	-10.57	-5.68
E0-C-568	Institute of Earth Sciences, Heidelberg University	20.1	276.26	1673.74	25.43	-10.33	-6.07
E0-C-567	Elemtex Ltd., Cornwall	20.35	281.54	1668.46	25.49	-10.66	-5.14
E0-C-566	Institute of Earth Sciences, Heidelberg University	20.6	287.23	1662.77	25.68	-10.88	-5.04
E0-C-565	Elemtex Ltd., Cornwall	20.85	293.16	1656.84	26.12	-11.31	-4.29
E0-C-564	Institute of Earth Sciences, Heidelberg University	21.1	298.80	1651.20	26.95	-11.37	-4.82
E0-C-563	Elemtex Ltd., Cornwall	21.35	304.01	1645.99	27.93	-11.56	-4.71
E0-C-562	Institute of Earth Sciences, Heidelberg University	21.6	309.03	1640.97	28.99	-11.83	-5.30
E0-C-561	Elemtex Ltd., Cornwall	21.85	313.76	1636.24	30.06	-11.62	-5.06
E0-C-560	Institute of Earth Sciences, Heidelberg University	22.1	317.88	1632.12	30.92	-11.65	-5.01
E0-C-559	Elemtex Ltd., Cornwall	22.35	321.63	1628.37	31.60	-11.57	-4.82
E0-C-558	Institute of Earth Sciences, Heidelberg University	22.6	325.44	1624.56	32.02	-11.62	-5.15
E0-C-557	Elemtex Ltd., Cornwall	22.85	328.92	1621.08	32.41	-11.30	-4.93
E0-C-556	Institute of Earth Sciences, Heidelberg University	23.1	332.36	1617.64	32.74	-11.43	-5.38
E0-C-555	Elemtex Ltd., Cornwall	23.35	335.60	1614.40	33.07	-11.41	-5.14
E0-C-554	Institute of Earth Sciences, Heidelberg University	23.6	339.20	1610.80	32.96	-11.53	-5.73
E0-C-553	Elemtex Ltd., Cornwall	23.85	342.63	1607.37	32.78	-11.27	-5.24
E0-C-552	Institute of Earth Sciences, Heidelberg University	24.1	345.67	1604.33	32.53	-11.33	-5.44
E0-C-551	Elemtex Ltd., Cornwall	24.35	348.50	1601.50	32.29	-10.56	-5.15
E0-C-550	Institute of Earth Sciences, Heidelberg University	24.6	351.60	1598.40	32.11	-9.92	-5.53
E0-C-549	Elemtex Ltd., Cornwall	24.85	354.95	1595.05	31.81	-9.02	-4.91
E0-C-548	Elemtex Ltd., Cornwall	25.1	358.66	1591.34	31.34	-8.89	-5.36
E0-C-547	Elemtex Ltd., Cornwall	25.35	361.76	1588.24	30.96	-8.13	-4.70
E0-C-545	Elemtex Ltd., Cornwall	25.85	368.28	1581.72	30.10	-9.95	-4.90
E0-C-544	Elemtex Ltd., Cornwall	26.1	371.73	1578.27	29.65	-9.96	-5.02
E0-C-543	Elemtex Ltd., Cornwall	26.35	374.40	1575.60	29.56	-9.57	-5.15
E0-C-542	Institute of Earth Sciences, Heidelberg University	26.6	377.19	1572.81	29.25	-9.73	-5.05
E0-C-541	Elemtex Ltd., Cornwall	26.85	380.61	1569.39	28.78	-10.30	-4.80
E0-C-540	Institute of Earth Sciences, Heidelberg University	27.1	383.71	1566.29	28.31	-10.19	-5.50
E0-C-539	Elemtex Ltd., Cornwall	27.35	386.61	1563.39	28.10	-9.62	-5.36
E0-C-538	Institute of Earth Sciences, Heidelberg University	27.6	389.45	1560.55	27.99	-9.63	-5.67
E0-C-537	Elemtex Ltd., Cornwall	27.85	392.28	1557.72	28.06	-9.81	-5.62
E0-C-536	Institute of Earth Sciences, Heidelberg University	28.1	395.53	1554.47	27.80	-9.09	-5.94
E0-C-535	Elemtex Ltd., Cornwall	28.35	398.50	1551.50	27.53	-9.04	-5.30
E0-C-534	Institute of Earth Sciences, Heidelberg University	28.6	401.24	1548.76	27.45	-9.40	-5.10
E0-C-533	Elemtex Ltd., Cornwall	28.85	404.08	1545.92	27.24	-9.61	-4.36
E0-C-532	Institute of Earth Sciences, Heidelberg University	29.1	406.86	1543.14	27.06	-10.59	-4.83
E0-C-531	Elemtex Ltd., Cornwall	29.35	409.64	1540.36	26.72	-9.64	-4.33
E0-C-530	Institute of Earth Sciences, Heidelberg University	29.6	412.12	1537.88	26.58	-9.99	-4.70
E0-C-529	Elemtex Ltd., Cornwall	29.85	414.76	1535.24	26.32	-10.24	-4.45
E0-C-528	Institute of Earth Sciences, Heidelberg University	30.1	417.23	1532.77	26.09	-10.43	-4.76
E0-C-527	Elemtex Ltd., Cornwall	30.35	419.88	1530.12	25.88	-10.69	-4.61
E0-C-526	Institute of Earth Sciences, Heidelberg University	30.6	422.39	1527.61	25.72	-10.51	-4.90
E0-C-525	Elemtex Ltd., Cornwall	30.85	424.80	1525.20	25.52	-10.58	-4.63
E0-C-524	Institute of Earth Sciences, Heidelberg University	31.1	427.41	1522.59	25.33	-10.76	-5.07
E0-C-523	Elemtex Ltd., Cornwall	31.35	430.10	1519.90	25.10	-10.69	-5.08

E0-C-522	Institute of Earth Sciences, Heidelberg University	31.6	432.68	1517.32	24.89	-10.69	-5.10
E0-C-521	Elemtex Ltd., Cornwall	31.85	435.29	1514.71	24.61	-11.11	-5.13
E0-C-520	Institute of Earth Sciences, Heidelberg University	32.1	437.91	1512.09	24.27	-10.83	-5.30
E0-C-519	Elemtex Ltd., Cornwall	32.35	440.57	1509.43	23.92	-10.67	-5.14
E0-C-518	Institute of Earth Sciences, Heidelberg University	32.6	443.17	1506.83	23.57	-11.13	-5.34
E0-C-517	Elemtex Ltd., Cornwall	32.85	445.61	1504.39	23.24	-11.58	-5.09
E0-C-516	Institute of Earth Sciences, Heidelberg University	33.1	448.21	1501.79	22.84	-11.13	-5.38
E0-C-515	Elemtex Ltd., Cornwall	33.35	450.68	1499.32	22.46	-11.33	-5.17
E0-C-514	Institute of Earth Sciences, Heidelberg University	33.6	453.19	1496.81	22.14	-11.37	-5.48
E0-C-513	Elemtex Ltd., Cornwall	33.85	455.66	1494.34	21.79	-11.36	-5.17
E0-C-512	Institute of Earth Sciences, Heidelberg University	34.1	458.16	1491.84	21.31	-10.87	-5.37
E0-C-511	Elemtex Ltd., Cornwall	34.35	460.62	1489.38	20.85	-11.09	-5.11
E0-C-510	Institute of Earth Sciences, Heidelberg University	34.6	463.14	1486.86	20.61	-10.97	-5.65
E0-C-509	Elemtex Ltd., Cornwall	34.85	465.63	1484.37	20.51	-11.13	-5.35
E0-C-508	Institute of Earth Sciences, Heidelberg University	35.1	468.10	1481.90	20.34	-11.63	-5.66
E0-C-507	Elemtex Ltd., Cornwall	35.35	470.47	1479.53	20.22	-11.59	-5.38
E0-C-506	Institute of Earth Sciences, Heidelberg University	35.6	472.87	1477.13	20.11	-11.51	-5.50
E0-C-505	Elemtex Ltd., Cornwall	35.85	475.14	1474.86	20.10	-11.39	-5.04
E0-C-504	Institute of Earth Sciences, Heidelberg University	36.1	477.30	1472.70	19.96	-11.86	-5.39
E0-C-503	Elemtex Ltd., Cornwall	36.35	479.37	1470.63	19.95	-11.57	-5.10
E0-C-502	Institute of Earth Sciences, Heidelberg University	36.6	481.50	1468.50	19.97	-11.94	-5.59
E0-C-501	Elemtex Ltd., Cornwall	36.85	483.51	1466.49	20.11	-11.52	-5.14
E0-C-500	Elemtex Ltd., Cornwall	37.1	485.52	1464.48	20.37	-10.99	-5.22
E0-C-499	Elemtex Ltd., Cornwall	37.35	487.45	1462.55	20.64	-11.03	-5.34
E0-C-498	Elemtex Ltd., Cornwall	37.6	489.48	1460.52	20.85	-11.38	-5.25
E0-C-497	Elemtex Ltd., Cornwall	37.85	491.72	1458.28	21.21	-11.40	-5.28
E0-C-496	Elemtex Ltd., Cornwall	38.1	494.01	1455.99	21.55	-11.42	-5.38
E0-C-495	Elemtex Ltd., Cornwall	38.35	496.26	1453.74	21.99	-10.82	-5.18
E0-C-494	Elemtex Ltd., Cornwall	38.6	498.55	1451.45	22.38	-10.80	-4.98

Table S 5 Stable isotope data of speleothem E1. The age of each sample corresponds to the chronology discussed in the main text.

Sample ID	Lab	dft [cm]	Age [a BP]	Age [a AD]	Age error [a]	$\delta^{13}C$ [‰ VPDB]	$\delta^{18}O$ [‰ VPDB]
E1-001	Institute of Earth Sciences, Heidelberg University	0.56	12.17	1937.83	21.56	-9.82	-4.78
E1-002	Institute of Earth Sciences, Heidelberg University	0.66	12.67	1937.33	21.46	-9.76	-4.77
E1-003	Institute of Earth Sciences, Heidelberg University	0.76	13.21	1936.79	21.36	-9.15	-4.52
E1-004	Institute of Earth Sciences, Heidelberg University	0.86	13.66	1936.34	21.29	-9.72	-4.82
E1-005	Institute of Earth Sciences, Heidelberg University	0.96	14.11	1935.89	21.23	-9.89	-4.71
E1-006	Institute of Earth Sciences, Heidelberg University	1.06	14.55	1935.45	21.15	-10.40	-4.87
E1-007	Institute of Earth Sciences, Heidelberg University	1.16	14.98	1935.02	21.09	-10.97	-5.05
E1-008	Institute of Earth Sciences, Heidelberg University	1.26	15.41	1934.59	21.04	-11.72	-5.18
E1-009	Institute of Earth Sciences, Heidelberg University	1.36	15.86	1934.14	20.95	-11.61	-5.07
E1-010	Institute of Earth Sciences, Heidelberg University	1.46	16.27	1933.73	20.90	-10.94	-5.13
E1-011	Institute of Earth Sciences, Heidelberg University	1.56	16.74	1933.26	20.82	-10.71	-5.20
E1-012	Institute of Earth Sciences, Heidelberg University	1.66	17.26	1932.74	20.75	-10.67	-5.15
E1-013	Institute of Earth Sciences, Heidelberg University	1.76	17.69	1932.31	20.68	-10.97	-5.21
E1-014	Institute of Earth Sciences, Heidelberg University	1.86	18.19	1931.81	20.61	-11.46	-5.28
E1-015	Institute of Earth Sciences, Heidelberg University	1.96	18.64	1931.36	20.57	-11.66	-5.56
E1-016	Institute of Earth Sciences, Heidelberg University	2.06	19.12	1930.88	20.48	-11.15	-5.53
E1-017	Institute of Earth Sciences, Heidelberg University	2.16	19.61	1930.39	20.40	-10.51	-5.54
E1-018	Institute of Earth Sciences, Heidelberg University	2.26	20.10	1929.90	20.32	-9.60	-5.07
E1-019	Institute of Earth Sciences, Heidelberg University	2.36	20.65	1929.35	20.29	-10.31	-5.71
E1-020	Institute of Earth Sciences, Heidelberg University	2.46	21.13	1928.87	20.20	-10.70	-5.39
E1-021	Institute of Earth Sciences, Heidelberg University	2.56	21.60	1928.40	20.12	-10.41	-5.45
E1-022	Institute of Earth Sciences, Heidelberg University	2.66	22.09	1927.91	20.07	-10.14	-5.47
E1-023	Institute of Earth Sciences, Heidelberg University	2.76	22.62	1927.38	19.96	-10.69	-5.09
E1-024	Institute of Earth Sciences, Heidelberg University	2.86	23.05	1926.95	19.88	-11.32	-5.02
E1-025	Institute of Earth Sciences, Heidelberg University	2.96	23.53	1926.47	19.83	-11.38	-4.84
E1-026	Institute of Earth Sciences, Heidelberg University	3.06	24.01	1925.99	19.71	-10.13	-4.36
E1-027	Institute of Earth Sciences, Heidelberg University	3.16	24.48	1925.52	19.65	-9.92	-4.20
E1-028	Institute of Earth Sciences, Heidelberg University	3.26	24.93	1925.07	19.62	-9.41	-3.87
E1-029	Institute of Earth Sciences, Heidelberg University	3.36	25.40	1924.60	19.54	-9.20	-3.89
E1-030	Institute of Earth Sciences, Heidelberg University	3.46	25.84	1924.16	19.48	-9.19	-4.06
E1-031	Institute of Earth Sciences, Heidelberg University	3.56	26.35	1923.65	19.41	-9.14	-4.07
E1-032	Institute of Earth Sciences, Heidelberg University	3.66	26.88	1923.12	19.33	-9.16	-3.98
E1-033	Institute of Earth Sciences, Heidelberg University	3.76	27.34	1922.66	19.24	-9.24	-4.22
E1-034	Institute of Earth Sciences, Heidelberg University	3.86	27.75	1922.25	19.17	-9.65	-4.05
E1-035	Institute of Earth Sciences, Heidelberg University	3.96	28.22	1921.78	19.09	-10.42	-4.36
E1-036	Institute of Earth Sciences, Heidelberg University	4.06	28.68	1921.32	18.98	-10.30	-4.34
E1-037	Institute of Earth Sciences, Heidelberg University	4.16	29.17	1920.83	18.80	-10.57	-4.57
E1-038	Institute of Earth Sciences, Heidelberg University	4.26	29.62	1920.38	18.74	-10.28	-4.36
E1-039	Institute of Earth Sciences, Heidelberg University	4.36	30.09	1919.91	18.69	-11.11	-4.51
E1-040	Institute of Earth Sciences, Heidelberg University	4.46	30.54	1919.46	18.62	-11.20	-4.53
E1-041	Institute of Earth Sciences, Heidelberg University	4.56	31.02	1918.98	18.55	-11.22	-4.50
E1-042	Institute of Earth Sciences, Heidelberg University	4.66	31.47	1918.53	18.44	-10.79	-4.50
E1-043	Institute of Earth Sciences, Heidelberg University	4.76	31.95	1918.05	18.35	-10.62	-4.55
E1-044	Institute of Earth Sciences, Heidelberg University	4.86	32.43	1917.57	18.28	-10.93	-4.72
E1-045	Institute of Earth Sciences, Heidelberg University	4.96	32.88	1917.12	18.21	-11.14	-4.65
E1-046	Institute of Earth Sciences, Heidelberg University	5.06	33.38	1916.62	18.12	-11.78	-4.86
E1-047	Institute of Earth Sciences, Heidelberg University	5.16	33.86	1916.14	18.06	-11.39	-4.69
E1-048	Institute of Earth Sciences, Heidelberg University	5.26	34.43	1915.57	18.01	-10.15	-4.33
E1-049	Institute of Earth Sciences, Heidelberg University	5.36	34.90	1915.10	17.89	-10.29	-4.42
E1-050	Institute of Earth Sciences, Heidelberg University	5.46	35.33	1914.67	17.82	-10.10	-4.30
E1-051	Institute of Earth Sciences, Heidelberg University	5.56	35.77	1914.23	17.76	-10.66	-4.73
E1-052	Institute of Earth Sciences, Heidelberg University	5.66	36.23	1913.77	17.69	-11.41	-4.87
E1-053	Institute of Earth Sciences, Heidelberg University	5.76	36.71	1913.29	17.61	-11.13	-4.73
E1-054	Institute of Earth Sciences, Heidelberg University	5.86	37.18	1912.82	17.52	-10.58	-4.42
E1-055	Institute of Earth Sciences, Heidelberg University	5.96	37.63	1912.37	17.46	-11.31	-4.66
E1-056	Institute of Earth Sciences, Heidelberg University	6.06	38.10	1911.90	17.38	-11.74	-4.90
E1-057	Institute of Earth Sciences, Heidelberg University	6.16	38.54	1911.46	17.31	-11.67	-4.88
E1-058	Institute of Earth Sciences, Heidelberg University	6.26	39.10	1910.90	17.26	-11.61	-4.77
E1-059	Institute of Earth Sciences, Heidelberg University	6.36	39.56	1910.44	17.17	-11.72	-4.88
E1-060	Institute of Earth Sciences, Heidelberg University	6.46	40.08	1909.92	17.11	-11.65	-4.87
E1-061	Institute of Earth Sciences, Heidelberg University	6.56	40.61	1909.39	16.95	-11.77	-4.90
E1-062	Institute of Earth Sciences, Heidelberg University	6.66	41.09	1908.91	16.89	-11.94	-4.88
E1-063	Institute of Earth Sciences, Heidelberg University	6.76	41.55	1908.45	16.79	-11.90	-4.95
E1-064	Institute of Earth Sciences, Heidelberg University	6.86	42.02	1907.98	16.66	-12.04	-5.11
E1-065	Institute of Earth Sciences, Heidelberg University	6.96	42.57	1907.43	16.54	-11.91	-5.21
E1-066	Institute of Earth Sciences, Heidelberg University	7.06	43.03	1906.97	16.48	-11.63	-5.19
E1-067	Institute of Earth Sciences, Heidelberg University	7.16	43.53	1906.47	16.44	-11.22	-5.08
E1-068	Institute of Earth Sciences, Heidelberg University	7.26	44.06	1905.94	16.41	-11.60	-5.20
E1-069	Institute of Earth Sciences, Heidelberg University	7.36	44.56	1905.44	16.30	-11.37	-5.10
E1-070	Institute of Earth Sciences, Heidelberg University	7.46	45.08	1904.92	16.16	-11.41	-4.97
E1-071	Institute of Earth Sciences, Heidelberg University	7.71	46.39	1903.61	16.01	-11.04	-4.90
E1-072	Institute of Earth Sciences, Heidelberg University	7.96	47.62	1902.38	15.79	-9.98	-4.56
E1-073	Institute of Earth Sciences, Heidelberg University	8.21	48.94	1901.06	15.49	-10.88	-4.77
E1-074	Institute of Earth Sciences, Heidelberg University	8.46	50.21	1899.79	15.32	-11.50	-4.72

E1-075	Institute of Earth Sciences, Heidelberg University	8.71	51.47	1898.53	15.09	-11.54	-4.71
E1-076	Institute of Earth Sciences, Heidelberg University	8.96	52.77	1897.23	14.85	-11.73	-4.67
E1-078	Institute of Earth Sciences, Heidelberg University	9.46	55.53	1894.47	14.73	-11.26	-4.47
E1-079	Institute of Earth Sciences, Heidelberg University	9.71	56.99	1893.01	14.80	-11.32	-4.65
E1-080	Institute of Earth Sciences, Heidelberg University	9.96	58.57	1891.43	15.00	-11.44	-4.66
E1-081	Institute of Earth Sciences, Heidelberg University	10.21	60.13	1889.87	14.97	-11.09	-4.62
E1-082	Institute of Earth Sciences, Heidelberg University	10.46	61.61	1888.39	14.81	-11.28	-4.65
E1-083	Institute of Earth Sciences, Heidelberg University	10.71	63.24	1886.76	14.73	-11.22	-4.70
E1-084	Institute of Earth Sciences, Heidelberg University	10.96	64.77	1885.23	14.56	-11.07	-4.65
E1-085	Institute of Earth Sciences, Heidelberg University	11.21	66.50	1883.50	14.31	-10.95	-4.43
E1-086	Institute of Earth Sciences, Heidelberg University	11.46	68.18	1881.82	14.05	-10.96	-4.50
E1-087	Institute of Earth Sciences, Heidelberg University	11.71	69.92	1880.08	13.80	-11.42	-4.58
E1-088	Institute of Earth Sciences, Heidelberg University	11.96	71.74	1878.26	13.58	-11.42	-4.53
E1-089	Institute of Earth Sciences, Heidelberg University	12.21	73.59	1876.41	13.35	-11.29	-4.75
E1-090	Institute of Earth Sciences, Heidelberg University	12.46	75.38	1874.62	13.15	-11.21	-4.63
E1-091	Institute of Earth Sciences, Heidelberg University	12.71	77.25	1872.75	13.00	-11.24	-4.62
E1-092	Institute of Earth Sciences, Heidelberg University	12.96	79.08	1870.92	12.92	-11.16	-4.50
E1-093	Institute of Earth Sciences, Heidelberg University	13.21	80.90	1869.10	12.84	-11.28	-4.51
E1-094	Institute of Earth Sciences, Heidelberg University	13.46	82.73	1867.27	12.84	-11.32	-4.54
E1-095	Institute of Earth Sciences, Heidelberg University	13.71	84.57	1865.43	12.81	-11.15	-4.41
E1-096	Institute of Earth Sciences, Heidelberg University	13.96	86.40	1863.60	12.77	-11.08	-4.65
E1-097	Institute of Earth Sciences, Heidelberg University	14.21	88.22	1861.78	12.66	-11.46	-4.47
E1-098	Institute of Earth Sciences, Heidelberg University	14.46	90.00	1860.00	12.61	-11.32	-4.31
E1-099	Institute of Earth Sciences, Heidelberg University	14.71	91.77	1858.23	12.58	-11.47	-4.41
E1-100	Institute of Earth Sciences, Heidelberg University	14.96	93.55	1856.45	12.50	-11.23	-5.28
E1-101	Institute of Earth Sciences, Heidelberg University	15.21	95.31	1854.69	12.44	-10.34	-4.45
E1-102	Institute of Earth Sciences, Heidelberg University	15.46	97.10	1852.90	12.39	-9.92	-4.31
E1-103	Institute of Earth Sciences, Heidelberg University	15.71	98.83	1851.17	12.34	-9.72	-4.32
E1-104	Institute of Earth Sciences, Heidelberg University	15.96	100.59	1849.41	12.26	-9.47	-4.66
E1-105	Institute of Earth Sciences, Heidelberg University	16.21	102.32	1847.68	12.17	-9.65	-4.87
E1-106	Institute of Earth Sciences, Heidelberg University	16.46	104.06	1845.94	12.09	-9.67	-4.94
E1-107	Institute of Earth Sciences, Heidelberg University	16.71	105.77	1844.23	12.00	-9.32	-4.80
E1-108	Institute of Earth Sciences, Heidelberg University	16.96	107.51	1842.49	11.93	-9.35	-4.71
E1-109	Institute of Earth Sciences, Heidelberg University	17.21	109.21	1840.79	11.86	-9.46	-4.89
E1-110	Institute of Earth Sciences, Heidelberg University	17.46	110.93	1839.07	11.81	-9.11	-4.88
E1-111	Institute of Earth Sciences, Heidelberg University	17.71	112.60	1837.40	11.76	-9.35	-5.08
E1-112	Institute of Earth Sciences, Heidelberg University	17.96	114.33	1835.67	11.72	-9.38	-4.99
E1-113	Institute of Earth Sciences, Heidelberg University	18.21	116.01	1833.99	11.67	-9.28	-4.65
E1-114	Institute of Earth Sciences, Heidelberg University	18.46	117.65	1832.35	11.64	-9.25	-4.81
E1-115	Institute of Earth Sciences, Heidelberg University	18.71	119.31	1830.69	11.62	-9.42	-4.80
E1-116	Institute of Earth Sciences, Heidelberg University	18.96	120.99	1829.01	11.57	-9.15	-5.11
E1-117	Institute of Earth Sciences, Heidelberg University	19.21	122.60	1827.40	11.52	-9.20	-4.54
E1-118	Institute of Earth Sciences, Heidelberg University	19.46	124.19	1825.81	11.49	-8.82	-4.22
E1-119	Institute of Earth Sciences, Heidelberg University	19.71	125.73	1824.27	11.46	-9.01	-4.38
E1-120	Institute of Earth Sciences, Heidelberg University	19.96	127.27	1822.73	11.43	-9.04	-4.31
E1-121	Institute of Earth Sciences, Heidelberg University	20.21	128.79	1821.21	11.40	-8.90	-4.39
E1-122	Institute of Earth Sciences, Heidelberg University	20.46	130.32	1819.68	11.39	-8.91	-4.36
E1-123	Institute of Earth Sciences, Heidelberg University	20.71	131.83	1818.17	11.34	-9.51	-4.64
E1-124	Institute of Earth Sciences, Heidelberg University	20.96	133.24	1816.76	11.25	-9.35	-4.89
E1-125	Institute of Earth Sciences, Heidelberg University	21.21	134.70	1815.30	11.20	-9.23	-4.52
E1-126	Institute of Earth Sciences, Heidelberg University	21.46	136.12	1813.88	11.10	-9.45	-4.53
E1-127	Institute of Earth Sciences, Heidelberg University	21.71	137.37	1812.63	11.04	-9.61	-4.57
E1-128	Institute of Earth Sciences, Heidelberg University	21.96	138.59	1811.41	10.96	-9.56	-4.77
E1-129	Institute of Earth Sciences, Heidelberg University	22.21	139.89	1810.11	10.73	-9.93	-4.91
E1-130	Institute of Earth Sciences, Heidelberg University	22.46	141.07	1808.93	10.52	-9.51	-4.77
E1-131	Institute of Earth Sciences, Heidelberg University	22.71	142.30	1807.70	10.29	-9.64	-4.83
E1-133	Institute of Earth Sciences, Heidelberg University	23.21	145.18	1804.82	9.48	-9.26	-4.68
E1-134	Institute of Earth Sciences, Heidelberg University	23.46	146.76	1803.24	8.91	-8.94	-4.75
E1-135	Institute of Earth Sciences, Heidelberg University	23.71	148.45	1801.55	8.20	-8.66	-4.38
E1-136	Institute of Earth Sciences, Heidelberg University	23.96	150.48	1799.52	6.94	-9.58	-4.48
E1-137	Institute of Earth Sciences, Heidelberg University	24.21	151.52	1798.48	6.47	-9.41	-4.29
E1-138	Institute of Earth Sciences, Heidelberg University	24.46	152.10	1797.90	6.52	-9.64	-4.24
E1-139	Institute of Earth Sciences, Heidelberg University	24.71	152.29	1797.71	7.10	-9.72	-4.36
E1-140	Institute of Earth Sciences, Heidelberg University	24.96	152.45	1797.55	7.83	-10.18	-4.61
E1-141	Institute of Earth Sciences, Heidelberg University	25.21	153.04	1796.96	7.98	-10.01	-4.99
E1-142	Institute of Earth Sciences, Heidelberg University	25.46	153.44	1796.56	8.45	-10.14	-4.99
E1-143	Institute of Earth Sciences, Heidelberg University	25.71	154.05	1795.95	8.75	-10.30	-4.90
E1-144	Institute of Earth Sciences, Heidelberg University	25.96	154.76	1795.24	8.83	-10.07	-4.88
E1-145	Institute of Earth Sciences, Heidelberg University	26.21	155.54	1794.46	8.91	-10.33	-5.03
E1-146	Institute of Earth Sciences, Heidelberg University	26.46	156.31	1793.69	9.05	-10.07	-5.02
E1-147	Institute of Earth Sciences, Heidelberg University	26.71	157.29	1792.71	9.02	-10.46	-5.38
E1-148	Institute of Earth Sciences, Heidelberg University	26.96	158.30	1791.70	9.02	-10.29	-5.64
E1-149	Institute of Earth Sciences, Heidelberg University	27.21	159.40	1790.60	8.95	-10.06	-5.63
E1-150	Institute of Earth Sciences, Heidelberg University	27.46	160.60	1789.40	8.90	-10.25	-5.42
E1-151	Institute of Earth Sciences, Heidelberg University	27.71	161.83	1788.17	8.80	-10.13	-5.33
E1-152	Institute of Earth Sciences, Heidelberg University	27.96	163.06	1786.94	8.73	-9.90	-5.15
E1-154	Institute of Earth Sciences, Heidelberg University	28.46	165.54	1784.46	8.67	-9.91	-5.23
E1-155	Institute of Earth Sciences, Heidelberg University	28.71	166.73	1783.27	8.73	-9.99	-5.27
E1-156	Institute of Earth Sciences, Heidelberg University	28.96	168.03	1781.97	8.66	-9.77	-5.25
E1-158	Institute of Earth Sciences, Heidelberg University	29.46	170.58	1779.42	8.57	-9.65	-5.16

E1-159	Institute of Earth Sciences, Heidelberg University	29.71	171.83	1778.17	8.58	-9.15	-4.50
E1-160	Institute of Earth Sciences, Heidelberg University	29.96	172.95	1777.05	8.62	-9.63	-4.66
E1-161	Institute of Earth Sciences, Heidelberg University	30.21	174.10	1775.90	8.72	-8.96	-4.35
E1-162	Institute of Earth Sciences, Heidelberg University	30.46	175.27	1774.73	8.76	-9.75	-4.78
E1-163	Institute of Earth Sciences, Heidelberg University	30.71	176.29	1773.71	8.79	-10.13	-4.81
E1-165	Institute of Earth Sciences, Heidelberg University	31.21	178.46	1771.54	8.69	-10.15	-4.50
E1-166	Institute of Earth Sciences, Heidelberg University	31.46	179.61	1770.39	8.48	-10.22	-4.37
E1-167	Institute of Earth Sciences, Heidelberg University	31.71	180.71	1769.29	8.31	-10.55	-4.44
E1-168	Institute of Earth Sciences, Heidelberg University	31.96	181.88	1768.12	8.13	-10.90	-4.96
E1-169	Institute of Earth Sciences, Heidelberg University	32.21	182.97	1767.03	7.93	-10.96	-5.08
E1-170	Institute of Earth Sciences, Heidelberg University	32.46	184.16	1765.84	7.67	-10.74	-5.28
E1-171	Institute of Earth Sciences, Heidelberg University	32.71	185.45	1764.55	7.33	-10.05	-5.42
E1-172	Institute of Earth Sciences, Heidelberg University	32.96	186.59	1763.41	7.15	-9.77	-4.99
E1-175	Institute of Earth Sciences, Heidelberg University	33.71	190.03	1759.97	6.66	-10.10	-4.26
E1-176	Institute of Earth Sciences, Heidelberg University	33.96	191.01	1758.99	6.64	-9.91	-4.04
E1-180	Institute of Earth Sciences, Heidelberg University	34.96	194.61	1755.39	6.62	-10.72	-4.42
E1-181	Institute of Earth Sciences, Heidelberg University	35.21	195.41	1754.59	6.53	-10.77	-4.47
E1-182	Institute of Earth Sciences, Heidelberg University	35.46	196.11	1753.89	6.40	-11.07	-4.72
E1-183	Institute of Earth Sciences, Heidelberg University	35.71	196.82	1753.18	6.14	-11.19	-4.85
E1-184	Institute of Earth Sciences, Heidelberg University	35.96	197.56	1752.44	5.93	-11.00	-5.40
E1-185	Institute of Earth Sciences, Heidelberg University	36.21	198.21	1751.79	5.73	-10.96	-5.94
E1-186	Institute of Earth Sciences, Heidelberg University	36.46	198.94	1751.06	5.56	-11.00	-6.15
E1-187	Institute of Earth Sciences, Heidelberg University	36.71	199.60	1750.40	5.39	-10.58	-6.07
E1-188	Institute of Earth Sciences, Heidelberg University	36.96	200.32	1749.68	5.35	-10.49	-6.24
E1-189	Institute of Earth Sciences, Heidelberg University	37.21	201.07	1748.93	5.44	-10.13	-5.98
E1-190	Institute of Earth Sciences, Heidelberg University	37.46	201.88	1748.12	5.67	-9.88	-5.73
E1-191	Institute of Earth Sciences, Heidelberg University	37.71	202.65	1747.35	5.85	-9.96	-5.96
E1-192	Institute of Earth Sciences, Heidelberg University	37.96	203.42	1746.58	5.92	-10.03	-5.98
E1-193	Institute of Earth Sciences, Heidelberg University	38.21	204.26	1745.74	6.17	-9.71	-5.94
E1-194	Institute of Earth Sciences, Heidelberg University	38.46	205.04	1744.96	6.30	-10.09	-5.74
E1-195	Institute of Earth Sciences, Heidelberg University	38.71	205.85	1744.15	6.44	-10.46	-5.33
E1-196	Institute of Earth Sciences, Heidelberg University	38.96	206.73	1743.27	6.64	-10.30	-5.10
E1-197	Institute of Earth Sciences, Heidelberg University	39.21	207.66	1742.34	6.65	-9.73	-4.89
E1-199	Institute of Earth Sciences, Heidelberg University	39.71	209.66	1740.34	6.71	-9.94	-4.32
E1-200	Institute of Earth Sciences, Heidelberg University	39.96	210.72	1739.28	6.76	-10.84	-4.55
E1-201	Institute of Earth Sciences, Heidelberg University	40.21	211.74	1738.26	6.77	-10.79	-5.41
E1-202	Institute of Earth Sciences, Heidelberg University	40.46	212.80	1737.20	6.78	-10.40	-5.36
E1-203	Institute of Earth Sciences, Heidelberg University	40.71	213.87	1736.13	6.78	-10.36	-5.17
E1-204	Institute of Earth Sciences, Heidelberg University	40.96	214.94	1735.06	6.80	-10.19	-4.94
E1-205	Institute of Earth Sciences, Heidelberg University	41.21	216.01	1733.99	6.83	-10.12	-4.41
E1-206	Institute of Earth Sciences, Heidelberg University	41.46	217.14	1732.86	6.86	-10.19	-4.41
E1-207	Institute of Earth Sciences, Heidelberg University	41.71	218.25	1731.75	6.91	-10.30	-4.20
E1-208	Institute of Earth Sciences, Heidelberg University	41.96	219.35	1730.65	6.97	-10.22	-4.18
E1-209	Institute of Earth Sciences, Heidelberg University	42.21	220.48	1729.52	7.06	-10.27	-4.27
E1-210	Institute of Earth Sciences, Heidelberg University	42.46	221.68	1728.32	7.18	-10.37	-4.33
E1-211	Institute of Earth Sciences, Heidelberg University	42.71	222.80	1727.20	7.32	-10.55	-4.30
E1-212	Institute of Earth Sciences, Heidelberg University	42.96	223.98	1726.02	7.47	-10.89	-4.46
E1-213	Institute of Earth Sciences, Heidelberg University	43.21	225.14	1724.86	7.62	-10.99	-4.60
E1-215	Institute of Earth Sciences, Heidelberg University	43.71	227.46	1722.54	8.01	-10.92	-4.80
E1-216	Institute of Earth Sciences, Heidelberg University	43.96	228.64	1721.36	8.20	-11.01	-5.00
E1-217	Institute of Earth Sciences, Heidelberg University	44.21	229.83	1720.17	8.42	-10.82	-4.97
E1-219	Institute of Earth Sciences, Heidelberg University	44.71	232.26	1717.74	8.84	-10.74	-5.12
E1-220	Institute of Earth Sciences, Heidelberg University	44.96	233.46	1716.54	9.03	-10.98	-5.19
E1-221	Institute of Earth Sciences, Heidelberg University	45.21	234.65	1715.35	9.25	-10.80	-5.16
E1-222	Institute of Earth Sciences, Heidelberg University	45.46	235.84	1714.16	9.46	-10.30	-4.87
E1-223	Institute of Earth Sciences, Heidelberg University	45.71	237.03	1712.97	9.65	-10.29	-4.65
E1-224	Institute of Earth Sciences, Heidelberg University	45.96	238.17	1711.83	9.82	-10.39	-4.76
E1-225	Institute of Earth Sciences, Heidelberg University	46.21	239.35	1710.65	10.01	-10.30	-4.87
E1-226	Institute of Earth Sciences, Heidelberg University	46.46	240.57	1709.43	10.19	-10.35	-4.88
E1-227	Institute of Earth Sciences, Heidelberg University	46.71	241.71	1708.29	10.39	-10.64	-5.16
E1-228	Institute of Earth Sciences, Heidelberg University	46.96	242.89	1707.11	10.59	-10.36	-5.09
E1-229	Institute of Earth Sciences, Heidelberg University	47.21	244.08	1705.92	10.80	-10.55	-5.18
E1-230	Institute of Earth Sciences, Heidelberg University	47.46	245.26	1704.74	11.00	-10.40	-5.32
E1-231	Institute of Earth Sciences, Heidelberg University	47.71	246.44	1703.56	11.18	-10.58	-5.10
E1-232	Institute of Earth Sciences, Heidelberg University	47.96	247.60	1702.40	11.29	-10.77	-5.55
E1-233	Institute of Earth Sciences, Heidelberg University	48.21	248.69	1701.31	11.40	-10.78	-5.48
E1-234	Institute of Earth Sciences, Heidelberg University	48.46	249.71	1700.29	11.50	-11.04	-5.54
E1-235	Institute of Earth Sciences, Heidelberg University	48.71	250.67	1699.33	11.41	-10.61	-5.41
E1-236	Institute of Earth Sciences, Heidelberg University	48.96	251.59	1698.41	11.40	-11.23	-5.79
E1-240	Institute of Earth Sciences, Heidelberg University	49.96	254.15	1695.85	9.38	-10.47	-5.03
E1-243	Institute of Earth Sciences, Heidelberg University	50.71	254.61	1695.39	6.71	-10.44	-5.58
E1-244	Institute of Earth Sciences, Heidelberg University	50.96	254.95	1695.05	6.39	-10.57	-5.57
E1-245	Institute of Earth Sciences, Heidelberg University	51.21	255.44	1694.56	6.47	-10.52	-5.46
E1-246	Institute of Earth Sciences, Heidelberg University	51.46	256.00	1694.00	6.64	-10.92	-5.66
E1-247	Institute of Earth Sciences, Heidelberg University	51.71	256.64	1693.36	7.10	-10.50	-5.58
E1-248	Institute of Earth Sciences, Heidelberg University	51.96	257.78	1692.22	8.34	-10.67	-5.39
E1-249	Institute of Earth Sciences, Heidelberg University	52.21	259.15	1690.85	9.69	-10.65	-5.27
E1-250	Institute of Earth Sciences, Heidelberg University	52.46	261.37	1688.63	11.90	-10.77	-5.43
E1-251	Institute of Earth Sciences, Heidelberg University	52.71	263.13	1686.87	13.10	-10.80	-5.51
E1-252	Institute of Earth Sciences, Heidelberg University	52.96	264.89	1685.11	14.23	-10.62	-5.41

E1-253	Institute of Earth Sciences, Heidelberg University	53.21	266.43	1683.57	15.11	-10.75	-5.21
E1-254	Institute of Earth Sciences, Heidelberg University	53.46	267.72	1682.28	15.66	-10.56	-4.94
E1-255	Institute of Earth Sciences, Heidelberg University	53.71	268.88	1681.12	16.06	-10.69	-4.43
E1-256	Institute of Earth Sciences, Heidelberg University	53.96	270.40	1679.60	16.69	-11.18	-5.24
E1-257	Institute of Earth Sciences, Heidelberg University	54.21	271.81	1678.19	16.92	-11.30	-5.24
E1-258	Institute of Earth Sciences, Heidelberg University	54.46	273.31	1676.69	16.98	-10.81	-5.11
E1-259	Institute of Earth Sciences, Heidelberg University	54.71	274.98	1675.02	17.13	-11.14	-5.02
E1-260	Institute of Earth Sciences, Heidelberg University	54.96	276.63	1673.37	17.13	-11.30	-5.10
E1-261	Institute of Earth Sciences, Heidelberg University	55.21	278.34	1671.66	17.19	-11.02	-4.97
E1-262	Institute of Earth Sciences, Heidelberg University	55.46	280.25	1669.75	17.42	-11.08	-5.11
E1-263	Institute of Earth Sciences, Heidelberg University	55.71	282.00	1668.00	17.65	-10.88	-5.15
E1-264	Institute of Earth Sciences, Heidelberg University	55.96	283.83	1666.17	17.83	-11.14	-5.18
E1-266	Institute of Earth Sciences, Heidelberg University	56.46	287.62	1662.38	18.07	-10.94	-5.27
E1-267	Institute of Earth Sciences, Heidelberg University	56.71	289.58	1660.42	18.25	-11.14	-5.17
E1-268	Institute of Earth Sciences, Heidelberg University	56.96	291.58	1658.42	18.56	-10.75	-5.28
E1-269	Institute of Earth Sciences, Heidelberg University	57.21	293.70	1656.30	19.01	-10.85	-5.09
E1-270	Institute of Earth Sciences, Heidelberg University	57.46	295.59	1654.41	19.37	-11.02	-5.01
E1-271	Institute of Earth Sciences, Heidelberg University	57.71	297.39	1652.61	19.83	-11.29	-4.88
E1-272	Institute of Earth Sciences, Heidelberg University	57.96	299.24	1650.76	20.45	-11.38	-5.00
E1-273	Institute of Earth Sciences, Heidelberg University	58.21	300.95	1649.05	20.86	-11.38	-4.97
E1-274	Institute of Earth Sciences, Heidelberg University	58.46	302.65	1647.35	21.29	-12.41	-7.14
E1-275	Institute of Earth Sciences, Heidelberg University	58.71	304.18	1645.82	21.74	-11.64	-4.78
E1-277	Institute of Earth Sciences, Heidelberg University	59.21	307.23	1642.77	22.69	-11.92	-4.87
E1-279	Institute of Earth Sciences, Heidelberg University	59.71	309.69	1640.31	23.40	-11.79	-4.83
E1-283	Institute of Earth Sciences, Heidelberg University	61.7	375.07	1574.93	40.65	-11.82	-4.82
E1-284	Institute of Earth Sciences, Heidelberg University	61.95	375.98	1574.02	40.28	-11.50	-4.55
E1-285	Institute of Earth Sciences, Heidelberg University	62.2	376.95	1573.05	39.80	-11.50	-4.93
E1-286	Institute of Earth Sciences, Heidelberg University	62.45	377.86	1572.14	39.22	-10.63	-4.98
E1-287	Institute of Earth Sciences, Heidelberg University	62.7	378.82	1571.18	38.84	-10.67	-4.99
E1-288	Institute of Earth Sciences, Heidelberg University	62.95	379.73	1570.27	38.54	-11.15	-5.31
E1-289	Institute of Earth Sciences, Heidelberg University	63.2	380.67	1569.33	38.20	-11.22	-5.48
E1-290	Institute of Earth Sciences, Heidelberg University	63.45	381.57	1568.43	37.79	-11.63	-5.65
E1-291	Institute of Earth Sciences, Heidelberg University	63.7	382.45	1567.55	37.31	-11.77	-5.62
E1-292	Institute of Earth Sciences, Heidelberg University	63.95	383.31	1566.69	37.02	-11.76	-5.88
E1-293	Institute of Earth Sciences, Heidelberg University	64.2	384.22	1565.78	36.60	-11.44	-5.69
E1-294	Institute of Earth Sciences, Heidelberg University	64.45	385.06	1564.94	36.19	-11.44	-5.48
E1-295	Institute of Earth Sciences, Heidelberg University	64.7	386.21	1563.79	35.53	-11.14	-5.57
E1-296	Institute of Earth Sciences, Heidelberg University	64.95	387.18	1562.82	35.13	-10.96	-5.63
E1-297	Institute of Earth Sciences, Heidelberg University	65.2	387.95	1562.05	34.72	-10.89	-5.64
E1-298	Institute of Earth Sciences, Heidelberg University	65.45	388.88	1561.12	34.28	-10.71	-5.07
E1-299	Institute of Earth Sciences, Heidelberg University	65.7	389.67	1560.33	33.99	-10.87	-5.10
E1-300	Institute of Earth Sciences, Heidelberg University	65.95	390.56	1559.44	33.76	-10.63	-5.13
E1-301	Institute of Earth Sciences, Heidelberg University	66.2	391.37	1558.63	33.45	-10.78	-5.45
E1-302	Institute of Earth Sciences, Heidelberg University	66.45	392.22	1557.78	33.15	-10.97	-5.55
E1-303	Institute of Earth Sciences, Heidelberg University	66.7	393.00	1557.00	32.80	-10.70	-5.55
E1-305	Institute of Earth Sciences, Heidelberg University	67.2	394.78	1555.22	31.98	-9.85	-5.68
E1-306	Institute of Earth Sciences, Heidelberg University	67.45	395.71	1554.29	31.54	-10.35	-5.81
E1-307	Institute of Earth Sciences, Heidelberg University	67.7	396.62	1553.38	31.17	-10.08	-5.69
E1-308	Institute of Earth Sciences, Heidelberg University	67.95	397.64	1552.36	30.71	-10.20	-5.70
E1-309	Institute of Earth Sciences, Heidelberg University	68.2	398.46	1551.54	30.33	-10.23	-5.42
E1-310	Institute of Earth Sciences, Heidelberg University	68.45	399.31	1550.69	29.90	-10.33	-5.50
E1-311	Institute of Earth Sciences, Heidelberg University	68.7	400.20	1549.80	29.49	-10.24	-5.24
E1-312	Institute of Earth Sciences, Heidelberg University	68.95	401.07	1548.93	29.01	-10.41	-5.61
E1-313	Institute of Earth Sciences, Heidelberg University	69.2	401.95	1548.05	28.57	-10.19	-5.69
E1-314	Institute of Earth Sciences, Heidelberg University	69.45	402.90	1547.10	28.13	-10.13	-5.89
E1-315	Institute of Earth Sciences, Heidelberg University	69.7	403.78	1546.22	27.67	-10.02	-5.95
E1-316	Institute of Earth Sciences, Heidelberg University	69.95	404.65	1545.35	27.18	-10.09	-5.82
E1-317	Institute of Earth Sciences, Heidelberg University	70.2	405.51	1544.49	26.68	-10.23	-5.62
E1-318	Institute of Earth Sciences, Heidelberg University	70.45	406.19	1543.81	26.36	-10.20	-5.48
E1-319	Institute of Earth Sciences, Heidelberg University	70.7	407.15	1542.85	25.64	-10.27	-5.38
E1-320	Institute of Earth Sciences, Heidelberg University	70.95	408.08	1541.92	25.01	-9.97	-5.13
E1-321	Institute of Earth Sciences, Heidelberg University	71.2	408.92	1541.08	24.44	-10.02	-5.10
E1-322	Institute of Earth Sciences, Heidelberg University	71.45	409.76	1540.24	24.01	-9.96	-5.19
E1-323	Institute of Earth Sciences, Heidelberg University	71.7	410.69	1539.31	23.28	-9.89	-5.20
E1-324	Institute of Earth Sciences, Heidelberg University	71.95	411.58	1538.42	22.53	-9.85	-5.14
E1-325	Institute of Earth Sciences, Heidelberg University	72.2	412.25	1537.75	22.21	-9.91	-5.29
E1-326	Institute of Earth Sciences, Heidelberg University	72.45	413.06	1536.94	21.69	-9.83	-5.35
E1-327	Institute of Earth Sciences, Heidelberg University	72.7	413.91	1536.09	20.94	-10.00	-5.47
E1-328	Institute of Earth Sciences, Heidelberg University	72.95	414.89	1535.11	20.00	-9.83	-5.30
E1-329	Institute of Earth Sciences, Heidelberg University	73.2	415.70	1534.30	19.55	-10.19	-5.65
E1-330	Institute of Earth Sciences, Heidelberg University	73.45	416.57	1533.43	18.66	-9.88	-5.49
E1-331	Institute of Earth Sciences, Heidelberg University	73.7	417.43	1532.57	18.08	-9.99	-5.41
E1-333	Institute of Earth Sciences, Heidelberg University	74.2	419.34	1530.66	16.30	-10.01	-5.52
E1-334	Institute of Earth Sciences, Heidelberg University	74.45	420.29	1529.71	15.46	-10.03	-5.52
E1-335	Institute of Earth Sciences, Heidelberg University	74.7	421.36	1528.64	14.40	-10.12	-5.52
E1-336	Institute of Earth Sciences, Heidelberg University	74.95	422.24	1527.76	13.71	-10.17	-5.34
E1-337	Institute of Earth Sciences, Heidelberg University	75.2	422.98	1527.02	13.60	-9.47	-4.78
E1-338	Institute of Earth Sciences, Heidelberg University	75.45	423.82	1526.18	13.73	-9.43	-4.71
E1-339	Institute of Earth Sciences, Heidelberg University	75.7	424.61	1525.39	13.71	-9.46	-4.62
E1-340	Institute of Earth Sciences, Heidelberg University	75.95	425.30	1524.70	13.62	-9.04	-4.47

E1-341	Institute of Earth Sciences, Heidelberg University	76.2	426.12	1523.88	13.37	-8.90	-4.34
E1-342	Institute of Earth Sciences, Heidelberg University	76.45	426.96	1523.04	13.28	-9.21	-4.41
E1-343	Institute of Earth Sciences, Heidelberg University	76.7	427.69	1522.31	13.20	-9.27	-4.38
E1-344	Institute of Earth Sciences, Heidelberg University	76.95	428.38	1521.62	13.13	-9.78	-4.92
E1-345	Institute of Earth Sciences, Heidelberg University	77.2	429.21	1520.79	13.01	-9.39	-4.83
E1-346	Institute of Earth Sciences, Heidelberg University	77.45	429.86	1520.14	13.14	-8.97	-5.18
E1-347	Institute of Earth Sciences, Heidelberg University	77.7	430.73	1519.27	13.06	-9.38	-5.07
E1-348	Institute of Earth Sciences, Heidelberg University	77.95	431.66	1518.34	12.97	-9.62	-5.22
E1-349	Institute of Earth Sciences, Heidelberg University	78.2	432.51	1517.49	12.95	-9.71	-5.29
E1-350	Institute of Earth Sciences, Heidelberg University	78.45	433.32	1516.68	12.99	-9.86	-5.23
E1-351	Institute of Earth Sciences, Heidelberg University	78.7	434.01	1515.99	13.02	-10.14	-5.63
E1-352	Institute of Earth Sciences, Heidelberg University	78.95	434.82	1515.18	13.10	-9.96	-5.56
E1-353	Institute of Earth Sciences, Heidelberg University	79.2	435.66	1514.34	13.05	-10.00	-5.89
E1-354	Institute of Earth Sciences, Heidelberg University	79.45	436.43	1513.57	13.11	-9.95	-5.88
E1-355	Institute of Earth Sciences, Heidelberg University	79.7	437.22	1512.78	13.13	-9.99	-5.87
E1-356	Institute of Earth Sciences, Heidelberg University	79.95	438.07	1511.93	13.08	-10.40	-6.20
E1-357	Institute of Earth Sciences, Heidelberg University	80.2	438.95	1511.05	13.17	-9.61	-5.81
E1-358	Institute of Earth Sciences, Heidelberg University	80.45	439.72	1510.28	13.12	-10.17	-5.97
E1-359	Institute of Earth Sciences, Heidelberg University	80.7	440.46	1509.54	13.13	-9.77	-5.82
E1-360	Institute of Earth Sciences, Heidelberg University	80.95	441.23	1508.77	13.26	-9.81	-5.92
E1-361	Institute of Earth Sciences, Heidelberg University	81.2	442.08	1507.92	13.33	-10.36	-6.37
E1-362	Institute of Earth Sciences, Heidelberg University	81.45	442.86	1507.14	13.52	-9.86	-6.13
E1-363	Institute of Earth Sciences, Heidelberg University	81.7	443.71	1506.29	13.41	-9.74	-6.19
E1-364	Institute of Earth Sciences, Heidelberg University	81.95	444.47	1505.53	13.66	-10.33	-6.25
E1-365	Institute of Earth Sciences, Heidelberg University	82.2	445.24	1504.76	13.75	-10.35	-7.09
E1-366	Institute of Earth Sciences, Heidelberg University	82.45	445.97	1504.03	13.66	-10.05	-6.23
E1-367	Institute of Earth Sciences, Heidelberg University	82.7	446.77	1503.23	13.66	-10.24	-6.54
E1-368	Institute of Earth Sciences, Heidelberg University	82.95	447.53	1502.47	13.89	-10.50	-6.10
E1-369	Institute of Earth Sciences, Heidelberg University	83.2	448.37	1501.63	13.92	-10.12	-6.17
E1-370	Institute of Earth Sciences, Heidelberg University	83.45	449.24	1500.76	13.88	-10.58	-6.08
E1-371	Institute of Earth Sciences, Heidelberg University	83.7	450.07	1499.93	13.75	-10.19	-5.82
E1-372	Institute of Earth Sciences, Heidelberg University	83.95	450.84	1499.16	13.82	-9.96	-5.59
E1-374	Institute of Earth Sciences, Heidelberg University	84.45	452.36	1497.64	13.58	-10.41	-4.89
E1-375	Institute of Earth Sciences, Heidelberg University	84.7	453.12	1496.88	13.36	-9.99	-5.05
E1-376	Institute of Earth Sciences, Heidelberg University	84.95	453.92	1496.08	13.22	-10.06	-4.75
E1-377	Institute of Earth Sciences, Heidelberg University	85.2	454.61	1495.39	12.91	-10.22	-4.48
E1-378	Institute of Earth Sciences, Heidelberg University	85.45	455.37	1494.63	12.98	-9.36	-4.35
E1-379	Institute of Earth Sciences, Heidelberg University	85.7	456.20	1493.80	12.95	-10.28	-4.60
E1-380	Institute of Earth Sciences, Heidelberg University	85.95	456.99	1493.01	12.84	-10.66	-4.58
E1-381	Institute of Earth Sciences, Heidelberg University	86.2	457.79	1492.21	12.70	-11.16	-4.71
E1-382	Institute of Earth Sciences, Heidelberg University	86.45	458.50	1491.50	12.68	-11.04	-4.45
E1-384	Institute of Earth Sciences, Heidelberg University	86.95	460.25	1489.75	13.01	-11.59	-5.11
E1-385	Institute of Earth Sciences, Heidelberg University	87.2	461.08	1488.92	13.30	-11.60	-5.27
E1-387	Institute of Earth Sciences, Heidelberg University	87.7	462.96	1487.04	14.30	-11.60	-5.38
E1-388	Institute of Earth Sciences, Heidelberg University	87.95	463.84	1486.16	14.73	-11.50	-5.35
E1-389	Institute of Earth Sciences, Heidelberg University	88.2	464.75	1485.25	15.21	-11.03	-5.43
E1-390	Institute of Earth Sciences, Heidelberg University	88.45	465.67	1484.33	15.72	-11.37	-5.49
E1-391	Institute of Earth Sciences, Heidelberg University	88.7	466.61	1483.39	16.19	-11.36	-5.64
E1-392	Institute of Earth Sciences, Heidelberg University	88.95	467.62	1482.38	16.53	-11.13	-5.54
E1-393	Institute of Earth Sciences, Heidelberg University	89.2	468.58	1481.42	16.82	-11.17	-5.50
E1-394	Institute of Earth Sciences, Heidelberg University	89.45	469.67	1480.33	17.36	-11.04	-5.78
E1-395	Institute of Earth Sciences, Heidelberg University	89.7	470.74	1479.26	18.05	-10.92	-5.58
E1-396	Institute of Earth Sciences, Heidelberg University	89.95	471.90	1478.10	18.47	-11.29	-5.51
E1-397	Institute of Earth Sciences, Heidelberg University	90.2	473.22	1476.78	19.00	-11.24	-5.48
E1-398	Institute of Earth Sciences, Heidelberg University	90.45	474.60	1475.40	19.89	-11.11	-5.26
E1-399	Institute of Earth Sciences, Heidelberg University	90.7	476.49	1473.51	20.39	-11.06	-5.28
E1-400	Institute of Earth Sciences, Heidelberg University	90.95	478.90	1471.10	20.37	-11.32	-5.39
E1-401	Institute of Earth Sciences, Heidelberg University	91.2	481.73	1468.27	20.16	-11.48	-5.65
E1-402	Institute of Earth Sciences, Heidelberg University	91.45	484.92	1465.08	20.34	-11.27	-5.70
E1-403	Institute of Earth Sciences, Heidelberg University	91.7	488.12	1461.88	21.04	-11.15	-5.61
E1-404	Institute of Earth Sciences, Heidelberg University	91.95	490.74	1459.26	21.83	-11.12	-5.42
E1-405	Institute of Earth Sciences, Heidelberg University	92.2	492.70	1457.30	22.76	-11.15	-5.54
E1-406	Institute of Earth Sciences, Heidelberg University	92.45	494.06	1455.94	23.81	-11.40	-5.56
E1-408	Institute of Earth Sciences, Heidelberg University	92.95	496.41	1453.59	25.75	-11.60	-6.08
E1-409	Institute of Earth Sciences, Heidelberg University	93.2	497.50	1452.50	26.96	-11.51	-5.99
E1-410	Institute of Earth Sciences, Heidelberg University	93.45	498.53	1451.47	28.12	-11.68	-6.25
E1-411	Institute of Earth Sciences, Heidelberg University	93.7	499.36	1450.64	29.07	-11.57	-6.17
E1-412	Institute of Earth Sciences, Heidelberg University	93.95	500.21	1449.79	29.87	-11.44	-6.34
E1-413	Institute of Earth Sciences, Heidelberg University	94.2	500.95	1449.05	30.84	-11.56	-6.27
E1-414	Institute of Earth Sciences, Heidelberg University	94.45	501.74	1448.26	31.66	-11.32	-6.32
E1-415	Institute of Earth Sciences, Heidelberg University	94.7	502.57	1447.43	32.59	-11.26	-5.98
E1-416	Institute of Earth Sciences, Heidelberg University	94.95	503.36	1446.64	33.41	-11.36	-5.48
E1-417	Institute of Earth Sciences, Heidelberg University	95.2	504.28	1445.72	34.29	-11.71	-5.79
E1-418	Institute of Earth Sciences, Heidelberg University	95.45	505.25	1444.75	35.22	-10.96	-5.52
E1-419	Institute of Earth Sciences, Heidelberg University	95.7	506.22	1443.78	36.12	-10.08	-4.91

Table S 6 Stable isotope data of speleothem E23-3. The age of each sample corresponds to the chronology discussed in the main text.

Sample ID	Lab	dft [cm]	Age [a BP]	Age [a AD]	Age error [a]	$\delta^{13}C$ [‰ VPDB]	$\delta^{18}O$ [‰ VPDB]
E23-3-001	Institute of Earth Sciences, Heidelberg University	0.15	-70.84	2020.84		-11.92	-5.04
E23-3-002	Institute of Earth Sciences, Heidelberg University	0.4	-68.93	2018.93		-12.31	-5.02
E23-3-003	Institute of Earth Sciences, Heidelberg University	0.65	-67.34	2017.34		-12.07	-4.95
E23-3-004	Institute of Earth Sciences, Heidelberg University	0.9	-65.61	2015.61		-12.28	-5.08
E23-3-005	Institute of Earth Sciences, Heidelberg University	1.15	-64.11	2014.11		-12.26	-5.28
E23-3-006	Institute of Earth Sciences, Heidelberg University	1.4	-62.56	2012.56		-11.73	-5.18
E23-3-007	Institute of Earth Sciences, Heidelberg University	1.65	-61.20	2011.20		-11.76	-5.24
E23-3-008	Institute of Earth Sciences, Heidelberg University	1.9	-59.28	2009.28		-11.93	-4.73
E23-3-009	Institute of Earth Sciences, Heidelberg University	2.15	-57.55	2007.55		-11.50	-4.30
E23-3-010	Institute of Earth Sciences, Heidelberg University	2.4	-56.60	2006.60		-11.15	-4.19
E23-3-011	Institute of Earth Sciences, Heidelberg University	2.65	-55.78	2005.78		-11.08	-4.20
E23-3-012	Institute of Earth Sciences, Heidelberg University	2.9	-54.74	2004.74		-11.03	-4.22
E23-3-013	Institute of Earth Sciences, Heidelberg University	3.15	-53.94	2003.94		-10.88	-4.21
E23-3-014	Institute of Earth Sciences, Heidelberg University	3.4	-52.32	2002.32		-11.13	-4.21
E23-3-015	Institute of Earth Sciences, Heidelberg University	3.65	-50.80	2000.80		-11.02	-4.19
E23-3-016	Institute of Earth Sciences, Heidelberg University	3.9	-50.02	2000.02		-10.73	-4.22
E23-3-017	Institute of Earth Sciences, Heidelberg University	4.15	-49.37	1999.37		-10.56	-4.22
E23-3-018	Institute of Earth Sciences, Heidelberg University	4.4	-48.07	1998.07		-10.00	-4.03
E23-3-019	Institute of Earth Sciences, Heidelberg University	4.65	-47.09	1997.09		-10.36	-4.17
E23-3-020	Institute of Earth Sciences, Heidelberg University	4.9	-46.44	1996.44		-10.79	-4.26
E23-3-021	Institute of Earth Sciences, Heidelberg University	5.15	-45.26	1995.26		-11.31	-4.51
E23-3-022	Institute of Earth Sciences, Heidelberg University	5.4	-44.11	1994.11		-11.00	-4.37
E23-3-023	Institute of Earth Sciences, Heidelberg University	5.65	-42.97	1992.97		-10.89	-4.47
E23-3-024	Institute of Earth Sciences, Heidelberg University	5.9	-40.83	1990.83		-10.20	-4.10
E23-3-025	Institute of Earth Sciences, Heidelberg University	6.15	-40.25	1990.25		-9.68	-3.99
E23-3-026	Institute of Earth Sciences, Heidelberg University	6.4	-38.74	1988.74		-10.48	-4.26
E23-3-027	Institute of Earth Sciences, Heidelberg University	6.65	-37.85	1987.85		-10.06	-4.20
E23-3-028	Institute of Earth Sciences, Heidelberg University	6.9	-36.77	1986.77		-11.07	-4.48
E23-3-029	Institute of Earth Sciences, Heidelberg University	7.15	-35.73	1985.73		-11.02	-4.82
E23-3-030	Institute of Earth Sciences, Heidelberg University	7.4	-35.14	1985.14		-11.38	-5.01
E23-3-031	Institute of Earth Sciences, Heidelberg University	7.65	-34.13	1984.13		-11.16	-5.03
E23-3-032	Institute of Earth Sciences, Heidelberg University	7.9	-33.14	1983.14		-10.60	-4.59
E23-3-033	Institute of Earth Sciences, Heidelberg University	8.15	-32.46	1982.46		-10.74	-4.33
E23-3-034	Institute of Earth Sciences, Heidelberg University	8.4	-31.84	1981.84		-10.17	-4.04
E23-3-035	Institute of Earth Sciences, Heidelberg University	8.65	-31.11	1981.11		-11.24	-4.19
E23-3-036	Institute of Earth Sciences, Heidelberg University	8.9	-30.36	1980.36		-10.91	-3.93
E23-3-037	Institute of Earth Sciences, Heidelberg University	9.15	-29.34	1979.34		-11.06	-4.21
E23-3-038	Institute of Earth Sciences, Heidelberg University	9.4	-28.52	1978.52		-11.13	-4.28
E23-3-039	Institute of Earth Sciences, Heidelberg University	9.65	-27.78	1977.78		-10.92	-4.21
E23-3-040	Institute of Earth Sciences, Heidelberg University	9.9	-26.88	1976.88		-11.13	-4.33
E23-3-041	Institute of Earth Sciences, Heidelberg University	10.15	-26.10	1976.10		-10.91	-4.34
E23-3-042	Institute of Earth Sciences, Heidelberg University	10.4	-24.99	1974.99		-10.60	-4.34
E23-3-043	Institute of Earth Sciences, Heidelberg University	10.65	-23.68	1973.68		-10.89	-4.53
E23-3-044	Institute of Earth Sciences, Heidelberg University	10.9	-21.98	1971.98		-11.15	-4.60
E23-3-045	Institute of Earth Sciences, Heidelberg University	11.15	-20.60	1970.60		-11.33	-4.81
E23-3-046	Institute of Earth Sciences, Heidelberg University	11.4	-19.45	1969.45		-10.81	-4.56
E23-3-047	Institute of Earth Sciences, Heidelberg University	11.65	-18.19	1968.19		-10.43	-4.36
E23-3-048	Institute of Earth Sciences, Heidelberg University	11.9	-17.44	1967.44		-10.39	-4.04
E23-3-049	Institute of Earth Sciences, Heidelberg University	12.15	-16.80	1966.80		-10.51	-4.01
E23-3-050	Institute of Earth Sciences, Heidelberg University	12.4	-15.60	1965.60		-10.74	-4.16
E23-3-051	Institute of Earth Sciences, Heidelberg University	12.65	-13.78	1963.78		-11.25	-4.30
E23-3-052	Institute of Earth Sciences, Heidelberg University	12.9	-12.95	1962.95		-10.77	-4.35
E23-3-053	Institute of Earth Sciences, Heidelberg University	13.15	-11.51	1961.51		-10.82	-4.34
E23-3-054	Institute of Earth Sciences, Heidelberg University	13.4	-10.77	1960.77			
E23-3-055	Institute of Earth Sciences, Heidelberg University	13.65	-10.16	1960.16		-11.02	-4.50
E23-3-056	Institute of Earth Sciences, Heidelberg University	13.9	-9.47	1959.47		-11.21	-4.66
E23-3-057	Institute of Earth Sciences, Heidelberg University	14.15	-8.57	1958.57		-10.88	-4.47
E23-3-058	Institute of Earth Sciences, Heidelberg University	14.4	-7.59	1957.59		-11.33	-4.73
E23-3-059	Institute of Earth Sciences, Heidelberg University	14.65	-6.70	1956.70		-11.35	-4.91
E23-3-060	Institute of Earth Sciences, Heidelberg University	14.9	-5.56	1955.56		-10.61	-4.93
E23-3-061	Institute of Earth Sciences, Heidelberg University	15.15	-4.74	1954.74		-9.91	-5.06
E23-3-062	Institute of Earth Sciences, Heidelberg University	15.4	-4.16	1954.16		-11.05	-5.37
E23-3-063	Institute of Earth Sciences, Heidelberg University	15.65	-3.53	1953.53		-10.43	-5.34
E23-3-064	Institute of Earth Sciences, Heidelberg University	15.9	-2.90	1952.90		-10.26	-5.27
E23-3-065	Institute of Earth Sciences, Heidelberg University	16.15	-2.33	1952.33		-10.81	-5.44
E23-3-066	Institute of Earth Sciences, Heidelberg University	16.4	-1.69	1951.69		-10.07	-5.22
E23-3-067	Institute of Earth Sciences, Heidelberg University	16.65	-0.99	1950.99		-10.45	-4.79
E23-3-068	Institute of Earth Sciences, Heidelberg University	16.9	-0.35	1950.35		-10.81	-4.60
E23-3-069	Institute of Earth Sciences, Heidelberg University	17.15	0.28	1949.72		-10.27	-4.23
E23-3-070	Institute of Earth Sciences, Heidelberg University	17.4	0.90	1949.10		-11.51	-4.65
E23-3-071	Institute of Earth Sciences, Heidelberg University	17.65	1.43	1948.57		-9.73	-4.08
E23-3-072	Institute of Earth Sciences, Heidelberg University	17.9	1.85	1948.15		-10.90	-4.17
E23-3-073	Institute of Earth Sciences, Heidelberg University	18.15	2.27	1947.73		-9.90	-4.15
E23-3-074	Institute of Earth Sciences, Heidelberg University	18.4	2.67	1947.33		-9.84	-4.30
E23-3-075	Institute of Earth Sciences, Heidelberg University	18.65	3.16	1946.84		-10.69	-4.40
E23-3-076	Institute of Earth Sciences, Heidelberg University	18.9	3.79	1946.21		-11.53	-4.60

E23-3-077	Institute of Earth Sciences, Heidelberg University	19.15	4.43	1945.57	-10.60	-4.32
E23-3-078	Institute of Earth Sciences, Heidelberg University	19.4	5.11	1944.89	-10.98	-4.33
E23-3-079	Institute of Earth Sciences, Heidelberg University	19.65	6.01	1943.99	-11.36	-4.58
E23-3-080	Institute of Earth Sciences, Heidelberg University	19.9	6.62	1943.38	-10.26	-4.24
E23-3-081	Institute of Earth Sciences, Heidelberg University	20.15	7.14	1942.86	-10.23	-4.35
E23-3-082	Institute of Earth Sciences, Heidelberg University	20.4	7.57	1942.43	-9.43	-4.12
E23-3-083	Institute of Earth Sciences, Heidelberg University	20.65	8.06	1941.94	-10.98	-4.43
E23-3-084	Institute of Earth Sciences, Heidelberg University	20.9	8.72	1941.28	-11.42	-4.65
E23-3-085	Institute of Earth Sciences, Heidelberg University	21.15	9.43	1940.57	-11.43	-4.79
E23-3-086	Institute of Earth Sciences, Heidelberg University	21.4	10.27	1939.73	-11.71	-4.97
E23-3-087	Institute of Earth Sciences, Heidelberg University	21.65	11.31	1938.69	-11.29	-4.97
E23-3-088	Institute of Earth Sciences, Heidelberg University	21.9	12.05	1937.95	-11.28	-5.14
E23-3-089	Institute of Earth Sciences, Heidelberg University	22.15	12.52	1937.48	-10.04	-4.78
E23-3-090	Institute of Earth Sciences, Heidelberg University	22.4	12.97	1937.03	-11.03	-5.22
E23-3-091	Institute of Earth Sciences, Heidelberg University	22.65	13.46	1936.54	-10.02	-5.13
E23-3-092	Institute of Earth Sciences, Heidelberg University	22.9	14.00	1936.00	-10.41	-5.20
E23-3-093	Institute of Earth Sciences, Heidelberg University	23.15	15.12	1934.88	-9.89	-5.14
E23-3-094	Institute of Earth Sciences, Heidelberg University	23.4	15.75	1934.25	-10.93	-5.12
E23-3-095	Institute of Earth Sciences, Heidelberg University	23.65	16.43	1933.57	-12.33	-5.44
E23-3-096	Institute of Earth Sciences, Heidelberg University	23.9	17.08	1932.92	-11.50	-4.97
E23-3-097	Institute of Earth Sciences, Heidelberg University	24.15	17.62	1932.38	-11.81	-5.09
E23-3-098	Institute of Earth Sciences, Heidelberg University	24.4	18.15	1931.85	-10.89	-4.64
E23-3-099	Institute of Earth Sciences, Heidelberg University	24.65	18.70	1931.30	-11.79	-4.88
E23-3-100	Institute of Earth Sciences, Heidelberg University	24.9	19.21	1930.79	-10.74	-4.68
E23-3-101	Institute of Earth Sciences, Heidelberg University	25.15	19.52	1930.48	-10.76	-4.46
E23-3-102	Institute of Earth Sciences, Heidelberg University	25.4	19.74	1930.26	-11.75	-4.79
E23-3-103	Institute of Earth Sciences, Heidelberg University	25.65	20.03	1929.97	-11.26	-4.67
E23-3-104	Institute of Earth Sciences, Heidelberg University	25.9	20.41	1929.59	-12.28	-4.85
E23-3-105	Institute of Earth Sciences, Heidelberg University	26.15	20.89	1929.11	-12.09	-4.88
E23-3-106	Institute of Earth Sciences, Heidelberg University	26.4	21.62	1928.38	-11.49	-4.87
E23-3-107	Institute of Earth Sciences, Heidelberg University	26.65	22.55	1927.45		
E23-3-108	Institute of Earth Sciences, Heidelberg University	26.9	23.68	1926.32	-11.93	-5.08
E23-3-109	Institute of Earth Sciences, Heidelberg University	27.15	25.89	1924.11	-11.89	-4.86
E23-3-110	Institute of Earth Sciences, Heidelberg University	27.4	27.56	1922.44	-11.97	-4.90
E23-3-111	Institute of Earth Sciences, Heidelberg University	27.65	31.91	1918.09	-11.98	-4.75
E23-3-112	Institute of Earth Sciences, Heidelberg University	27.9	33.43	1916.57	-11.87	-4.70
E23-3-113	Institute of Earth Sciences, Heidelberg University	28.15	35.50	1914.50	-12.26	-5.28
E23-3-114	Institute of Earth Sciences, Heidelberg University	28.4	36.54	1913.46	-11.90	-5.71
E23-3-115	Institute of Earth Sciences, Heidelberg University	28.65	37.82	1912.18	-11.00	-5.40
E23-3-116	Institute of Earth Sciences, Heidelberg University	28.9	39.16	1910.84	-10.92	-5.17
E23-3-117	Institute of Earth Sciences, Heidelberg University	29.15	40.85	1909.15	-11.57	-5.23
E23-3-118	Institute of Earth Sciences, Heidelberg University	29.4	41.91	1908.09	-11.96	-4.92
E23-3-119	Institute of Earth Sciences, Heidelberg University	29.65	44.77	1905.23	-11.91	-4.72
E23-3-120	Institute of Earth Sciences, Heidelberg University	29.9	49.30	1900.70	-10.15	0.89
E23-3-121	Institute of Earth Sciences, Heidelberg University	30.4	52.02	1897.98	-12.17	-4.72
E23-3-122	Institute of Earth Sciences, Heidelberg University	30.9	54.35	1895.65	-11.96	-4.87
E23-3-123	Institute of Earth Sciences, Heidelberg University	31.4	56.13	1893.87	-11.45	-4.95
E23-3-124	Institute of Earth Sciences, Heidelberg University	31.9	57.58	1892.42	-11.74	-5.36
E23-3-125	Institute of Earth Sciences, Heidelberg University	32.4	59.10	1890.90	-11.39	-5.28
E23-3-126	Institute of Earth Sciences, Heidelberg University	32.9	61.95	1888.05	-11.02	-4.97
E23-3-127	Institute of Earth Sciences, Heidelberg University	33.4	64.54	1885.46	-11.07	-4.63
E23-3-128	Institute of Earth Sciences, Heidelberg University	33.9	67.55	1882.45	-12.04	-4.83
E23-3-129	Institute of Earth Sciences, Heidelberg University	34.4	69.94	1880.06	-11.65	-4.77
E23-3-130	Institute of Earth Sciences, Heidelberg University	34.9	71.94	1878.06	-11.55	-4.85
E23-3-131	Institute of Earth Sciences, Heidelberg University	35.4	74.42	1875.58	-11.73	-4.98
E23-3-132	Institute of Earth Sciences, Heidelberg University	35.9	77.93	1872.07	-11.18	-4.44
E23-3-133	Institute of Earth Sciences, Heidelberg University	36.4	80.22	1869.78	-11.54	-4.38
E23-3-134	Institute of Earth Sciences, Heidelberg University	36.9	81.81	1868.19	-11.67	-4.70
E23-3-135	Institute of Earth Sciences, Heidelberg University	37.4	83.50	1866.50	-11.51	-4.77
E23-3-136	Institute of Earth Sciences, Heidelberg University	37.9	85.31	1864.69	-11.17	-4.35
E23-3-137	Institute of Earth Sciences, Heidelberg University	38.4	86.95	1863.05	-11.05	-4.42
E23-3-138	Institute of Earth Sciences, Heidelberg University	38.9	89.79	1860.21	-11.10	-4.48
E23-3-139	Institute of Earth Sciences, Heidelberg University	39.4	92.10	1857.90	-10.55	-4.37
E23-3-140	Institute of Earth Sciences, Heidelberg University	39.9	94.14	1855.86	-10.74	-4.41
E23-3-141	Institute of Earth Sciences, Heidelberg University	40.4	95.81	1854.19	-10.51	-4.36
E23-3-142	Institute of Earth Sciences, Heidelberg University	40.9	97.24	1852.76	-10.57	-4.49
E23-3-143	Institute of Earth Sciences, Heidelberg University	41.4	98.42	1851.58	-10.06	-4.64
E23-3-144	Institute of Earth Sciences, Heidelberg University	41.9	100.47	1849.53	-8.48	-0.85
E23-3-145	Institute of Earth Sciences, Heidelberg University	42.4	102.31	1847.69	-9.47	-4.72
E23-3-146	Institute of Earth Sciences, Heidelberg University	42.9	105.51	1844.49	-9.72	-4.89
E23-3-147	Institute of Earth Sciences, Heidelberg University	43.4	108.70	1841.30		
E23-3-148	Institute of Earth Sciences, Heidelberg University	43.9	112.10	1837.90	-10.34	-5.41
E23-3-149	Institute of Earth Sciences, Heidelberg University	44.4	114.86	1835.14	-10.06	-4.81
E23-3-150	Institute of Earth Sciences, Heidelberg University	44.9	117.68	1832.32	-10.49	-4.71
E23-3-151	Institute of Earth Sciences, Heidelberg University	45.4	119.95	1830.05	-10.21	-5.09
E23-3-152	Institute of Earth Sciences, Heidelberg University	45.9	122.38	1827.62	-10.40	-5.18
E23-3-153	Institute of Earth Sciences, Heidelberg University	46.4	124.44	1825.56	-10.12	-5.11
E23-3-154	Institute of Earth Sciences, Heidelberg University	46.9	126.61	1823.39	-9.99	-4.99
E23-3-155	Institute of Earth Sciences, Heidelberg University	47.4	129.45	1820.55	-9.92	-5.08
E23-3-156	Institute of Earth Sciences, Heidelberg University	47.9	131.49	1818.51	-10.08	-5.11

E23-3-157	Institute of Earth Sciences, Heidelberg University	48.4	133.25	1816.75	-10.20	-5.38
E23-3-158	Institute of Earth Sciences, Heidelberg University	48.9	135.13	1814.87	-9.82	-4.96
E23-3-159	Institute of Earth Sciences, Heidelberg University	49.4	136.67	1813.33	-9.91	-4.35
E23-3-160	Institute of Earth Sciences, Heidelberg University	49.9	138.95	1811.05	-9.85	-4.20
E23-3-161	Institute of Earth Sciences, Heidelberg University	50.4	140.43	1809.57	-9.72	-4.07
E23-3-162	Institute of Earth Sciences, Heidelberg University	50.9	141.69	1808.31	-9.45	-3.97
E23-3-163	Institute of Earth Sciences, Heidelberg University	51.4	142.84	1807.16	-9.08	-3.79
E23-3-164	Institute of Earth Sciences, Heidelberg University	51.9	144.21	1805.79	-9.30	-3.96
E23-3-165	Institute of Earth Sciences, Heidelberg University	52.4	145.59	1804.41	-9.33	-3.98
E23-3-166	Institute of Earth Sciences, Heidelberg University	52.9	147.11	1802.89	-9.83	-4.31
E23-3-167	Institute of Earth Sciences, Heidelberg University	53.4	149.03	1800.97	-10.19	-4.47
E23-3-168	Institute of Earth Sciences, Heidelberg University	53.9	151.04	1798.96	-10.14	-4.50
E23-3-169	Institute of Earth Sciences, Heidelberg University	54.4	153.45	1796.55	-10.19	-4.57
E23-3-170	Institute of Earth Sciences, Heidelberg University	54.9	155.12	1794.88	-9.88	-4.61
E23-3-171	Institute of Earth Sciences, Heidelberg University	55.4	156.87	1793.13	-9.87	-4.61
E23-3-172	Institute of Earth Sciences, Heidelberg University	55.9	159.45	1790.55	-9.77	-4.54
E23-3-173	Institute of Earth Sciences, Heidelberg University	56.4	161.10	1788.90	-10.37	-4.54
E23-3-174	Institute of Earth Sciences, Heidelberg University	56.9	162.68	1787.32	-11.43	-4.68
E23-3-175	Institute of Earth Sciences, Heidelberg University	57.4	164.59	1785.41	-10.90	-5.17
E23-3-176	Institute of Earth Sciences, Heidelberg University	57.9	166.98	1783.02	-11.06	-5.17
E23-3-177	Institute of Earth Sciences, Heidelberg University	58.4	168.47	1781.53	-10.63	-4.94
E23-3-178	Institute of Earth Sciences, Heidelberg University	58.9	169.89	1780.11	-10.90	-5.57
E23-3-179	Institute of Earth Sciences, Heidelberg University	59.4	171.29	1778.71	-11.02	-5.68
E23-3-180	Institute of Earth Sciences, Heidelberg University	59.9	172.37	1777.63	-10.92	-5.39
E23-3-181	Institute of Earth Sciences, Heidelberg University	60.4	173.23	1776.77	-10.13	-5.10
E23-3-182	Institute of Earth Sciences, Heidelberg University	60.9	174.46	1775.54	-10.38	-5.29
E23-3-183	Institute of Earth Sciences, Heidelberg University	61.4	175.95	1774.05	-10.58	-5.40
E23-3-184	Institute of Earth Sciences, Heidelberg University	61.9	177.35	1772.65	-10.14	-5.47
E23-3-185	Institute of Earth Sciences, Heidelberg University	62.4	178.83	1771.17	-10.10	-5.46
E23-3-186	Institute of Earth Sciences, Heidelberg University	62.9	179.58	1770.42	-9.85	-5.49
E23-3-187	Institute of Earth Sciences, Heidelberg University	63.4	180.60	1769.40	-10.05	-5.28
E23-3-188	Institute of Earth Sciences, Heidelberg University	63.9	182.15	1767.85	-10.22	-5.12
E23-3-189	Institute of Earth Sciences, Heidelberg University	64.4	184.76	1765.24	-9.82	-4.60
E23-3-190	Institute of Earth Sciences, Heidelberg University	64.9	187.18	1762.82	-10.65	-4.71
E23-3-191	Institute of Earth Sciences, Heidelberg University	65.4	188.47	1761.53	-11.58	-5.20
E23-3-192	Institute of Earth Sciences, Heidelberg University	65.9	189.97	1760.03	-9.77	-5.20
E23-3-193	Institute of Earth Sciences, Heidelberg University	66.4	191.51	1758.49	-9.93	-5.23
E23-3-194	Institute of Earth Sciences, Heidelberg University	66.9	194.00	1756.00	-9.69	-4.89
E23-3-195	Institute of Earth Sciences, Heidelberg University	67.4	195.74	1754.26	-9.63	-4.72
E23-3-196	Institute of Earth Sciences, Heidelberg University	67.9	198.99	1751.01	-9.60	-4.57
E23-3-197	Institute of Earth Sciences, Heidelberg University	68.4	202.12	1747.88	-10.17	-4.71
E23-3-198	Institute of Earth Sciences, Heidelberg University	68.9	204.38	1745.62	-11.72	-6.17
E23-3-199	Institute of Earth Sciences, Heidelberg University	69.4	207.75	1742.25	-11.33	-6.07
E23-3-200	Institute of Earth Sciences, Heidelberg University	69.9	210.56	1739.44	-10.79	-5.52
E23-3-201	Institute of Earth Sciences, Heidelberg University	70.4	213.02	1736.98	-11.35	-5.01
E23-3-202	Institute of Earth Sciences, Heidelberg University	70.9	214.54	1735.46	-11.45	-5.36
E23-3-203	Institute of Earth Sciences, Heidelberg University	71.4	215.59	1734.41	-11.21	-5.57
E23-3-204	Institute of Earth Sciences, Heidelberg University	71.9	216.54	1733.46	-10.47	-5.29
E23-3-205	Institute of Earth Sciences, Heidelberg University	72.4	218.02	1731.98	-9.88	-4.53
E23-3-206	Institute of Earth Sciences, Heidelberg University	72.9	219.91	1730.09	-9.74	-4.24
E23-3-207	Institute of Earth Sciences, Heidelberg University	73.4	221.84	1728.16	-10.02	-4.07
E23-3-208	Institute of Earth Sciences, Heidelberg University	73.9	224.76	1725.24	-9.86	-4.14
E23-3-209	Institute of Earth Sciences, Heidelberg University	74.4	226.42	1723.58		
E23-3-210	Institute of Earth Sciences, Heidelberg University	74.9	227.89	1722.11	-11.05	-4.82
E23-3-211	Institute of Earth Sciences, Heidelberg University	75.4	230.48	1719.52	-10.55	-4.84
E23-3-212	Institute of Earth Sciences, Heidelberg University	75.9	232.68	1717.32	-10.23	-4.76
E23-3-213	Institute of Earth Sciences, Heidelberg University	76.4	234.55	1715.45	-10.20	-4.62
E23-3-214	Institute of Earth Sciences, Heidelberg University	76.9	236.35	1713.65	-10.12	-4.67
E23-3-215	Institute of Earth Sciences, Heidelberg University	77.4	238.27	1711.73	-10.12	-4.69
E23-3-216	Institute of Earth Sciences, Heidelberg University	77.9	240.58	1709.42	-10.34	-4.74
E23-3-217	Institute of Earth Sciences, Heidelberg University	78.4	242.42	1707.58	-10.50	-4.98
E23-3-218	Institute of Earth Sciences, Heidelberg University	78.9	243.49	1706.51	-10.04	-4.98
E23-3-219	Institute of Earth Sciences, Heidelberg University	79.4	244.31	1705.69	-9.89	-4.97
E23-3-220	Institute of Earth Sciences, Heidelberg University	79.9	245.11	1704.89	-10.26	-5.04
E23-3-221	Institute of Earth Sciences, Heidelberg University	80.4	246.17	1703.83	-10.67	-5.10
E23-3-222	Institute of Earth Sciences, Heidelberg University	80.9	249.05	1700.95	-10.17	-5.01
E23-3-223	Institute of Earth Sciences, Heidelberg University	81.4	251.06	1698.94	-10.78	-5.39
E23-3-224	Institute of Earth Sciences, Heidelberg University	81.9	252.88	1697.12	-10.40	-5.44
E23-3-225	Institute of Earth Sciences, Heidelberg University	82.4	254.82	1695.18	-10.75	-5.48
E23-3-226	Institute of Earth Sciences, Heidelberg University	82.9			-7.92	-4.73
E23-3-227	Institute of Earth Sciences, Heidelberg University	83.4			-8.62	-5.00
E23-3-228	Institute of Earth Sciences, Heidelberg University	83.9			-8.66	-4.89

Formatted: Normal

Page 19: [1] Deleted	Sophie Warken	8/11/26 2:29:00 PM

1.1.1

Page 25: [2] Deleted	Sophie Warken	8/11/26 2:29:00 PM